

Quantum electrodynamics of non-demolition detection of single microwave photon by superconducting qubit array

P. Navez, A. G. Balanov, S. E. Savel'ev, A. M. Zagoskin

Department of Physics, Loughborough University, Loughborough LE11 3TU, United Kingdom

(Dated: December 6, 2022)

By consistently applying the formalism of quantum electrodynamics we developed a comprehensive theoretical framework describing the interaction of single microwave photons with an array of superconducting transmon qubits in a waveguide cavity resonator. In particular, we analyse the effects of microwave photons on the array's response to a weak probe signal exciting the resonator. The study reveals that a high quality factor cavities provide better spectral resolution of the response, while cavities with moderate quality factor allow better sensitivity for a single photon detection. Remarkably, our analysis showed that a single-photon signal can be detected by even a sole qubit in cavity under the realistic range of system parameters. We also discuss how quantum properties of the microwave radiation and electrodynamic properties of resonators affect the response of qubits' array. Our results provide an efficient theoretical background for informing the development and design of quantum devices consisting of arrays of qubits, especially for those using a cavity where an explicit expression for the transmission or reflection is required.

I. INTRODUCTION

Microwaves are a natural frequency range for superconducting qubits, which makes them especially attractive for applications related to detecting a single microwave photons [1–3], where one has to contend with strong ambient noise. These important studies relates not only to pivotal technological applications, but also to paradigm building research such as searching of galactic axions [4–6], one of dark matter candidates. Due to all these reasons, experimental and theoretical studies of the interaction of a microwave radiation with arrays of qubits attract increasing research attention [7–13].

Despite a significant progress over the last decades in the theoretical investigation of the interaction of superconducting qubit systems with electromagnetic field (EMF) [14–18], the applied approaches are predominantly based on rather qualitative descriptions of the system under consideration to effective equations, which limits applicability of such models by very specific problems. Here we develop a consistent and comprehensive theory of a quantized electromagnetic field interacting with a transmon qubits embedded in a superconducting waveguide cavity.

The main distinctive feature of our approach [3, 6, 19–23] is that we start from a consistent non-relativistic quantum electrodynamics (QED) formalism describing both photon and Cooper pair fields, where decoherence is derived explicitly. Within this framework we distinguish the cavity mode from the external mode, as the photon field, while the transmon field has to be built as superpositions of two mode state describing tunnelling through Josephson junctions as the electron field. This description enables us to express the model parameters in terms of fundamental quantities associated with the architectural geometry of a system consisting of transmons and coplanar waveguide lines.

Usually, when using a resonator waveguide, the qubits are probed theoretically by making use of the power spec-

tral function or correlation function providing the spectral properties [24, 25]. However this analysis is not explicitly related to the transmission or reflection factor that is really measured. Many missing informations occur, as for instance the intensity peak, that may be crucial for a full experimental characterization.

In this work, we apply the developed theoretical framework to a microwave photon detection scheme based on the Stark shift response to the probe beam to calculate explicitly the transmission signal, depending on the parameters of resonant cavity and the properties of the photons to detect. We also discuss some conditions where the system under study is capable of working as a single photon detector.

Other proposals on the single photon detection [26], in particular based on the itinerant photon [27–29], exist in the literature but they do not employ explicitly a probe beam used for a subsequent transmission analysis of the Stark shift profile. In contrast in our work, the performance of a detection relies on the ability of this macroscopic transmitted beam to probe a single photon signal, which can be interpreted as an amplification process.

If the actual trends in single photon detection is to separate the storage cavity from the measurement cavity to read out the qubit [30], it is at the cost of using a time protocol of different pulses and adiabatic coupling and decoupling processes by means of a magnetic field, preventing the possibility of a continuous measurement. Our approach aims at benefiting from this last property in order to characterize the nature of the beam of single photon entering into the cavity. It could be viewed as a more involved theoretical description of the early experiment [20] with an emphasis on the quantum state discrimination (coherent, incoherent, thermal) under various parameter conditions, including the possibility of using many qubits.

The paper is organized as follows. In Section II we provide theoretical approaches leading to a practical model

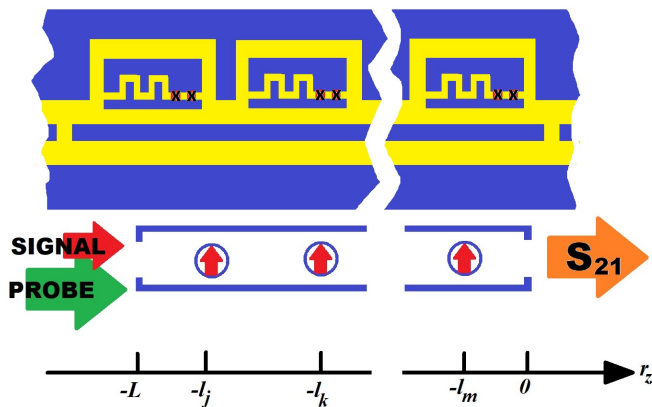


FIG. 1. (Color online) **Upper panel:** Artistic rendering of the QED device with an array of transmon qubits; yellow color corresponds to insulator region, blue shows the superconductor region; crosses indicate the position of the Josephson junctions. **Lower panel:** Schematic representation of the QED circuit associated with the device depicted in the upper panel; blue box with open edges is a cavity resonator; ovals with vertical arrow are the qubits; horizontal arrows represent the input signal, probe field and measured transmission S_{21} ; axis is used to indicate the positions $-l_j$ of the j^{th} transmon along the direction r_z (the origin is placed after the device as the usual convention in transmission line theory [31]).

that allows to describe the transmission signal. In Section III, we discuss the results obtained for various parameters conditions before ending with the conclusion in Section IV. All accounts explained in those sections are explicitly detailed in the appendices.

II. MODELLING

A generic quantum electrodynamics (QED) description of a qubit array embedded in a microwave waveguide is discussed in appendices A, B and C. Here we consider a QED system, which represents an array of transmon qubits coupled to a coplanar waveguide resonator, see Fig.1. The upper part of the figure shows an artistic image of the system, while the lower panel provides with its schematic representation. In the schematic representation, the probe (green arrow online) and signal (red arrow online) fields form the input and transmission S_{21} (orange arrow online) is the output for the measurement.

In appendix A, we define the 3D Hamiltonian for EMF and quantum Cooper pair field and transform it into the more convenient dipole representation. In appendix B, we use a restricted set of basis for the Cooper field that describes the tunneling at the Josephson junction while, in appendix C, we restrict the basis to the TME modes. For the transverse electromagnetic components propagating within the waveguide in the direction r_z as time t changes, the two canonically conjugated field variables

are the integrated nonlocal flux $\hat{\Phi}_B(r_z, t)$ through the insulator region surrounding perpendicularly the signal (blue line in the middle) and an infinitesimal charge element $dQ(r_z, t)$. They obey the nontrivial commutation relations:

$$[\hat{\Phi}_B(r'_z, t), \partial_{r_z} \hat{Q}(r_z, t)] = i\hbar\delta(r_z - r'_z). \quad (1)$$

For freely propagating electromagnetic waves, these operators are related to the local potential $V(r_z, t)$ through the Lenz law $\hat{V}(r_z, t) = -\partial_t \hat{\Phi}_B(r_z, t)$ and the local current $I(r_z, t)$ through charge conservation $\partial_{r_z} \hat{I}(r_z, t) = -\partial_t \partial_{r_z} \hat{Q}(r_z, t)$.

The transmons denoted by $j = 1 \dots N$ are arranged in an array near the waveguide. They are formed of two superconducting islands shaped as interlocking combs (to increase mutual capacitance) and connected by a pair of Josephson junctions. The electrodynamics of transmon qubits can be described in terms of the real charge operators $\hat{q}_j(t)$ of the Cooper pair having charge $2e$ on each side of the islands and their conjugated flux operators $\hat{\Phi}_j(t)$ that correspond to the phase difference between the wave functions of the two macroscopic quantum states, associated to each island, multiplied by $(2e)/\hbar$.

Similarly, for the longitudinal modes related to j^{th} transmon the nontrivial commutation relations read

$$[\hat{\Phi}_j(t), \hat{q}_{j'}(t)] = i\hbar\delta_{j,j'}. \quad (2)$$

Although for the description of both the waveguide and the qubit we use similar type of variables, they have some differences. Namely, the charge on the surface of the waveguide is determined by the Gauss theorem for the electric field. It is induced by a transverse mode of the electromagnetic field and differs from the one $\hat{q}_{j'}$ resulting from a longitudinal Coulombian field commonly referred to plasmon excitations.

Unlike the case of bulk superconductors, the (plasmon) frequencies of our Josephson structure lie within the microwave range. Therefore these excitations have their own dynamics, which needs to be taken into account. More details are given in appendices B and C. Despite the above fundamental difference between the introduced charge components, the defined set of canonically conjugated variables allows to describe a quantum device as a circuit of lump elements (quantum circuit). Such a description greatly simplifies the understanding of the underlying physics since the proposed derivation allows a unambiguous well-defined physical representation of these variables in Fig.1.

Using the outcomes of appendices A-C with the addition of the description of the resonator in appendix D and a unitary transformation on transmon variables in appendix E, we derive the Hamiltonian in terms of these

quantum circuit variables:

$$\hat{H} = - \sum_{j=1}^N E_{J,j} \cos \left[\frac{2e}{\hbar} (\hat{\Phi}_j - f_j \hat{\Phi}_B(-l_j)) \right] + \frac{\hat{q}_j^2}{2C_j} + \int_{-\infty}^{\infty} dr_z \left[\frac{\partial_{r_z} \hat{Q}^2(r_z)}{2C'} + \frac{\partial_{r_z} \hat{\Phi}_B^2(r_z)}{2L'} \right] + \frac{\hat{Q}_-^2(-L) + \hat{Q}_+^2(0)}{2C}, \quad (3)$$

where $E_{J,j}$ is the Josephson junction energy responsible for an inductance-like coupling with the EMF and C_j the capacitance of the transmon. The geometric prefactor f_j controls the effective flux inside the transmon and $-l_j$ is the position of the qubit inside the cavity (see Fig. 1). L' and C' are the line inductance and capacitance respectively and C is the capacitance at the ends of the cavity having length L (see Fig.1). Since the capacitances C are placed longitudinally, their charge corresponds precisely to the effective charge accumulated through the waveguide line. The integration has to be taken over the whole length of the waveguide which is assumed infinite from both sides. The integrated charge $\hat{Q}_{\pm}(r_z, t) = \pm \int_{\pm\infty}^{r_z} \partial_{r_z} \hat{Q}(r_z, t) dr_z$ is a nonlocal operator, which is opposite to the charge accumulated throughout the waveguide. The integration is from the left side of the waveguide $-$ or from the right side $+$.

Note, the presence of a cavity suppresses the super-radiative relaxation rate that scales like N^3 as observed experimentally in [13] in order to remain mainly with the dephasing rate $\Gamma_{\phi,j}$ and some other additional rates Γ_j coming from other decay into other electric modes (TM or TE).

After restricting consideration by two first transmon energy levels, the Hamiltonian (3) is rewritten in appendix E in a nonlocal form using new field operator and a qubit variable as:

$$\hat{H} = \int_{-\infty}^{\infty} dr_z \frac{\hat{\alpha}^2(r_z) + c^2 \partial_{r_z} \hat{\alpha}^2(r_z)}{2} + \frac{\hat{Q}_-^2(-L) + \hat{Q}_+^2(0)}{2C} + \sum_{j=1}^N \frac{\hbar \omega_j}{2} \hat{\sigma}_j^z - \sqrt{\hbar c \kappa_j} \hat{\sigma}_j^x \hat{\alpha}(-l_j), \quad (4)$$

where the flux is now identified as $\hat{\Phi}_B(r_z) = \hat{\alpha}(r_z)/\sqrt{C'}$ and the charge has now a non local expression: $\hat{Q}_{\mp}(r_z) = \pm \int_{\mp\infty}^{r_z} dr'_z \sqrt{C'} \hat{\alpha}(r'_z)$. The new parameters of the Hamiltonian (4) are $c = 1/\sqrt{L'C'}$, $\hbar \omega_j = \sqrt{4e^2 E_{J,j}/C_j} - e^2/(2C_j)$ and $\kappa_j = \frac{2e}{\hbar} f_j \sqrt{E_{J,j} \omega_j / (2cC')}$. Then the non-trivial commutation relation between the conjugate variables becomes:

$$[\hat{\alpha}(r_z, t), \hat{\alpha}(r'_z, t)] = i\hbar \delta(r_z - r'_z). \quad (5)$$

Note that the Heisenberg equations imply that the conjugated momentum is not a time derivative $\hat{\alpha}(r_z, t) \neq \partial_t \hat{\alpha}(r_z, t)$. Depending on the waveguide architecture, the propagation speed c can be significantly smaller than the speed of light in the free space. For example, in the

specific case of coplanar waveguide depicted in Fig. 15 of appendix C, C' should be substituted by an efficient capacitance C'_{eff} , which accounts also the interface current to the dielectric materials composing the waveguide. Such consideration corrects the estimated speed of propagation c and allows to improve previous theoretical description [32, 33].

As shown in appendix E, the quantities of interest available for measurement in experiment are the forward (+) and backward wave (-) quantum operators propagating throughout the waveguide:

$$\hat{A}_{\pm}(r_z, t) = \frac{\hat{V}(r_z, t) \pm Z \hat{I}(r_z, t)}{2\sqrt{Z}} = \pm c^{3/2} \partial_{r_z} \hat{\alpha}(r_z, t) - c^{1/2} \hat{\alpha}(r_z, t), \quad (6)$$

where the impedance is $Z = \sqrt{L'/C'}$.

Taking the temporal Fourier transform, the transmission of the signal is $S_{21} = \langle \hat{A}_{\omega,+}(0) \rangle / \langle \hat{A}_{\omega,+}^{in}(0) \rangle$, where $\hat{A}_{\omega,+}^{in}(r_z)$ is the input field operator, while the full operator $\hat{A}_{\omega,+}(r_z) = \hat{A}_{\omega,+}^{in}(r_z) + \hat{A}_{\omega,+}^{sc}(r_z)$ contains the scattering contribution $\hat{A}_{\omega,+}^{sc}(r_z)$ resulting from the interaction of EMF with the cavity and the qubits.

Despite the simplification in terms of qubits, the Hamiltonian (4) cannot still be solved exactly in the continuous limit. For a high quality cavity however, it is possible to separate the continuous field of the waveguide and the other degree of freedom inside the cavity. In appendix F, these cavity modes are determined in terms of the two end capacitances C assumed to be small in comparison to the line capacitance C' , i.e. $C \ll C'L$. In the leading order, we obtain the harmonics $\omega_{n,0} = n\pi c/L$ for any natural integer. To the next orders, the frequency shift and the half-width are:

$$\omega_n - \omega_{n,0} = -\frac{2C}{C'L} \omega_{n,0}, \quad \gamma_n = \frac{4c}{L} \left(\frac{C\omega_{n,0}}{cC'} \right)^2, \quad (7)$$

in agreement with the reference [34]. The quality factor of n^{th} mode is defined as:

$$\mathcal{Q}_n = \frac{\omega_n}{\gamma_n} \cong \frac{C'L}{2\omega_{n,0} Z C^2}. \quad (8)$$

It differs from the definition in [34], where $\mathcal{Q}_n = C'L/(2\omega_{n,0} R_L C^2)$ with R_L being the resistance outside the resonator, usually chosen to match the line impedance Z . Within our consideration, we don't use any resistance since, in the situation where the qubits are absent, a lossless cavity does not dissipate any energy but rather scatters part of its energy. Therefore, the finite linewidth previously associated with dissipation through the effective external load resistance is understood in our case in terms of impedances of the EMF without any dissipation. The expression (8) does not account for the quality factor saturation [34]. The latter can be explained by the additional currents at the dielectric interfaces.

In appendix H, we restrict the cavity dynamics to the first mode $n = 1$ described in terms of the annihilation operator \hat{a}_1 with a frequency close to the qubit frequencies and apply the rotating wave approximation. We arrive eventually at the Jaynes-Cumming Hamiltonian for many qubits [35] which additionally contains the external backward and forward fields:

$$\begin{aligned} \frac{\hat{H}(t)}{\hbar} = & \sum_{j=1}^N -\frac{\delta\omega_j}{2} \hat{\sigma}_j^z + g_j (\hat{a}_1^\dagger \hat{\sigma}_j^- + \hat{a}_1 \hat{\sigma}_j^+) + (\omega_c - \omega) \hat{a}_1^\dagger \hat{a}_1 \\ & + i \sqrt{\frac{\gamma_c}{\hbar\omega_c}} \sum_{\pm} \hat{A}_{\pm}^{in}(0, t) (\hat{a}_1 e^{-i\omega t} - \hat{a}_1^\dagger e^{i\omega t}). \end{aligned} \quad (9)$$

Here, the coupling $g_j = \kappa_j \cos(\pi l_j/L)/\sqrt{\pi}$ depends on the position of the qubits, while the cavity frequency $\omega_c = \omega_1$ and the damping $\gamma_c = \gamma_1$ are adjusted to the first resonance mode. The latter induces a decay rate of the qubits as a result of the Purcell effect. At the difference of a similar scheme described in [8], the input field $\hat{A}_{\pm}^{in}(0, t) = \langle \hat{A}_{\pm}^{in}(0, t) \rangle + \delta \hat{A}_{\pm}^{in}(0, t)$ not only accounts for the classical coherent part of the field but also for the quantum part of the field which either corresponds to the fluctuating vacuum mode viewed as an input quantum noise [36] or the incoherent mode to be detected. This is an interesting fundamental feature that these two apparently unrelated contributions originate from one unique quantum field. A similar expression appears in absence of the cavity in the appendix G and leads to similar developments in [37, 38].

The Hamiltonian (9) with such a time dependent quantum operator is generally treated using the master equation approach or stochastic techniques [36]. The former is used in our work in order to get analytical expressions derived in Appendices G and H. In complement to this approach, the line transmission S_{21} is determined for a coherent forward field passing through the cavity in appendices F and H. For a frequency ω_p close to the first resonance mode of the cavity, it is a sum of two contributions from the cavity and from the qubits:

$$\begin{aligned} S_{21} = S_{21}^{cv} + S_{21}^{qb} = \\ \sum_{\pm} \frac{-i\gamma_c/2}{\omega_p \mp \omega_c + i\gamma_c/2} \left[1 \pm \sqrt{\frac{\hbar\omega_c}{\gamma_c}} \sum_{j=1}^N \frac{g_j \langle \hat{\sigma}_{\omega_p, j}^{\mp} \rangle}{\langle \hat{A}_{\omega_p, \pm}^{in}(0) \rangle} \right] \end{aligned} \quad (10)$$

Comparing with earlier works [24, 39], this last expression suggests that, since the transmission factor is only sensitive to the lowering and raising operators, the qubit state does not have to be prepared in a superposition of ground and excited states for an effective action. As a consequence, the discrete photon set inside a cavity is monitored continuously using a coherent probe beam tuned at the qubit frequency without any additional protocol required.

III. RESULTS AND DISCUSSIONS

A. Setup

As detailed in appendix I and illustrated in Fig.1, the setup involves two continuous beams: the weak photon signal beams with a flux \mathcal{J} is tuned at the cavity resonance $\omega = \omega_c$; a second coherent probe beam of frequency ω_p close to the qubit frequencies.

For the purpose of quantum non-demolition measurements (QND) [24], the cavity and qubit frequencies, ω_c and ω_j respectively, must be strongly detuned such that their difference much larger compared to the coupling $|\omega_j - \omega_c| \gg g_j$. Then, as shown in appendix H, the inelastic processes are suppressed, and the effective qubit-cavity interaction has the form photon number-dependent qubit energy shift with the Hamiltonian terms $\chi_j \hat{\sigma}_j^z \hat{a}_1^\dagger \hat{a}_1$. The energy shift $\chi_j = g_j^2/(\omega_j - \omega_c)$ is usually referred as the Stark shift and must be very low in comparison to the microwave frequencies. The latter discriminates the peaks of cavity associated to different photon population in the probe transmission spectrum.

Using the formula for the relaxation rate $\Gamma_j = \kappa_j^2/\omega_j$ in appendix F in absence of a cavity, the constant χ_j is estimated using the data available in [13]. Namely the radiative relaxation rate $\Gamma_j \sim 2\pi 6.4\text{MHz}$ and the qubit frequency $\omega_j \sim 2\pi 8\text{GHz}$, we estimate the coupling $g_j \sim \kappa_j/2 \sim \sqrt{\omega_j \Gamma_j}/2 \sim 2\pi 100\text{MHz}$ and deduce $\chi_j \sim 2\pi 10\text{MHz}$ for $|\omega_j - \omega_c| \sim 2\pi 1\text{GHz}$.

In presence of a cavity with the relaxation rate γ_c , we add phenomenologically two other damping mechanisms associated to the qubits [7, 38]. The first accounts for the qubit radiative time $T_{1,j} = 1/\Gamma_j$ decaying in other modes than in the TEM mode, while the second for the dephasing time (lifetime of coherent superposition of qubits state not described explicitly in our formalism) $T_{2,j} = 1/\Gamma_{\phi,j}$. We shall choose the best value $\Gamma_{\phi,j} = 2\pi 250\text{kHz}$ obtained in [13] keeping in mind that these are difficult to control in the fabrication process. Although the origin of the time $T_{2,j}$ has been thoroughly discussed in [8], the possibility of other decay electromagnetic modes (TE or TM) included in $T_{1,j} = 1/\Gamma_j$ has not been mentioned and could be negligible in an optimal designed circuit [13]. In contrast, according to our estimation of the experimental data [38] in appendix F, these other modes contribute to 90% of the relaxation in comparison to the TEM mode.

The quantum input states under consideration are detailed in appendix I and are described as follows:

1. **Coherent state:** This state has non zero amplitude average $\langle \hat{a}_1 \rangle \neq 0$ with a well defined phase with infinite decoherence time and is the most common input radiation produced by a microwave source.
2. **Incoherent state:** This state is monochromatic and has a decoherence time τ_c much larger than the

cavity lifetime $2/\gamma_c$ with the zero amplitude average and thus no defined phase. These input radiations may be produced by a fluorescent source resulting from a spontaneous emission of artificial atoms.

3. **Thermal state:** A quantum state with a much smaller decoherence time τ_c such that $\tau_c\chi_j \ll 1$ has a much larger broadening of its frequency spectrum. Once it passes through the cavity, it cannot be distinguished from a thermal state resulting from a black body radiation. In comparison with the coherent and incoherent cases, for the thermal case, we note a much more important increase of line broadening, as well as a reduction of the photon flux once $\tau_c < 2/\gamma_c$.

Quite generally, the calculation of the transmission S_{21}^ν is done in appendix I for the three cases of photon signal above with the labelings $\nu = \text{coh, inc, th}$ as a function of the probe frequency ω_p . We obtain the general analytical formulas (I14) (I32) and (I45) combined with (I21) that allow to deal with imperfect situations of absence of line resolution.

B. Well-resolved spectrum: $\gamma_c \ll \chi_j$

For the positive frequency ω_p close to the qubit frequencies and the signal frequency ω with a photon flux per unit of time \mathcal{J} exactly tuned at the cavity resonance $\omega = \omega_c$ and $\gamma_c \ll \chi_j$, the transmission can be approximated as:

$$S_{21}^\nu \cong -\frac{i\gamma_c}{2(\omega_p - \omega_c)} + \sum_{j=1}^N \sum_{n=0}^{\infty} \frac{iP_\nu(n)\gamma_c\chi_j/[2(\omega_j - \omega_c)]}{\omega_p - [\omega_j + 2\chi_j n - i(\Gamma_\nu(n) + \Gamma_j/2 + \Gamma_{\phi,j})]} \quad (11)$$

where $P_\nu(n)$ is the probability distribution and $\Gamma_\nu(n)$ is the decay rate due to the cavity with explicit expressions given in table I for various input quantum states of the signal field ν . Note that the formula for $\Gamma_\nu(n)$ agrees for coherent state with the one derived in [25] using the spectral power for the spin. In contrast, a more fundamental approach allows to determine explicitly the intensity peak for the transmission.

For the validity of formula Eq.(11) in the incoherent case, we need also to satisfy the high quality factor condition $\gamma_c \ll (1 + \bar{n})(\Gamma_j/2 + \Gamma_{\phi,j})/\bar{n}$.

For one qubit, the graphs for the transmission are displayed in Figs.2, 3, 4, 6 and 8 and represent a sideband comb structure whose the distribution determines the nature and the average of the signal. The other graphs in Fig.5 or 9 display too much broadening to be approximated by Eq.(11) despite the possible line resolution for the incoherent case. Fig.2 corresponds to the observed Stark shift with the best to date values of coupling and quality factor so far obtained in current experiments,

State	ν	$P_\nu(n)$	$\Gamma_\nu(n)$	\bar{n}
Vacuum	0	$\delta_{n,0}$	0	0
Coherent	coh	$e^{-\bar{n}}\bar{n}^n/n!$	$(n + \bar{n})\gamma_c/2$	$2\mathcal{J}/\gamma_c$
Incoherent	inc	$\bar{n}^n/(\bar{n} + 1)^{n+1}$	$n\gamma_c/2$	$2\mathcal{J}/\gamma_c$
Thermal	th	$\bar{n}^n/(\bar{n} + 1)^{n+1}$	$[(2\bar{n} + 1)n + \bar{n}]\gamma_c$	$\tau_c\mathcal{J}$

TABLE I. Representation of the probability distribution and cavity decay rate for a given average photon number inside the cavity \bar{n} . The index ν labels the various analyzed quantum states while $\nu = 0$ corresponds to the background response without any signal $\bar{n} = 0$. The last column shows the proportionality relation between the cavity photon average and the photon flux \mathcal{J} .

while other figures represent results for less perfect devices.

The probe beam acts in the range around the qubit frequency so that the transmission due to the cavity S_{21}^{cv} in the first term of Eq.(11) is far off resonance and therefore can be neglected as shown in Fig.2 where the imaginary part for large ω_p is close to zero. In contrast in Figs.3,4 and 8, the imaginary part becomes asymptotically negative and may introduce a significant background noise if not well distinguished from the signal in the real part.

As shown in Fig.6, the increase of the qubit number contributes to suppress the background from the cavity and increase the sensitivity to the signal detection.

As far as the sensitivity of the probe is concerned, the transmission of qubit for the spectrum scales at resonance like $g_j^2/(\omega_j - \omega_c)^2$ which is always a very small quantity and this imposes that $\gamma_c \gg \Gamma_j, \Gamma_{\phi,j}$ in order to have a high response. Therefore a high quality factor is not desired unless the qubit decay rate and dephasing are negligible. Since dephasing is about 250kHz, a similar value has to be chosen for the cavity linewidth for an optimum transmission.

C. Lower quality factor regime $\gamma_c \gg \chi_j$

The case of low broadening of the spectral line may be difficult to achieve experimentally since it requires high quality factor and extreme high sensitivity of the response signal.

In the weak coupling regime and for $\chi_j \ll \sqrt{\gamma_c(\Gamma_j/2 + \Gamma_{\phi,j})}$, the line amplitude vanishes except for the main line, but the signal amplitude increases due to the lower quality factor allowing for a better transmission of the probe beam. We find in appendix I the same results for the coherent and thermal cases:

$$S_{21}^{\text{coh}} = S_{21}^{\text{th}} = S_{21}^{cv} + \sum_{j=1}^N \frac{i\gamma_c\chi_j/[2(\omega_j - \omega_c)]}{\omega_p - [\omega_j + 2\chi_j\bar{n} - i(\Gamma_j/2 + \Gamma_{\phi,j})]} \quad (12)$$

The position of the unique peak is displaced by the offset $2\chi_j\bar{n}$ in comparison to the situation of vacuum signal.

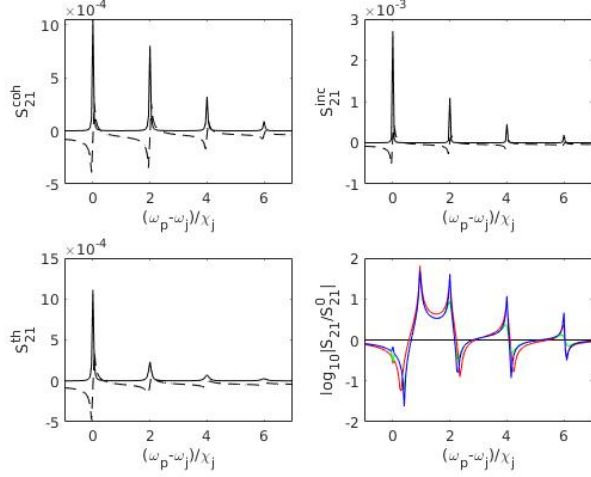


FIG. 2. Transmission S_{21}^ν through the cavity containing one qubit and the average signal photon number $\bar{n} = 1$. System parameters: Values: $\omega_j = 2\pi$ 10GHz, $\omega_c = 2\pi$ 9GHz, $\chi_j = 2\pi$ 10MHz, $\gamma_c = 2\pi$ 100kHz, $\Gamma_j + 2\Gamma_{\phi,j} = 2\pi$ 250kHz
Panels 1-3: Real (solid line) and imaginary (dashed line) of S_{21}^ν for the coherent (panel 1), incoherent (2) or thermal (3) photon field. Peaks are labeled by the actual photon number n . Peak heights are proportional to $P_\nu(n)$ with linewidths: $\Gamma_\nu(n) + \Gamma_j/2 + \Gamma_{\phi,j}$.

Panel 4: Transmission relative to the case of no signal, $|S_{21}^\nu|/|S_{21}^0|$, for coherent (red), incoherent (blue) and thermal (green) photon field. Transmission S_{21}^ν for a cavity containing one qubit with an average signal photon number $\bar{n} = 1$.

For the incoherent case the transmission is strongly suppressed due to the large uncertainty of the phase leading to additional broadening. Using the Kummer special function (detailed in Appendix I), we find:

$$S_{21}^{\text{inc}} = S_{21}^{cv} + \sum_{j=1}^N \frac{i\gamma_c U\left(1, 1, \frac{\omega_p - \omega_j + i(\Gamma_j/2 + \Gamma_{\phi,j})}{2\bar{n}\chi_j}\right)}{(\omega_j - \omega_c)4\bar{n}}. \quad (13)$$

In this context, the transmission of the pure vacuum state is higher than the one of the mixed incoherent state which acts as an inhibitor of the probe beam propagation.

Even in presence of large broadening, it is nevertheless still possible to discriminate in the probe response between coherent or thermal and incoherent states in the weak Stark coupling regime as seen in Fig.7.

D. Influence of a finite coherence time for $\gamma_c\tau_c \ll 1$

The infinite coherence time limit corresponds to the ideal case of the thermal state case. Once the coherence time τ_c becomes smaller, both the probe response and the line resolution deteriorate. Figure 10 illustrates these features for realistic experimental values.

We did not address however the crossover case: $\gamma_c\tau_c \geq 1$ for which a more elaborated theory is required. How-

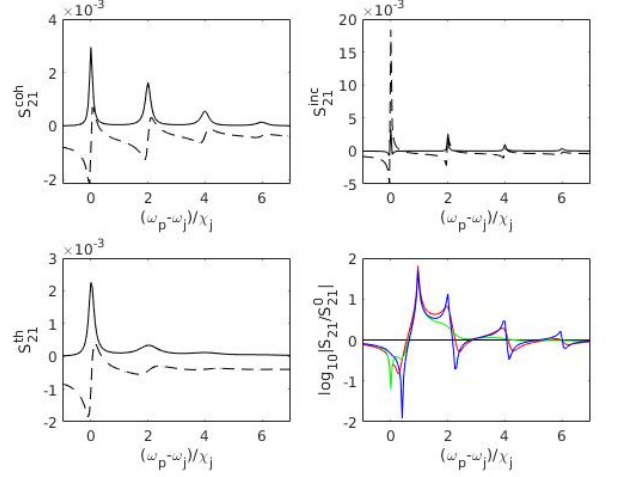


FIG. 3. Same as Fig.2 for a lower cavity quality factor. Parameters: $\omega_j = 2\pi$ 10GHz, $\omega_c = 2\pi$ 9GHz, $\chi_j = 2\pi$ 10MHz, $\gamma_c = 2\pi$ 1MHz, $\Gamma_j + 2\Gamma_{\phi,j} = 2\pi$ 250kHz.

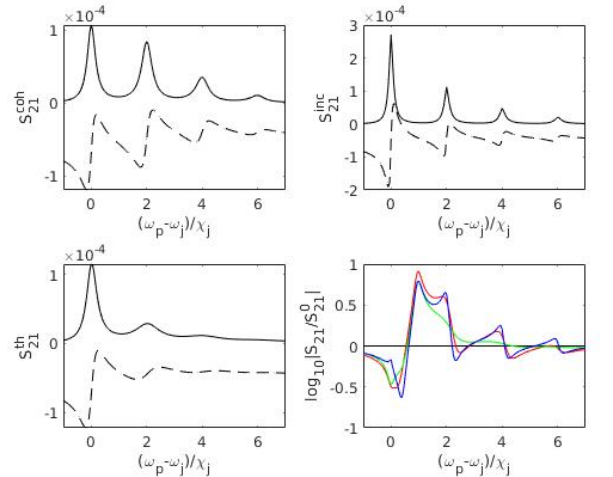


FIG. 4. Same as Fig.2 for lower Stark shift. Parameters: $\omega_j = 2\pi$ 10GHz, $\omega_c = 2\pi$ 9GHz, $\chi_j = 2\pi$ 1MHz, $\gamma_c = 2\pi$ 100kHz, $\Gamma_j + 2\Gamma_{\phi,j} = 2\pi$ 250kHz.

ever, by interpolation with the incoherent case, we could obtain a rough idea of the outcome in this regime. The validity of such an interpolation has not yet been proved from our present approach and would require more theoretical investigation.

E. Detuned case: $\omega \neq \omega_c$

The proposed setup implies an exact knowledge of the single photon frequency to be detected. Deviations from this frequency with respect to the cavity one deteriorate the quality of the probe response. Fig.11 illustrates how

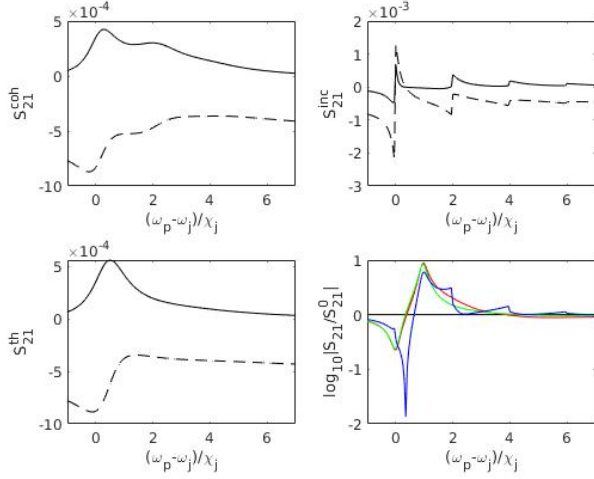


FIG. 5. Same as Fig.2 for lower Stark shift and quality factor. Parameters: $\omega_j = 2\pi$ 10GHz, $\omega_c = 2\pi$ 9GHz, $\chi_j = 2\pi$ 1MHz, $\gamma_c = 2\pi$ 1MHz, $\Gamma_j + 2\Gamma_{\phi,j} = 2\pi$ 250kHz.

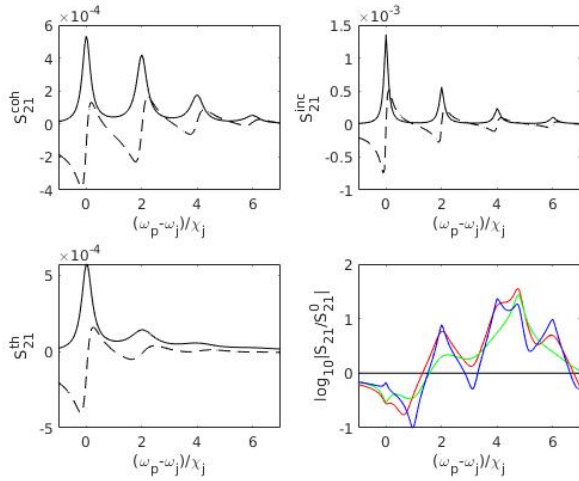


FIG. 6. Same as Fig.4 for 5 qubits. Parameters: $\omega_j = 2\pi$ 10GHz, $\omega_c = 2\pi$ 9GHz, $\chi_j = 2\pi$ 1MHz, $\gamma_c = 2\pi$ 1MHz, $\Gamma_j + 2\Gamma_{\phi,j} = 2\pi$ 250kHz.

the quality of the response is affected significantly by this indetermination for coherent state and incoherent state respectively, once the detuning is of order of γ_c .

F. Non-identical and interacting qubits

The probe response to the signal increases proportionally to the number of qubits, but only if all the essential qubit parameters ($\omega_j, \Gamma_j, \Gamma_{\phi,j}, \chi_j$) are identical. In reality, due to the difficulty of manufacturing the qubit with high precision [13], these parameters will likely demonstrate a dispersion of the order of at least 10%.

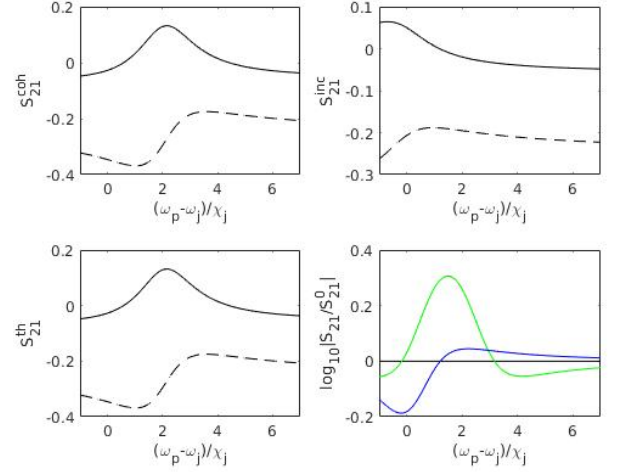


FIG. 7. Same as Fig.2 in the limit of very low quality factor. The thermal case becomes indistinguishable from the coherent case. Parameters: $\omega_j = 2\pi$ 10GHz, $\omega_c = 2\pi$ 9GHz, $\chi_j = 2\pi$ 100kHz, $\gamma_c = 2\pi$ 500MHz, $\Gamma_j + 2\Gamma_{\phi,j} = 2\pi$ 250kHz.

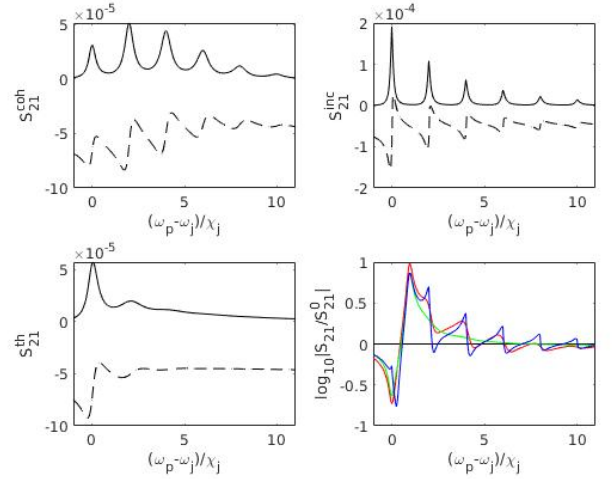


FIG. 8. Same as Fig.4 for $\bar{n} = 2$ for high quality factor. Parameters: $\omega_j = 2\pi$ 10GHz, $\omega_c = 2\pi$ 9GHz, $\chi_j = 2\pi$ 1MHz, $\gamma_c = 2\pi$ 100kHz, $\Gamma_j + 2\Gamma_{\phi,j} = 2\pi$ 250kHz.

In principle, a properly tuned interqubit coupling (e.g., due to mutual capacitance) can mitigate the effects of dispersion and optimize the signal-to-noise ratio and achieve the theoretical Heisenberg limit of sensitivity [39]. A rigorous analysis of this situation in a realistic experimental setup requires a special consideration.

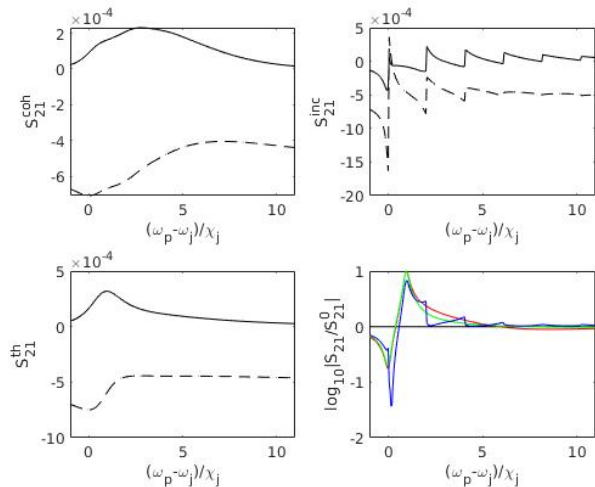


FIG. 9. Same as Fig.5 for $\bar{n} = 2$ in the limit of very low quality factor. Parameters: $\omega_j = 2\pi$ 10GHz, $\omega_c = 2\pi$ 9GHz, $\chi_j = 2\pi$ 1MHz, $\gamma_c = 2\pi$ 1MHz, $\Gamma_j + 2\Gamma_{\phi,j} = 2\pi$ 250kHz.

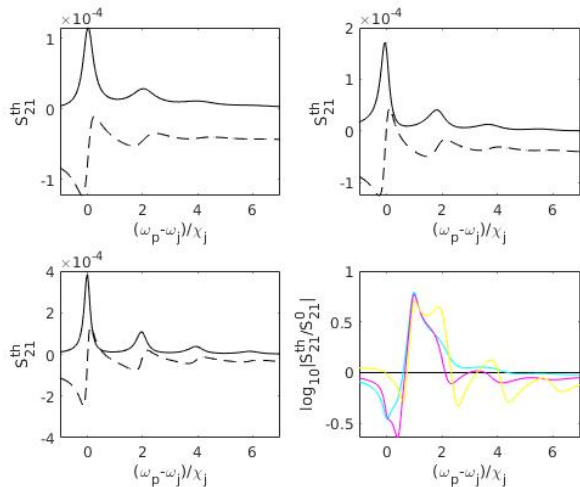


FIG. 10. Same as Fig.4 for three values of the coherence time $\tau_c = (10^{-12}, 10^{-9}, 10^{-8})\text{sec}/2\pi$ with their respective colors: cyan, magenta and yellow for the panel 4. Parameters: $\omega_j = 2\pi$ 10GHz, $\omega_c = 2\pi$ 9GHz, $\chi_j = 2\pi$ 1MHz, $\gamma_c = 2\pi$ 100kHz, $\Gamma_j + 2\Gamma_{\phi,j} = 2\pi$ 250kHz.

IV. CONCLUSIONS AND PERSPECTIVES

Using the consistent QED approach, we have developed a general formalism for treating the system of trans-

mon qubits in a waveguide cavity interacting with low-intensity electromagnetic field. In limiting cases, our results are in accordance with earlier calculations based on the phenomenological descriptions of the system. As an example, we have obtained solutions for non-interacting qubits in the presence of three realistic versions of the

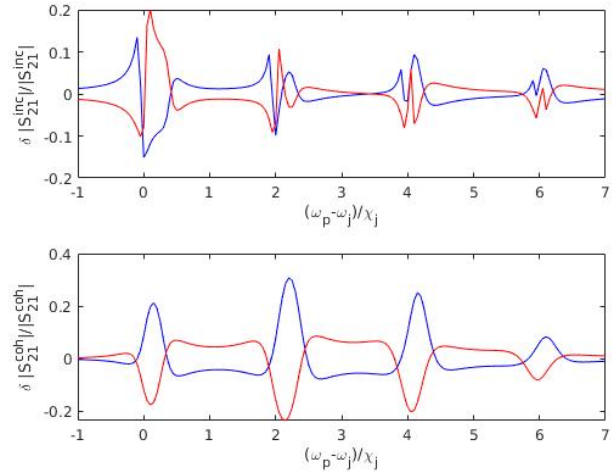


FIG. 11. Relative error for values of Fig.4 for the coherent case in panel 1 and incoherent case in panel 2 and two values of the detuning $\omega - \omega_c = -\gamma_c/3, \gamma_c/3$ corresponding to the blue and red curves respectively. Parameters: $\omega_j = 2\pi$ 10GHz, $\omega_c = 2\pi$ 9GHz, $\chi_j = 2\pi$ 1MHz, $\gamma_c = 2\pi$ 100kHz, $\Gamma_j + 2\Gamma_{\phi,j} = 2\pi$ 250kHz.

photon field: coherent, incoherent and thermal. Our approach is particularly relevant for the quantitative treatment of transmon-based detectors of microwave photons that requires an explicit expression for the transmission.

The formalism can be further applied to the more interesting case of strongly interacting qubits, which should achieve the over-SQL Heisenberg limit of sensitivity.

Acknowledgments: This work was performed in the framework of the EU project SUPERGALAX (Grant agreement ID: 863313). PN thanks Artur Sowa for his hospitality and fruitful discussions during his visit at the University of Saskatchewan.

[1] A. Blais, R.-S. Huang, A. Wallraff, S. M. Girvin, and R. J. Schoelkopf, Phys. Rev. A **69**, 062320 (2004).

[2] J. P. Pekola and B. Karimi, Phys. Rev. X **12**, 011026 (2022).

- [3] A. M. Zagoskin, *Quantum engineering: theory and design of quantum coherent structures* (Cambridge University Press, 2011).
- [4] L. D. Duffy and K. van Bibber, *New Journal of Physics* **11**, 105008 (2009).
- [5] C. Beck, *Physics of the Dark Universe* **7-8**, 6 (2015).
- [6] A. V. Dixit, S. Chakram, K. He, A. Agrawal, R. K. Naik, D. I. Schuster, and A. Chou, *Phys. Rev. Lett.* **126**, 141302 (2021).
- [7] H. Paik, D. I. Schuster, L. S. Bishop, G. Kirchmair, G. Catelani, A. P. Sears, B. R. Johnson, M. J. Reagor, L. Frunzio, L. I. Glazman, S. M. Girvin, M. H. Devoret, and R. J. Schoelkopf, *Phys. Rev. Lett.* **107**, 240501 (2011).
- [8] J. Koch, T. M. Yu, J. Gambetta, A. A. Houck, D. I. Schuster, J. Majer, A. Blais, M. H. Devoret, S. M. Girvin, and R. J. Schoelkopf, *Phys. Rev. A* **76**, 042319 (2007).
- [9] G. Wendin, *Reports on Progress in Physics* **80**, 106001 (2017).
- [10] A. Wallraff, D. I. Schuster, A. Blais, L. Frunzio, R.-S. Huang, J. Majer, S. Kumar, S. M. Girvin, and R. J. Schoelkopf, *Nature* **431**, 162 (2004).
- [11] E. Il'ichev, N. Oukhanski, A. Izmalkov, T. Wagner, M. Grajcar, H.-G. Meyer, A. Y. Smirnov, A. Maassen van den Brink, M. H. S. Amin, and A. M. Zagoskin, *Phys. Rev. Lett.* **91**, 097906 (2003).
- [12] I.-C. Hoi, C. M. Wilson, G. Johansson, J. Lindkvist, B. Peropadre, T. Palomaki, and P. Delsing, *New Journal of Physics* **15**, 025011 (2013).
- [13] J. D. Brehm, A. N. Poddubny, A. Stehli, T. Wolz, H. Rotzinger, and A. V. Ustinov, *npj Quantum Materials* **6** (2021), 10.1038/s41535-021-00310-z.
- [14] A. L. Rakhmanov, A. M. Zagoskin, S. Savel'ev, and F. Nori, *Physical Review B* **77**, 144507 (2008).
- [15] A. Zagoskin, A. Rakhmanov, S. Savel'ev, and F. Nori, *physica status solidi (b)* **246**, 955 (2009).
- [16] S. Savel'ev, A. Zagoskin, A. Rakhmanov, A. Omelyanchouk, Z. Washington, and F. Nori, *Physical Review A* **85**, 013811 (2012).
- [17] Z. Ivić, N. Lazarides, and G. Tsironis, *Scientific reports* **6**, 29374 (2016).
- [18] A. Asenjo-Garcia, M. Moreno-Cardoner, A. Albrecht, H. J. Kimble, and D. E. Chang, *Phys. Rev. X* **7**, 031024 (2017).
- [19] X. Gu, A. F. Kockum, A. Miranowicz, Y. xi Liu, and F. Nori, *Physics Reports* **718-719**, 1 (2017), microwave photonics with superconducting quantum circuits.
- [20] D. I. Schuster, A. A. Houck, J. A. Schreier, A. Wallraff, J. M. Gambetta, A. Blais, L. Frunzio, J. Majer, B. Johnson, M. H. Devoret, S. M. Girvin, and R. J. Schoelkopf, *Nature* **445**, 515 (2007).
- [21] K. Inomata, Z. Lin, K. Koshino, W. D. Oliver, J.-S. Tsai, T. Yamamoto, and Y. Nakamura, *Nature Communications* **7**, 12303 (2016).
- [22] G. S. Mazhorin, I. N. Moskalenko, I. S. Besedin, D. S. Shapiro, S. V. Remizov, W. V. Pogosov, D. O. Moskalev, A. A. Pishchimova, A. A. Dobronosova, I. A. Rodionov, and A. V. Ustinov, *Phys. Rev. A* **105**, 033519 (2022).
- [23] M. V. Fistul, O. Neyenhuys, A. B. Bocaz, M. Lisitskiy, and I. M. Eremin, *Phys. Rev. B* **105**, 104516 (2022).
- [24] A. M. Zagoskin, R. D. Wilson, M. Everitt, S. Savel'ev, D. R. Gulevich, J. Allen, V. K. Dubrovich, and E. Il'ichev, *Scientific Reports* **3** (2013), 10.1038/srep03464.
- [25] J. Gambetta, A. Blais, D. I. Schuster, A. Wallraff, L. Frunzio, J. Majer, M. H. Devoret, S. M. Girvin, and R. J. Schoelkopf, *Phys. Rev. A* **74**, 042318 (2006).
- [26] G. Romero, J. J. García-Ripoll, and E. Solano, *Phys. Rev. Lett.* **102**, 173602 (2009).
- [27] R. Lescanne, S. Deléglise, E. Albertinale, U. Réglade, T. Capelle, E. Ivanov, T. Jacqmin, Z. Leghtas, and E. Flurin, *Phys. Rev. X* **10**, 021038 (2020).
- [28] F. Helmer, M. Mariani, E. Solano, and F. Marquardt, *Phys. Rev. A* **79**, 052115 (2009).
- [29] B. Royer, A. L. Grimsmo, A. Choquette-Poitevin, and A. Blais, *Phys. Rev. Lett.* **120**, 203602 (2018).
- [30] B. R. Johnson, M. D. Reed, A. A. Houck, D. I. Schuster, L. S. Bishop, E. Ginossar, J. M. Gambetta, L. DiCarlo, L. Frunzio, S. M. Girvin, and R. J. Schoelkopf, *Nature Physics* **6**, 663 (2010).
- [31] D. M. Pozar, *Microwave engineering; 3rd ed.* (Wiley, Hoboken, NJ, 2005).
- [32] K. Watanabe, K. Yoshida, T. Aoki, and S. Kohjiro, *Japanese Journal of Applied Physics* **33**, 5708 (1994).
- [33] S. Gevorgian, L. Linner, and E. Kollberg, *IEEE Transactions on Microwave Theory and Techniques* **43**, 772 (1995).
- [34] M. Göppl, A. Fragner, M. Baur, R. Bianchetti, S. Filipp, J. M. Fink, P. J. Leek, G. Puebla, L. Steffen, and A. Wallraff, *Journal of Applied Physics* **104**, 113904 (2008), <https://doi.org/10.1063/1.3010859>.
- [35] J. Fink, M. Göppl, M. Baur, R. Bianchetti, P. Leek, A. Blais, and A. Wallraff, *Nature* **454**, 315 (2008).
- [36] C. W. Gardiner and P. Zoller, *Quantum Noise*, 2nd ed., edited by H. Haken (Springer, 2000).
- [37] K. Lalumière, B. C. Sanders, A. F. van Loo, A. Fedorov, A. Wallraff, and A. Blais, *Phys. Rev. A* **88**, 043806 (2013).
- [38] O. Astafiev, A. M. Zagoskin, A. A. Abdumalikov, Y. A. Pashkin, T. Yamamoto, K. Inomata, Y. Nakamura, and J. S. Tsai, *Science* **327**, 840 (2010).
- [39] P. Navez, A. G. Balanov, S. E. Savel'ev, and A. M. Zagoskin, *Phys. Rev. B* **103**, 064503 (2021).
- [40] L. H. Ryder, *Quantum Field Theory*, 2nd ed. (Cambridge University Press, 1996).
- [41] P. G. De Gennes, *Superconductivity of Metals and Alloys*, Advanced book classics (Perseus, Cambridge, MA, 1999).
- [42] C. Cohen-Tannoudji, B. Diu, and F. Laloë, *Quantum mechanics; 1st ed.* (Wiley, New York, NY, 1977) trans. of : Mécanique quantique. Paris : Hermann, 1973.
- [43] D. T. Pegg and S. M. Barnett, *Journal of Modern Optics* **44**, 225 (1997), <https://doi.org/10.1080/09500349708241868>.
- [44] L. Pitaevskii and S. Stringari, *Bose-Einstein condensation and superfluidity*, International Series of Monographs on Physics (OUP Oxford, 2016).
- [45] For a concrete calculation, we need to use the useful asymptotic expression $K(k) \sim \ln(4/\sqrt{1-k^2}) \simeq \ln(2) + \pi w_i/(2h_i)$.

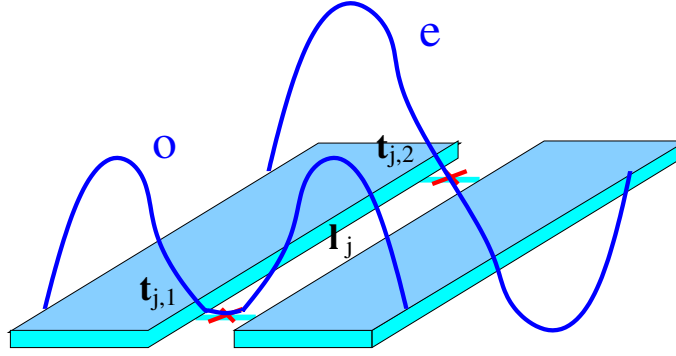


FIG. 12. Schematic representation of the ground (o) and excited (e) pair wavefunctions inside the transmon I_j . The red crosses represents the Josephson junctions placed at $\mathbf{t}_{j,1}$ and $\mathbf{t}_{j,2}$ respectively.

Appendix A: Quantum electrodynamics formulation

1. Quantum field Hamiltonian

Here we develop an effective Hamiltonian description of quantum dynamics of the electromagnetic field interacting with transmon qubits in a waveguide, improving on the earlier work [19].

Our goal is, starting from the full quantum electrodynamics (QED) of the system, to derive a reduced description valid at low temperatures and at low signal intensity, i.e., in the expected regime of its operation.

We consider the structure depicted in Fig.1 and assume for simplicity that its conducting parts are made of the same Type I, s-wave superconductor. At temperatures much less than the superconducting gap, the effects of quasiparticle excitations can be neglected ($k_B T \ll \Delta$). The superconductor can be described by the bosonic quantum spatiotemporal field $\hat{\psi}(\mathbf{r}, t)$ of Cooper pairs of charge $2e$ and mass m interacting with the vector potential $\hat{\mathbf{A}}(\mathbf{r}, t)$ of the quantized electromagnetic field in the Coulomb gauge $\nabla \cdot \hat{\mathbf{A}}(\mathbf{r}, t) = 0$. As point like particle, the Cooper pair gas must be seen as a whole in the bulk and not as having a momentum distribution but rather as condensed composite objects of electrons. Only their spatial distribution can change so that the field operator is written in terms of the electron operator $\hat{\psi}_{e,\sigma}(\mathbf{r}, t)$ with spin $\sigma = \uparrow, \downarrow$ as

$$\hat{\psi}(\mathbf{r}, t) = \int d^3 \mathbf{r}' F(\mathbf{r}') \hat{\psi}_{e,\uparrow}(\mathbf{r} + \mathbf{r}'/2, t) \hat{\psi}_{e,\downarrow}(\mathbf{r} - \mathbf{r}'/2, t), \quad (\text{A1})$$

where $F(\mathbf{r}')$ is the pairing function. We assume the nontrivial commutation relations [40]:

$$[\hat{\psi}(\mathbf{r}, t), \hat{\psi}^\dagger(\mathbf{r}', t)] = \delta^{(3)}(\mathbf{r} - \mathbf{r}'), \quad [\hat{A}^p(\mathbf{r}, t), \partial_t \hat{A}^q(\mathbf{r}', t)] = i \frac{\hbar}{\epsilon} \left(\delta_{p,q} - \frac{\nabla_{\mathbf{r}}^p \nabla_{\mathbf{r}'}^q}{(\nabla_{\mathbf{r}})^2} \right) \delta^{(3)}(\mathbf{r} - \mathbf{r}'), \quad (\text{A2})$$

with $p, q = r_x, r_y, r_z$ and where the inverse operator defines for any function $f(\mathbf{r})$ the nonlocal transformation: $(1/\nabla_{\mathbf{r}})^2 f(\mathbf{r}) = \int d^3 \mathbf{r}' (4\pi |\mathbf{r} - \mathbf{r}'|)^{-1} f(\mathbf{r}')$. The electric and magnetic fields are expressed through the vector potential in the standard way $\hat{\mathbf{E}}(\mathbf{r}, t) = -\partial_t \hat{\mathbf{A}}(\mathbf{r}, t)$ and $\hat{\mathbf{B}}(\mathbf{r}, t) = \nabla \times \hat{\mathbf{A}}(\mathbf{r}, t)$.

In this regime, we can write the low energy quantum Hamiltonian in terms of the time dependent operators as:

$$\begin{aligned} \hat{H} = & \int d^3 \mathbf{r} \frac{1}{2m} \left| \left(\frac{\hbar}{i} \nabla_{\mathbf{r}} - 2e \hat{\mathbf{A}}(\mathbf{r}, t) \right) \hat{\psi}(\mathbf{r}, t) \right|^2 + V_s(\mathbf{r}) |\hat{\psi}(\mathbf{r}, t)|^2 + \frac{1}{2} \int d^3 \mathbf{r}' \frac{(2e)^2 (|\hat{\psi}(\mathbf{r}', t)|^2 - n_s(\mathbf{r}')) (|\hat{\psi}(\mathbf{r}, t)|^2 - n_s(\mathbf{r}))}{4\pi \epsilon |\mathbf{r} - \mathbf{r}'|} \\ & + \frac{\epsilon}{2} \left[(\partial_t \hat{\mathbf{A}}(\mathbf{r}, t))^2 - c^2 \hat{\mathbf{A}}(\mathbf{r}, t) \cdot \nabla_{\mathbf{r}}^2 \hat{\mathbf{A}}(\mathbf{r}, t) \right]. \end{aligned} \quad (\text{A3})$$

The first term corresponds to the kinetic energy, the second is the lattice potential $V_s(\mathbf{r})$ which confines it inside the superconductors. It contains the contribution of the anomalous term due to pairing [41] and is assumed to be static and constant inside the superconductors and zero outside them. The third term describes the energy cost of local Cooper pair density exceeding the average local density of superconducting electrons, n_s . The fourth term is the energy of the transverse electromagnetic field energy. Replacing the operator by their expectation value $\langle \hat{\psi}(\mathbf{r}, t) \rangle$ and $\langle \hat{\mathbf{A}}(\mathbf{r}, t) \rangle$ in Eq.(A3), we recover a form analog to the Landau-Ginsburg Hamiltonian [41].

2. The dipole representation for the transmons

The transmons depicted in Fig.1 are a couple of superconducting islands with large mutual capacitance connected by two Josephson junctions which allows a control of the qubit frequency by a magnetic field. The superconductor volume in the circuit Ω is the sum of the waveguide volume Ω_0 and the transmon volumes Ω_j i.e. $\Omega = \Omega_0 + \sum_{j=1}^N \Omega_j$.

The transfer of charge at the junction creates an electric dipole that is sensitive to the electromagnetic field. In order to reflect this observation, the Hamiltonian is expressed in terms of polarisation operator $\hat{P}(\mathbf{r}, t)$ associated to each transmon. To this end, we use the Power-Zienau-Wolley transformation acting on each transmon [42]:

$$\hat{\psi}(\mathbf{r}, t) = \exp \left[i \frac{2e}{\hbar} \sum_{j=1}^N \xi_j(\mathbf{r}) \int_0^1 du \mathbf{r} \cdot \hat{\mathbf{A}}(\mathbf{l}_j + u(\mathbf{r} - \mathbf{l}_j), t) \right] \hat{\psi}'(\mathbf{r}, t), \quad (\text{A4})$$

where \mathbf{l}_j is the coordinate of the transmon j between the two Josephson junctions, see Fig.1, and the window function $\xi_j(\mathbf{r}) = 1$ for $\mathbf{r} \in \Omega_j$ and is zero otherwise. The expression (A4) takes into account of the phase accumulation within the transmon along the trajectory between the two junctions.

The new field $\hat{\psi}'(\mathbf{r}, t)$ no longer commutes with $\partial_t \hat{\mathbf{A}}(\mathbf{r}, t)$. We derive following commutation relation:

$$\begin{aligned} [\hat{\psi}'(\mathbf{r}, t), \partial_t \hat{\mathbf{A}}(\mathbf{r}'', t)] &= \left[\exp \left(-i \frac{2e}{\hbar} \sum_{j=1}^N \xi_j(\mathbf{r}) \int_0^1 du \mathbf{r} \cdot \hat{\mathbf{A}}(\mathbf{l}_j + u(\mathbf{r} - \mathbf{l}_j), t) \right) \hat{\psi}(\mathbf{r}, t), \partial_t \hat{\mathbf{A}}(\mathbf{r}'', t) \right] \\ &= \left[\exp \left(-i \frac{2e}{\hbar} \sum_{j=1}^N \xi_j(\mathbf{r}) \int_0^1 du \mathbf{r} \cdot \hat{\mathbf{A}}(\mathbf{l}_j + u(\mathbf{r} - \mathbf{l}_j), t) \right), \partial_t \hat{\mathbf{A}}(\mathbf{r}'', t) \right] \hat{\psi}(\mathbf{r}, t) \\ &= 2e \left(\mathbf{1} - \frac{\nabla_{\mathbf{r}''} \nabla_{\mathbf{r}''}}{(\nabla_{\mathbf{r}''})^2} \right) \sum_{j=1}^N \xi_j(\mathbf{r}) \mathbf{r} \int_0^1 du \delta^{(3)}(\mathbf{l}_j + u(\mathbf{r} - \mathbf{l}_j) - \mathbf{r}'') \\ &\quad \times \exp \left(-i \frac{2e}{\hbar} \sum_{j=1}^N \xi_j(\mathbf{r}) \int_0^1 du \mathbf{r} \cdot \hat{\mathbf{A}}(\mathbf{l}_j + u(\mathbf{r} - \mathbf{l}_j), t) \right) \hat{\psi}(\mathbf{r}, t) \\ &= \frac{2e}{\epsilon} \sum_{j=1}^N \xi_j(\mathbf{r}) \left(\mathbf{1} - \frac{\nabla_{\mathbf{r}''} \nabla_{\mathbf{r}''}}{(\nabla_{\mathbf{r}''})^2} \right) \mathbf{r} \int_0^1 du \delta^{(3)}(\mathbf{l}_j + u(\mathbf{r} - \mathbf{l}_j) - \mathbf{r}'') \hat{\psi}'(\mathbf{r}, t). \end{aligned} \quad (\text{A5})$$

In order to preserve the canonicity of the commutation relation for the creation/annihilation operators, we use the displacement current operator $\hat{\mathbf{D}}(\mathbf{r}, t)$ resulting from an unitary transformation on the vector potential time derivative. More explicitly, we define quantum constitutive relation: $\hat{\mathbf{D}}(\mathbf{r}, t) = -\epsilon \hat{\mathbf{A}}'(\mathbf{r}, t) = -\epsilon \partial_t \hat{\mathbf{A}}(\mathbf{r}, t) + \hat{\mathbf{P}}(\mathbf{r}, t)$ with the new vector potential such that $[\hat{\mathbf{A}}'(\mathbf{r}, t), \hat{\psi}'(\mathbf{r}, t)] = 0$. To satisfy this property, we use the transverse polarisation operator $\hat{\mathbf{P}}(\mathbf{r}, t)$ defined as:

$$\hat{\mathbf{P}}(\mathbf{r}, t) = \frac{2e}{\epsilon} \left(\mathbf{1} - \frac{\nabla_{\mathbf{r}} \nabla_{\mathbf{r}}}{(\nabla_{\mathbf{r}})^2} \right) \int d^3 \mathbf{r}' \sum_{j=1}^N \int_0^1 du \mathbf{r}' (|\hat{\psi}'(\mathbf{r}', t)|^2 - n_s(\mathbf{r}')) \delta^{(3)}(\mathbf{l}_j + u(\mathbf{r}' - \mathbf{l}_j) - \mathbf{r}) \quad (\text{A6})$$

$$[\hat{A}^p(\mathbf{r}, t), \hat{D}^q(\mathbf{r}', t)] = -i \hbar (\delta_{p,q} - \frac{\nabla_{\mathbf{r}}^p \nabla_{\mathbf{r}}^q}{(\nabla_{\mathbf{r}})^2}) \delta^{(3)}(\mathbf{r} - \mathbf{r}'). \quad (\text{A7})$$

This expression is written in terms of the charge distribution excess $2e (|\hat{\psi}'(\mathbf{r}', t)|^2 - n_s(\mathbf{r}'))$ for each transmon j which acts now as a electric dipole. Under this transformation, the new vector potential itself remains unchanged $\hat{\mathbf{A}}'(\mathbf{r}, t) = \hat{\mathbf{A}}(\mathbf{r}, t)$ but it is important to note the difference between its time derivative and its conjugate momentum.

$\partial_t \hat{\mathbf{A}}'(\mathbf{r}, t) \neq \hat{\mathbf{A}}'(\mathbf{r}, t)$. Applied to the Hamiltonian, this transformation will change the differential operator as:

$$\begin{aligned} & \left(\frac{\hbar}{i} \nabla_{\mathbf{r}} - 2e \hat{\mathbf{A}}(\mathbf{r}, t) \right)^2 \exp \left[i \frac{2e}{\hbar} \sum_{j=1}^N \xi_j(\mathbf{r}) \int_0^1 d\mathbf{u} \cdot \hat{\mathbf{A}}(\mathbf{l}_j + \mathbf{u}(\mathbf{r} - \mathbf{l}_j), t) \right] \hat{\psi}'(\mathbf{r}, t) = \\ & \exp \left[i \frac{2e}{\hbar} \sum_{j=1}^N \xi_j(\mathbf{r}) \int_0^1 d\mathbf{u} \cdot \hat{\mathbf{A}}(\mathbf{l}_j + \mathbf{u}(\mathbf{r} - \mathbf{l}_j), t) \right] \left(\frac{\hbar}{i} \nabla_{\mathbf{r}} - (2e) \sum_{j=1}^N \xi_j(\mathbf{r}) \int_0^1 d\mathbf{u} \hat{\mathbf{B}}(\mathbf{l}_j + \mathbf{u}(\mathbf{r} - \mathbf{l}_j), t) \times \mathbf{r} \right)^2 \hat{\psi}'(\mathbf{r}, t). \end{aligned} \quad (\text{A8})$$

Therefore, the Hamiltonian becomes:

$$\begin{aligned} \hat{H} = & \sum_{j=1}^N \int_{\Omega_j} d^3\mathbf{r} \frac{1}{2m} \left| \left(\frac{\hbar}{i} \nabla_{\mathbf{r}} - (2e) \int_0^1 d\mathbf{u} \hat{\mathbf{B}}(\mathbf{l}_j + \mathbf{u}(\mathbf{r} - \mathbf{l}_j), t) \times \mathbf{r} \right) \hat{\psi}'(\mathbf{r}, t) \right|^2 + \int_{\Omega_0} d^3\mathbf{r} \frac{1}{2m} \left| \left(\frac{\hbar}{i} \nabla_{\mathbf{r}} - (2e) \hat{\mathbf{A}}(\mathbf{r}, t) \right) \hat{\psi}'(\mathbf{r}, t) \right|^2 \\ & + \int_{\Omega_0} d^3\mathbf{r} V_s(\mathbf{r}) |\hat{\psi}'(\mathbf{r}, t)|^2 + \frac{1}{2} \int d^3\mathbf{r}' \frac{(2e)^2 (|\hat{\psi}'(\mathbf{r}', t)|^2 - n_s(\mathbf{r}')) (|\hat{\psi}'(\mathbf{r}, t)|^2 - n_s(\mathbf{r}))}{4\pi\epsilon|\mathbf{r} - \mathbf{r}'|} + \frac{\epsilon}{2} \left(\hat{\mathbf{A}}'(\mathbf{r}, t) - \frac{\hat{\mathbf{P}}(\mathbf{r}, t)}{\epsilon} \right)^2. \end{aligned} \quad (\text{A9})$$

The effect of the magnetic field can be neglected inside a superconductor due to the Meissner effect so that the vector potential is zero in the bulk of a superconductor.

Appendix B: The transmon quantum state description

1. The angular momentum representation

The quantum description of the transmon in terms of the flux charge variables at the Josephson junctions, starting from the consistent QED picture. Very often in literature, any quantum approach is developed by replacing phenomenologically these classical variables into canonically conjugated quantum operators. On the contrary in this section, we develop a consistent framework based on a fundamental quantum field theory from which we deduce flux charge operators, that are subsequently approximated as real variables in the classical limit.

In addition, as we shall see, the phase operator can be only defined formally as a discrete variables over the interval $[0, 2\pi)$. The continuum limit appears usually not well defined unless we artificially prolongate their domain beyond this interval to the whole set of real number [43].

We approximate the quantum field operator of the Cooper pair $\hat{\psi}(\mathbf{r}, t)$ considering only the two lowest-energy modes when describing the dynamics of the junctions in Fig.12. It allows a consistent description of a transmon using the angular momentum representation, that is transformed afterwards, into the approximate flux charge representation for the purpose of a qubit description.

Let us consider the case in the absence of the transverse electromagnetic field. Since every transmon subsystem is electrically neutral, we neglect the dipolar and multipolar Coulomb interaction between them and with the elements of the waveguide so that each transmon j is described by the one-mode approximation. Here the wave function $\psi_{j,\alpha}(\mathbf{r})$ describing the state with $N_{s,j}$ of pairs is a solution of the mean-field Hartree equation (or Gross-Pitaevskii equation [44]):

$$\left[-\frac{\hbar^2}{2m} \nabla_{\mathbf{r}}^2 + V_s(\mathbf{r}) + \int_{\Omega_j} d^3\mathbf{r}' \frac{(2e)^2 (|\psi_{j,\alpha}(\mathbf{r}')|^2 N_{s,j} - n_s(\mathbf{r}'))}{4\pi\epsilon|\mathbf{r} - \mathbf{r}'|} \right] \psi_{j,\alpha}(\mathbf{r}) = \mu_{j,\alpha}(N_{s,j}) \psi_{j,\alpha}(\mathbf{r}). \quad (\text{B1})$$

Here $j = 0, \dots, N$ labels the wave functions for each part of the system (waveguide and transmons), $\alpha = o, e$ labels the ground and excited states respectively and $\mu_{j,\alpha}(N_{s,j})$ is the corresponding chemical potential. The Hartree energy is obtained from the relation $dE_{j,\alpha}(N_{s,j})/dN_{s,j} = \mu_{j,\alpha}(N_{s,j})$. The total ground state energy is the sum of ground state energies $E_0 = \sum_{j=0}^N E_{j,o}(N_{s,j})$.

The wave function of the first excited state $\alpha = e$ has a single node changing sign at the Josephson junction, as illustrated in Fig.(12). Neglecting the influence of higher energy excited state, we can write approximately the quantum field operator as:

$$\hat{\psi}'(\mathbf{r}, t) \simeq \psi_0(\mathbf{r}) \hat{c}_0(t) + \sum_{j=1}^N \psi_{j,o}(\mathbf{r}) \hat{c}_{j,o}(t) + \psi_{j,e}(\mathbf{r}) \hat{c}_{j,e}(t). \quad (\text{B2})$$

Here $\int_{\Omega_j} d^3\mathbf{r} \psi_{j\alpha}^*(\mathbf{r})\psi_{j\alpha}(\mathbf{r}) = \delta_{\alpha\alpha'}$, $\xi_j(\mathbf{r})\psi_{j'\alpha}(\mathbf{r}) = \delta_{j,j'}\psi_{j\alpha}(\mathbf{r})$ and $\hat{c}_{j\alpha}$ is the annihilation operator. In other words, in the absence of external electromagnetic field, the general quantum state is a combination of the Fock states of the form $|\Psi\rangle = (\hat{c}_0^\dagger)^{N_{s,0}}/\sqrt{N_{s,0}!} \prod_{j=1}^N (\hat{c}_j^\dagger)^{N_{s,j,o}} (\hat{c}_{j\alpha}^\dagger)^{N_{s,j,e}} |0\rangle/\sqrt{N_{s,j,o}!N_{s,j,e}!}$ with the particle number constraint: $N_{s,j,e} + N_{s,j,o} = N_{s,j}$.

The energy difference between the excited and the ground state is Josephson energy $E_{J,j}(N_{s,j}) = E_{j,e}(N_{s,j}) - E_{j,o}(N_{s,j})$. Assuming for simplicity that the two island parts of the transmon are perfectly symmetric, we can define their localized states:

$$\psi_{j\pm}(\mathbf{r}) = \frac{\psi_{j,o}(\mathbf{r}) \pm \psi_{j,e}(\mathbf{r})}{\sqrt{2}}, \quad \hat{c}_{j\pm}(t) = \frac{\hat{c}_{j,o}(t) \pm \hat{c}_{j,e}(t)}{\sqrt{2}}. \quad (\text{B3})$$

With a good accuracy, we can consider these as orthonormal (wave functions almost do not overlap much each other) so that we satisfy the commutation relation $[\hat{c}_{j\pm}, \hat{c}_{j'\pm}^\dagger] = \delta_{j,j'}\delta_{\pm,\pm}$. Also, since the superconducting waveguide part is large and electrically neutral, the Cooper pair mode can be described by a coherent state and we can replace its quantum operators description with a c-number: $\hat{c}_0(t) \simeq \sqrt{N_{s,0}}$.

Therefore, the quantum field is rewritten as:

$$\hat{\psi}'(\mathbf{r}, t) \simeq \sqrt{N_{s,0}}\psi_0(\mathbf{r}) + \sum_{j=1}^N \sum_{\pm} \psi_{j,\pm}(\mathbf{r})\hat{c}_{j,\pm}(t). \quad (\text{B4})$$

As the wave functions of two different transmons do not overlap $\psi_{j,\pm}(\mathbf{r})\psi_{j',\pm}(\mathbf{r}) \simeq 0$ for $j \neq j'$, the density operator becomes:

$$|\hat{\psi}'(\mathbf{r}, t)|^2 = N_{s,0}|\psi_0(\mathbf{r})|^2 + \sum_{j=1}^N (|\psi_{j,+}(\mathbf{r})|^2 + |\psi_{j,-}(\mathbf{r})|^2)\hat{n}_j(t) + (|\psi_{j,+}(\mathbf{r})|^2 - |\psi_{j,-}(\mathbf{r})|^2)\hat{m}_j^z(t) + \sum_{\pm} \psi_{j,\pm}^*(\mathbf{r})\psi_{j,\mp}(\mathbf{r})\hat{m}_j^{\pm}(t) \quad (\text{B5})$$

$$\hat{n}_j(t) = \frac{\hat{c}_{j,+}^\dagger(t)\hat{c}_{j,+}(t) + \hat{c}_{j,-}^\dagger(t)\hat{c}_{j,-}(t)}{2}, \quad \hat{m}_j^z(t) = \frac{\hat{c}_{j,+}^\dagger(t)\hat{c}_{j,+}(t) - \hat{c}_{j,-}^\dagger(t)\hat{c}_{j,-}(t)}{2}, \quad \hat{m}_j^{\pm}(t) = \hat{c}_{j,\pm}^\dagger(t)\hat{c}_{j,\mp}(t), \quad (\text{B6})$$

where the operators $\hat{m}_j^z(t)$ and $\hat{m}_j^{\pm}(t)$ are subject to the algebra of the angular momentum operator and $\hat{n}_j(t)$ is the particle number operator for the transmon j . Indeed, $[\hat{m}_j^+, \hat{m}_j^-] = \hat{m}_j^z$, $[\hat{m}_j^z, \hat{m}_j^{\pm}] = \pm 2\hat{m}_j^{\pm}$. Similarly for the kinetic term, we obtain:

$$|\nabla\hat{\psi}'(\mathbf{r}, t)|^2 = N_0|\nabla\psi_0(\mathbf{r})|^2 + \sum_{j=1}^N (|\nabla\psi_{j,+}(\mathbf{r})|^2 + |\nabla\psi_{j,-}(\mathbf{r})|^2)\hat{n}_j(t) + (|\nabla\psi_{j,+}(\mathbf{r})|^2 - |\nabla\psi_{j,-}(\mathbf{r})|^2)\hat{m}_j^z(t) + \sum_{\pm} \nabla\psi_{j,\pm}(\mathbf{r})\nabla\psi_{j,\mp}(\mathbf{r})\hat{m}_j^{\pm}(t). \quad (\text{B7})$$

We substitute the expressions Eq.(B5) and Eq.(B7) into the Hamiltonian (A9), and apply the following simplifications:

1. In (A9), the magnetic field coupling term is neglected over the linear electric field coupling term $\hat{\mathbf{A}}(\mathbf{r}, t)$ with the polarisation term.
2. For a small intensity of the waveguide field, the quadratic term in the transverse polarisation term is neglected.
3. We chose eigenstates of \hat{n}_j with $N_{s,j}$ particles, approximating $|\psi_{j,+}(\mathbf{r})|^2 + |\psi_{j,-}(\mathbf{r})|^2 \simeq |\psi_j(\mathbf{r})|^2$
4. We use the Eq.(B1) to express the matrix element in terms of eigenenergies
5. We neglect the product term $\hat{m}_j^z(t)\hat{m}_{j'}^{\pm}(t)$ and $\hat{m}_j^{\pm}(t)\hat{m}_{j'}^{\pm}(t)$ in the Coulomb term as the overlapping integral over \mathbf{r} and \mathbf{r}' is very small.

As a result, the expressions (A9) becomes:

$$\begin{aligned}
\hat{H} = & E_0 + \sum_{j=1}^N \frac{E_{j,J}(N_{s,j})}{2} - \frac{\mu_{j,e}(N_{s,j}) - \mu_{j,o}(N_{s,j})}{2} (\hat{m}_j^-(t) + c.c.) \\
& + \frac{1}{2} \int d^3\mathbf{r}' \frac{(2e)^2 \sum_{j,j'=1}^N (|\psi_{j,+}(\mathbf{r})|^2 - |\psi_{j,-}(\mathbf{r})|^2) \hat{m}_j^z(t) (|\psi_{j',+}(\mathbf{r}')|^2 - |\psi_{j',-}(\mathbf{r}')|^2) \hat{m}_{j'}^z(t)}{4\pi\epsilon|\mathbf{r}-\mathbf{r}'|} \\
& + \frac{\epsilon}{2} \left[\hat{\mathbf{A}}^2(\mathbf{r}, t) - c^2 \hat{\mathbf{A}}(\mathbf{r}, t) \cdot \nabla_{\mathbf{r}}^2 \hat{\mathbf{A}}(\mathbf{r}, t) + \frac{N_{s,0} |(2e)\psi_0(\mathbf{r})|^2}{2\epsilon m} \hat{\mathbf{A}}^2(\mathbf{r}, t) \right] \\
& - \sum_{j=1}^N \int_0^1 du \int d^3\mathbf{r} \hat{\mathbf{A}}(\mathbf{l}_j + u(\mathbf{r} - \mathbf{l}_j), t) \cdot \mathbf{r} (2e) (|\psi_{j,+}(\mathbf{r})|^2 - |\psi_{j,-}(\mathbf{r})|^2) \hat{m}_j^z(t), \tag{B8}
\end{aligned}$$

where now we omit the prime in the time derivative of the vector potential. Assuming a linear dependence for the energy difference, we can further approximate: $\mu_{j,e}(N_{s,j}) - \mu_{j,o}(N_{s,j}) = dE_{j,J}(N_{s,j})/dN_{s,j} \cong E_{j,J}(N_{s,j})/N_{s,j}$.

2. The presence of the external uniform magnetic field

In the presence of a uniform magnetic field \mathbf{B}_0 , the vector potential contains in addition to the time-dependent waveguide field the classical component:

$$\hat{\mathbf{A}}(\mathbf{r}, t) \rightarrow \hat{\mathbf{A}}(\mathbf{r}, t) + \mathbf{A}_0(\mathbf{r}). \tag{B9}$$

Therefore, we add a phase $\theta_{j,\pm}(\mathbf{r})$ so that the quantum field parametrisation is modified into:

$$\hat{\psi}'(\mathbf{r}, t) \simeq \sqrt{N_{s,0}} \psi_0(\mathbf{r}) + \sum_{j=1}^N \sum_{\pm} \psi_{j,\pm}(\mathbf{r}) e^{i\theta_{j,\pm}(\mathbf{r})} \hat{c}_{j,\pm}(t). \tag{B10}$$

Substituting these expressions into Eq.(A9) and minimizing the energy, we obtain the London equation $\nabla_{\mathbf{r}}^2 \mathbf{A}_0(\mathbf{r}) = \frac{(2e)^2 n_s(\mathbf{r})}{\epsilon c^2 m} \mathbf{A}_0(\mathbf{r})$ where the Cooper pair density is approximated as $n_s(\mathbf{r}) \cong \sum_{j=0}^N N_{s,j} |\psi_{j,o}(\mathbf{r})|^2$. The solution of the latter is such that the asymptotic expression is $\frac{1}{2}(\mathbf{B}_0 \times \mathbf{r})$ and implies that surface current appears to avoid the magnetic field to penetrate the bulk. Therefore one deduces the phases $\theta_{j,\pm}(\mathbf{r}) = \int_{C_{j,\pm}} d\mathbf{r}' \cdot \mathbf{A}_0(\mathbf{r}')$ along a contour $C_{j,\pm}$ on the surface of the conducting islands starting from one junction located in Fig.12 at $\mathbf{t}_{j,1}$ and finishing at $\mathbf{r} \rightarrow \mathbf{t}_{j,2}$ so that it encloses the transmon loop at the other junction located at $\mathbf{t}_{j,2}$. Since the boundary condition imposes a zero normal component on the surface, the phases are independent on the choice of the contour path. We deduce the relation to the total flux crossing the transmon loop as $\Phi_{B_0} = \oint d\mathbf{S} \cdot \mathbf{B}_0 = \theta_{j,+}(\mathbf{t}_{j,2}) - \theta_{j,-}(\mathbf{t}_{j,2})$. As a result, the presence of the field changes the Hamiltonian into:

$$\sum_{j=1}^N \frac{E_{J_1,j}(N_{j,s}) + E_{J_2,j}(N_{j,s}) \exp(i2e\Phi_{B_0}/\hbar)}{2N_{j,s}} \hat{m}_j^+(t) + c.c. = \sum_{j=1}^N \frac{E_{J,j}(N_{j,s}, B_0)}{2N_{j,s}} \left[e^{i\varphi_j(N_{j,s}, B_0)} \hat{m}_j^+(t) + c.c. \right], \tag{B11}$$

where the reparametrization with the effective Josephson energy $E_{J,j}(B_0)$ and the phase $\varphi_j(N_{s,j}, B_0)$ is found in [8]. In what follows, the phase will be reabsorbed in the raising-lowering operators: $\hat{m}_j^{\pm}(t)$. Finally:

$$\begin{aligned}
\hat{H} = & E_0 + \sum_{j=1}^N \frac{E_{J,j}(N_{s,j})}{2} (2 - \hat{m}_j^-(t) - \hat{m}_j^+(t)) \\
& + \frac{1}{2} \int d^3\mathbf{r}' \frac{(2e)^2 (\sum_{j,j'=1}^N (|\psi_{j,+}(\mathbf{r})|^2 - |\psi_{j,-}(\mathbf{r})|^2) \hat{m}_j^z(t) (|\psi_{j',+}(\mathbf{r}')|^2 - |\psi_{j',-}(\mathbf{r}')|^2) \hat{m}_{j'}^z(t)}{4\pi\epsilon|\mathbf{r}-\mathbf{r}'|} \\
& + \frac{\epsilon}{2} \left[\hat{\mathbf{A}}^2(\mathbf{r}, t) - c^2 \hat{\mathbf{A}}(\mathbf{r}, t) \cdot \nabla_{\mathbf{r}}^2 \hat{\mathbf{A}}(\mathbf{r}, t) + \frac{N_{s,0} |(2e)\psi_0(\mathbf{r})|^2}{2\epsilon m} \hat{\mathbf{A}}^2(\mathbf{r}, t) \right] \\
& - \sum_{j=1}^N \int_0^1 du \int d^3\mathbf{r} \hat{\mathbf{A}}(\mathbf{l}_j + u(\mathbf{r} - \mathbf{l}_j), t) \cdot \mathbf{r} (2e) (|\psi_{j,+}(\mathbf{r})|^2 - |\psi_{j,-}(\mathbf{r})|^2) \hat{m}_j^z(t). \tag{B12}
\end{aligned}$$

3. Phase and charge basis formalism: charge qubit

We define the charge operator as: $\hat{q}_j(t) = (2e)\hat{m}_j^z(t)$ with the quantum numbers limited to integer value $m_j^z = -M, -M+1, \dots, M-1, M$. We define the phase basis through

$$|\phi_j\rangle \equiv |\tilde{m}_j\rangle = \sum_{m_j=-M}^M \frac{e^{im_j\phi_j}}{\sqrt{2M+1}} |m_j\rangle, \quad \phi_j = 2\pi\tilde{m}_j/(2M+1), \quad \tilde{m}_j = 0, \dots, 2M \quad (\text{B13})$$

$$|m_j\rangle = \frac{1}{\sqrt{2M+1}} \sum_{\tilde{m}_j=0}^{2M+1} e^{-i\frac{2\pi m_j \tilde{m}_j}{2M+1}} |\tilde{m}_j\rangle. \quad (\text{B14})$$

In this restricted set, we shall assume also the basis are defined modulo $2M+1$, i.e. $|m_j+2M+1\rangle_j = |m_j\rangle_j$ and $|\tilde{m}_j+2M+1\rangle_j = |\tilde{m}_j\rangle_j$. This assumption may not be correct especially for M not large. Nevertheless, once we achieve the limit $M \rightarrow \infty$ through this procedure, the phase operator goes from a set of discrete variables to a continuous one over the range $[0, 2\pi)$. From the above definition, we find:

$$\sum_{m_j=-M}^M |m_j+1\rangle\langle m_j| = \sum_{\tilde{m}_j=0}^{2M} e^{-i\phi_j} \frac{|\tilde{m}_j\rangle_j\langle\tilde{m}_j|}{2M+1} \stackrel{M \rightarrow \infty}{=} \int_0^{2\pi} \frac{d\phi_j}{2\pi} e^{-i\phi_j} |\phi_j\rangle\langle\phi_j| = e^{-i\hat{\phi}_j} \quad (\text{B15})$$

$$\hat{m}_j^s = \sum_{m_j=-M}^M m_j^s |m_j\rangle\langle m_j| = \sum_{\tilde{m}_j=0}^{2M} \sum_{\tilde{m}_j=0}^{2M} (-i\partial_{\phi_j'})^s \frac{\sin[(2M+1)(\phi_j - \phi_j')]}{\sin(\phi_j - \phi_j')} \frac{|\tilde{m}_j\rangle\langle\tilde{m}_j|}{2M+1} \quad (\text{B16})$$

$$\stackrel{M \rightarrow \infty}{=} \int_0^{2\pi} \frac{d\phi_j}{2\pi} (-i\partial_{\phi_j})^s |\phi_j\rangle\langle\phi_j| = \hat{\phi}_j^s. \quad (\text{B17})$$

In the new basis, $[e^{-i\hat{\phi}_j}, \hat{m}_j] = e^{-i\hat{\phi}_j}$ from which it follows that $[\hat{\phi}_j, \hat{m}_{j'}] = i\delta_{j,j'}$. Using the flux $\hat{\Phi}_j = (2e)\hat{\phi}_j/\hbar$ and charge variable, we rewrite it as $[\hat{\Phi}_j, \hat{q}_{j'}] = i\hbar\delta_{j,j'}$. The creation operator is approximated for large $M = N_{s,j}/2$ as:

$$\hat{m}_j^\pm = \sum_{m_j=-M}^M \sqrt{M(M+1) - m_j(m_j \pm 1)} |m_j \pm 1\rangle\langle m_j| \cong \frac{N_{s,j}}{2} e^{\mp i\hat{\phi}_j}. \quad (\text{B18})$$

In the language of these variables, the Hamiltonian (B12) becomes:

$$\begin{aligned} \hat{H} = & E_0 + \sum_{j=1}^N E_{J,j} \left[1 - \cos\left(\frac{2e}{\hbar}\hat{\Phi}_j(t)\right) \right] + \frac{1}{2} \sum_{j,j'=1}^N C_{j,j'}^{-1} \hat{q}_j(t)\hat{q}_{j'}(t) \\ & + \frac{\epsilon}{2} \left[\hat{\mathbf{A}}^2(\mathbf{r}, t) - c^2 \hat{\mathbf{A}}(\mathbf{r}, t) \cdot \nabla_{\mathbf{r}}^2 \hat{\mathbf{A}}(\mathbf{r}, t) + \frac{N_0 |(2e)\psi_0(\mathbf{r})|^2}{2\epsilon m} \hat{\mathbf{A}}^2(\mathbf{r}, t) \right] \\ & - \sum_{j=1}^N \int_0^1 du \int d^3\mathbf{r} \hat{\mathbf{A}}(\mathbf{l}_j + u(\mathbf{r} - \mathbf{l}_j), t) \cdot \mathbf{r} (|\psi_{j,+}(\mathbf{r})|^2 - |\psi_{j,-}(\mathbf{r})|^2) \hat{q}_j(t), \end{aligned} \quad (\text{B19})$$

where we define the capacitance:

$$C_{j,j'}^{-1} = \frac{1}{2} \int d^3\mathbf{r}' \frac{(\sum_{j,j'=1}^N (|\psi_{j,+}(\mathbf{r})|^2 - |\psi_{j,-}(\mathbf{r})|^2)(|\psi_{j',+}(\mathbf{r}')|^2 - |\psi_{j',-}(\mathbf{r}')|^2))}{4\pi\epsilon|\mathbf{r} - \mathbf{r}'|}, \quad (\text{B20})$$

where $E_{J,j}$ is the Josephson energy.

Appendix C: Quantum description of the electromagnetic field in the waveguide

1. General treatment for a waveguide in vacuum

In this section, we revisit the usual approach for the waveguide description in order to consistently account for quantum effects. The main results are as follows: 1) The capacitance which characterizes the electromagnetic wave propagation, differs from the static capacitance in presence of dielectric materials; 2) Explicit formulas for the speed

propagation v and impedance Z in a coplanar waveguide; 3) A formula for the coupling factor f_j between the electromagnetic field and transmon.

Consider a quantum electromagnetic field propagating along the superconducting wire axis of a constant cross section depicted in Fig.13. The property of translational invariance along the z axis is required for a good quality waveguide that does not emit radiation outside the device to eliminate the stray radiation. Due to experimental constraints, it is not generally strictly valid since the waveguide has a curved geometry. Therefore, using Eq.(B19), the Heisenberg equations for the vector potential field correspond to the quantum Ampere equations:

$$(c^2\partial_t^2 - \nabla_{\mathbf{r}}^2)\hat{\mathbf{A}}(\mathbf{r}, t) = \mu\hat{\mathbf{j}}_{\perp}(\mathbf{r}, t) \cong -\frac{N_{s,0}|(2e)\psi_0(\mathbf{r})|^2}{\epsilon c^2 m}\hat{\mathbf{A}}(\mathbf{r}, t) \cong \begin{cases} -\frac{n_s(2e)^2}{\epsilon c^2 m}\hat{\mathbf{A}}(\mathbf{r}, t) & \text{conductors} \\ 0 & \text{insulators} \end{cases}, \quad (\text{C1})$$

where n_s is Cooper pair density. The right hand side corresponds to a renormalized transverse current responsible for the dynamical Meissner effect.

We restrict our analysis to the only relevant TEM mode of the electromagnetic field. Then the vector potential operator can be approximated by $\hat{\mathbf{A}}(\mathbf{r}, t) = \hat{\alpha}(r_z, t)\mathbf{A}_{\perp}(\mathbf{r}_{\perp})$ where $\hat{\alpha}(r_z, t)$ is the quantum operator describing the electromagnetic propagation along the z axis and $\mathbf{A}_{\perp}(\mathbf{r}_{\perp}) = (A_{\perp}^x(\mathbf{r}_{\perp}), A_{\perp}^y(\mathbf{r}_{\perp}), 0)$ is a classical transverse vector field dependent only on the transverse coordinates $\mathbf{r}_{\perp} = (r_x, r_y, 0)$.

In the simplest configuration of two parallel plates at $(\pm D/2, r_y, r_z)$, for a plane wave $\langle \hat{\alpha}(r_z, t) \rangle \sim \exp[i(k_z r_z - \omega t)]$, the solution is a constant for A_{\perp}^z normal the conductor and zero otherwise. Note the absence of a parallel component inside the bulk with the London penetration length $\lambda_s = \sqrt{\epsilon c^2 m / (n_s (2e)^2)}$. As consequence a net electrical charge appears at the surface to compensate the discontinuity of the vector potential. This surface charge distribution has normally its own dynamics associated the plasma frequency $\omega_{pl} = c/\lambda_s$. Since generally the penetration depth $\lambda_s \ll 1/k$ for the wavelengths which we are concerned with (microwave), the surface charge responds instantaneously to the field and we can consider the limit $\lambda_s \rightarrow 0$ in the Ampere equation, so that the z component of the vector potential cancels out. It corresponds to neglecting the influence of the kinetic inductance due to current compared to the geometric (magnetic inductance) [34].

In the London gauge ($\nabla \cdot \hat{\mathbf{A}}(\mathbf{r}, t) = 0$), Eq.(C1) is transformed into a two-dimensional problem for the transverse electromagnetic component:

$$\nabla_{\perp}^2 \mathbf{A}_{\perp}(\mathbf{r}_{\perp}) = 0, \quad \mathbf{n} \times \mathbf{A}_{\perp} = 0 \text{ at the surface boundary}, \quad \nabla_{\perp} \cdot \mathbf{A}_{\perp}(\mathbf{r}_{\perp}) = 0, \quad (\text{C2})$$

where $\mathbf{n} = (n_x, n_y, 0)$ is the normal unit vector at the boundary and is pointing from the signal to the ground part of the waveguide. The transverse components are normalized such that $\int d^2\mathbf{r}_{\perp} \mathbf{A}_{\perp}^2(\mathbf{r}_{\perp}) = 1/\epsilon$. It is then possible to define a scalar potential $\mathbf{A}_{\perp} = \nabla_{\perp} \chi(\mathbf{r}_{\perp})$ so the problem reduces to the Laplace equation:

$$\nabla_{\perp}^2 \chi(\mathbf{r}_{\perp}) = 0, \quad \chi(\mathbf{r}_{\perp}) = \chi_s \text{ at signal wire}, \quad \chi(\mathbf{r}_{\perp}) = 0 \text{ at ground wire}. \quad (\text{C3})$$

These boundary conditions define the gauge of the vector potential and tells that the potential is set to χ_s at the z -axis ($r_x = 0$ and $r_y = 0$). The substitution of this approximated expression into the commutation relation and the integration over the transverse coordinate produce the non trivial commutation relation:

$$[\hat{\alpha}(r_z, t), \hat{\alpha}(r'_z, t)] = i\hbar\delta(r_z - r'_z). \quad (\text{C4})$$

Note again that in general $\hat{\alpha}(r_z, t) \neq \partial_t \hat{\alpha}(r_z, t)$.

2. Quantum circuit formulation of the waveguide

We assume a generic waveguide represented under the form of in Fig.13. In order to express the electromagnetic field in terms of the electrical circuit notations, we define the operator potential difference between the signal wire 1 and ground wire 2 as:

$$\hat{V}(r_z, t) = -\int_2^1 d\mathbf{r}'_{\perp} \cdot \hat{\mathbf{E}}(\mathbf{r}, t) = \int_2^1 d\mathbf{r}_{\perp} \cdot \mathbf{A}_{\perp}(\mathbf{r}_{\perp}) \hat{\alpha}(r_z, t) = \chi_s \hat{\alpha}(r_z, t). \quad (\text{C5})$$

According to this definition, the potential is the same everywhere at any point of the conducting surface since the vector potential is parallel to the normal vector. By extension, we also determine as shown in Fig.13 the equipotential in green and the force line in red between the two lines.

For each normal vector \mathbf{n} , we define the infinitesimal element $d\mathbf{s} = dr_s \mathbf{n}$ where $dr_s = n_x dr_y - n_y dr_x$ which is the variation along the equipotential in the xy plane. On an infinitesimal section of size dr_z , the Gauss theorem defines an effective line charge that encloses the signal wire at the surface given by $d\hat{Q}(r_z, t) = \epsilon \oint d\mathbf{s} \cdot \hat{\mathbf{E}}(\mathbf{r}, t) dr_z =$

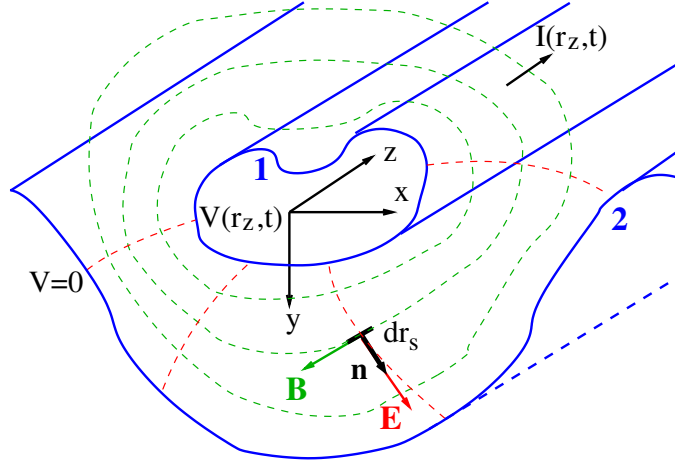


FIG. 13. Schematic representation of a linear waveguide with signal line (1) and ground line (2) with red electric field line and green magnetic line conformal to each other.

$-\epsilon \oint ds \cdot \mathbf{A}_\perp(\mathbf{r}_\perp) \hat{\alpha}(r_z, t) dr_z$ and opposite to the ground wire line charge. Using these definitions, we define the differential capacitance dC for this charge element as the proportionality factor between the operator of electric charge on the section of the waveguide and the local voltage operator $d\hat{Q}(r_z, t) = dC \hat{V}(r_z, t)$. Eliminating the operator $\hat{\alpha}(r_z, t)$ in the two expressions, we find explicitly:

$$dC = -\frac{\epsilon \oint ds \cdot \mathbf{A}_\perp(\mathbf{r}_\perp)}{\chi_s} dr_z, \quad (\text{C6})$$

which depends only on the waveguide geometry.

The current along the wires is related to the magnetic field according to the Ampere law Eq.(C1) expressed in a circulation integral form along a green line over the transverse plane so that the electric field does not contribute:

$$\hat{I}(r_z, t) = \frac{1}{\mu_0} \oint ds \cdot \nabla \times (\mathbf{A}_\perp(\mathbf{r}_\perp) \hat{\alpha}(r_z, t)) = \frac{1}{\mu_0} \oint ds \cdot \mathbf{A}_\perp(\mathbf{r}_\perp) \partial_{r_z} \hat{\alpha}(r_z, t). \quad (\text{C7})$$

The magnetic flux operator in this section is defined along a trajectory between the two wires (1 and 2) as:

$$d\hat{\Phi}_B(r_z, t) = \int_1^2 d\mathbf{r}_\perp \cdot \hat{\mathbf{B}}(\mathbf{r}, t) dr_z = \int_1^2 d\mathbf{r}_\perp \cdot \nabla \times \hat{\mathbf{A}}(\mathbf{r}, t) dr_z = \int_1^2 d\mathbf{r}_\perp \cdot \mathbf{A}_\perp(\mathbf{r}_\perp) \partial_{r_z} \hat{\alpha}(r_z, t) dr_z. \quad (\text{C8})$$

Integrating along r_z , the total flux is $\hat{\Phi}_B(r_z, t) = \int_1^2 d\mathbf{r}_\perp \cdot \mathbf{A}_\perp(\mathbf{r}_\perp) \hat{\alpha}(r_z, t)$. Note the quantum Lenz relation linking the flux and the potential: $\partial_t \hat{\Phi}_B(r_z, t) = -\hat{V}(r_z, t)$. The phase operator is related to the flux through: $\hat{\phi}_B(r_z, t) = (2e) \hat{\Phi}_B(r_z, t) / \hbar$. Similarly we can define the differential inductance dL through the proportionality relation $d\hat{\Phi}_B(r_z, t) = dL \hat{I}(r_z, t)$:

$$dL = \frac{\mu_0 \int_1^2 d\mathbf{r}_\perp \cdot \mathbf{A}_\perp(\mathbf{r}_\perp)}{\oint ds \cdot \mathbf{A}_\perp(\mathbf{r}_\perp)} dr_z = -\frac{\chi_s}{\epsilon c^2 \oint ds \cdot \mathbf{A}_\perp(\mathbf{r}_\perp)} dr_z, \quad (\text{C9})$$

that depends also only on the geometry of the waveguide. We deduce immediately the relation linking the line inductance and the line capacitance $(dL/dr_z)(dC/dr_z) = 1/c^2$. These expressions can be further simplified by carry out a partial integration on the normalization condition and by using the Laplace equation in:

$$\begin{aligned} 1/\epsilon &= \int d^2\mathbf{r}_\perp (\nabla\chi(\mathbf{r}_\perp))^2 = \oint ds \cdot (\nabla\chi(\mathbf{r}_\perp))\chi(\mathbf{r}_\perp)|_1^2 - \int d\mathbf{r}_\perp \chi(\mathbf{r}_\perp) \nabla^2 \chi(\mathbf{r}_\perp) \\ &= -\oint ds \cdot \mathbf{A}_\perp(\mathbf{r}_\perp) \chi_s. \end{aligned} \quad (\text{C10})$$

The last relation expresses all parameters in terms of the scalar potential χ_s . We find finally:

$$\partial_{r_z} \hat{\Phi}_B(r_z, t) = \chi_s \partial_{r_z} \hat{\alpha}(r_z, t), \quad \partial_{r_z} \hat{Q}(r_z, t) = \frac{1}{\chi_s} \hat{\alpha}(r_z, t), \quad L' = \frac{dL}{dr_z} = \frac{\chi_s^2}{c^2}, \quad C' = \frac{dC}{dr_z} = \frac{1}{\chi_s^2}. \quad (\text{C11})$$

Thus the electromagnetic part of the Hamiltonian can be rewritten as:

$$\int dr_z \frac{1}{2} \left[(\hat{\alpha}(r_z, t))^2 - c^2 \hat{\alpha}(r_z, t) \partial_z^2 \hat{\alpha}(r_z, t) \right] = \int \left[\frac{d\hat{Q}^2}{2dC} + \frac{d\hat{\Phi}_B^2}{2dL} \right] = \int dr_z \left[\frac{1}{2C'} \left(\frac{d\hat{Q}}{dr_z} \right)^2 + \frac{1}{2L'} \left(\frac{d\hat{\Phi}_B}{dr_z} \right)^2 \right] \quad (\text{C12})$$

with the non trivial commutations relation:

$$[\hat{\Phi}_B(r'_z, t), \partial_{r_z} \hat{Q}(r_z, t)] = i\hbar \delta(r_z - r'_z). \quad (\text{C13})$$

Let us note that the charge conservation law along the conductor expressed in differential form: $\partial_t \partial_{r_z} \hat{Q}(r_z, t) = -\partial_{r_z} \hat{I}(r_z, t)$ is deduced easily from the Heisenberg equation: $\partial_t \hat{\alpha}(r_z, t) = c^2 \partial_{r_z}^2 \hat{\alpha}(r_z, t)$ valid for a free em field. The self Coulombian energy associated to these surface charges is included in the Hamiltonian Eq.(C12) with another capacitance C_{coul} and leads to the renormalisation of the line capacitance $C' \rightarrow 1/(1/C' + 1/C_{coul})$.

Let us show the power of this approach on some examples. In the simplest case of parallel planes of large transverse width W and interdistance D , so that $\mathbf{A}_\perp(\mathbf{r}_\perp) = (A_\perp, 0, 0)$, we obtain

$$C' = \frac{dC}{dr_z} = \frac{\epsilon \int_{-W/2}^{W/2} dr_y}{\int_1^2 dr_x} = \frac{\epsilon W}{D}. \quad (\text{C14})$$

In the case of a coplanar waveguide of size w for the signal wire and s for the interspace represented in Fig.15 assuming the vacuum dielectric constant everywhere ($\epsilon_0 = \epsilon_1 = \epsilon_2$), we need to use two conformal transformations one on the upper and the other on lower half planes [32, 33]. For each areas, this process redefines up to a normalisation constant the effective width $W_0 \sim 2K(k_0)$ and the effective interdistance $D_0 \sim K(k'_0)$ where $k_0 = w/(w+2s)$ and $k'_0 = \sqrt{1-k_0^2}$ are arguments of the complete elliptic integral. As a result, we obtain $C' = \epsilon 2W_0/D_0 = \epsilon 4K(k_0)/K(k'_0)$, an extra factor 2 is added to include both half planes [32, 33].

Using $\mathbf{l}_j = (-l_j, \mathbf{l}_{j\perp})$, the Hamiltonian Eq.(B19) becomes:

$$\begin{aligned} \hat{H} = E_0 + \sum_{j=1}^N E_{J,j} \left[1 - \cos \left(\frac{2e}{\hbar} \hat{\Phi}_j(t) \right) \right] + \frac{1}{2} \sum_{j,j'=1}^N C_{j,j'}^{-1} \hat{q}_j(t) \hat{q}_{j'}(t) \\ + \int_{-\infty}^{\infty} dr_z \frac{1}{2} \left[(\hat{\alpha}(r_z, t))^2 - c^2 \hat{\alpha}(r_z, t) \partial_z^2 \hat{\alpha}(r_z, t) \right] - \sum_{j=1}^N f_j \frac{\hat{\alpha}(-l_j, t)}{\sqrt{C'}} \hat{q}_j(t), \end{aligned} \quad (\text{C15})$$

where we define the dimensionless parameter:

$$f_j = \sqrt{C'} \int_0^1 du \int d^3 \mathbf{r} \mathbf{A}_\perp(\mathbf{l}_{j\perp} + u(\mathbf{r} - \mathbf{l}_{j\perp})) \cdot \mathbf{r}_\perp (|\psi_{j,+}(\mathbf{r})|^2 - |\psi_{j,-}(\mathbf{r})|^2). \quad (\text{C16})$$

This complicated formula depends on the complicated architecture of the circuit but can nevertheless be interpreted as follows. Using the rough formula $C' \sim \epsilon \mathbf{l}$ where \mathbf{r} is the average spatial range of the microwave electric field in the xy plane and \mathbf{l} is the average distance between two wires, we estimate $\mathbf{A}_\perp(\mathbf{r}) \sim 1/\sqrt{\epsilon \mathbf{l}}$ from the normalisation. If \mathfrak{d} is the distance between the two islands of the transmon, we find the magnitude $f_j \sim \mathfrak{d}/\mathbf{l}$.

In what follows, we shall omit E_0 in Eq.(C15).

3. Generalisation to the dielectric-filled waveguide

In the experimentally relevant case when the insulating substrates (silicon oxide, sapphire, etc) are present [34], the permittivity parameter depends on the position $\epsilon(\mathbf{r}_\perp)$ keeping the permeability μ_0 constant and affect the speed of propagation. Repeating the reasoning of previous sections with such dependence in Eq.(B19), we generalize the equations for the transverse electromagnetic component as:

$$\nabla_\perp \times \mathbf{A}_\perp(\mathbf{r}_\perp) = 0, \quad \mathbf{n} \times \mathbf{A}_\perp(\mathbf{r}_\perp) = 0 \text{ at the surface boundary,} \quad \nabla_\perp \cdot (\epsilon(\mathbf{r}_\perp) \mathbf{A}_\perp(\mathbf{r}_\perp)) = 0. \quad (\text{C17})$$

These components are normalized such that $\int d^2 \mathbf{r}_\perp \epsilon(\mathbf{r}_\perp) \mathbf{A}_\perp^2(\mathbf{r}_\perp) = 1$. It is still possible to define a scalar potential via $\mathbf{A}_\perp(\mathbf{r}_\perp) = \nabla_\perp \chi(\mathbf{r}_\perp)$ so the problem reduces into the Laplace-like equation:

$$\nabla_\perp \cdot (\epsilon(\mathbf{r}_\perp) \nabla_\perp \chi(\mathbf{r}_\perp)) = 0, \quad \chi(\mathbf{r}_\perp) = \chi_s \text{ at signal wire,} \quad \chi(\mathbf{r}_\perp) = 0 \text{ at ground wire.} \quad (\text{C18})$$

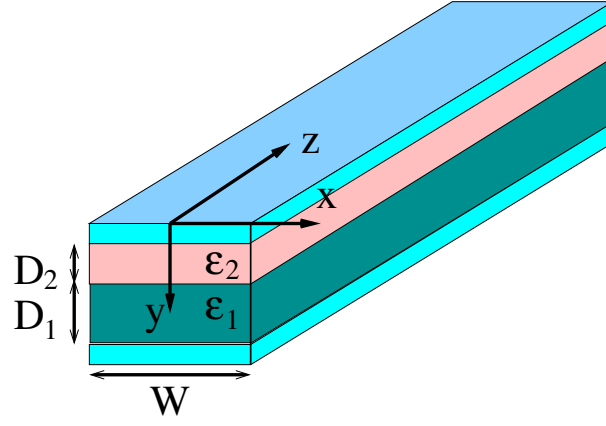


FIG. 14. Schematic representation of a waveguide made of two superconducting planes filled with two dielectrics.

We find that the propagation speed v is given by

$$v^2 = \frac{\int d^2\mathbf{r}_\perp \mathbf{A}_\perp^2(\mathbf{r}_\perp)}{\mu_0 \int d^2\mathbf{r}_\perp \epsilon(\mathbf{r}_\perp) \mathbf{A}_\perp^2(\mathbf{r}_\perp)} = \frac{\int d^2\mathbf{r}_\perp (\nabla_\perp \chi(\mathbf{r}_\perp))^2}{\mu_0} \neq c^2. \quad (\text{C19})$$

In order to have a first idea of the expected outcomes, let us estimate the speed for the simple case in Fig.14 of two parallel plane signal and ground wire of transverse width W filled with two separate dielectrics, one of permittivity ϵ_1 of thickness D_1 followed by another of permittivity ϵ_2 of thickness D_2 . Solving the equation, we obtain a different field $\mathbf{A}_\perp(\mathbf{r}_\perp) = (1/[\epsilon_i \sqrt{W(D_1/\epsilon_1 + D_2/\epsilon_2)}], 0, 0)$ for each dielectric $i = 1, 2$ (We neglect the edge effect). We obtain the phase velocity:

$$v = \sqrt{\frac{D_1/\epsilon_1^2 + D_2/\epsilon_2^2}{\mu_0(D_1/\epsilon_1 + D_2/\epsilon_2)}}. \quad (\text{C20})$$

This result unfortunately leads to the inequality $v \neq 1/\sqrt{L'C'}$ valid strictly for the vacuum case. The definitions Eqs.(C6),(C9) and (C11) are generalized into:

$$C' = \frac{\oint \epsilon(\mathbf{r}_\perp) \mathbf{A}_\perp(\mathbf{r}_\perp) \cdot d\mathbf{s}}{\int_1^2 d\mathbf{r}_\perp \cdot \mathbf{A}_\perp(\mathbf{r}_\perp)} = \frac{W}{(D_1/\epsilon_1 + D_2/\epsilon_2)}, \quad (\text{C21})$$

$$L' = \frac{\mu_0 \int_1^2 d\mathbf{r}_\perp \cdot \mathbf{A}_\perp(\mathbf{r}_\perp)}{\oint d\mathbf{s} \cdot \mathbf{A}_\perp(\mathbf{r}_\perp)} = \frac{\mu_0 \epsilon_2 (D_1/\epsilon_1 + D_2/\epsilon_2)}{W}, \quad (\text{C22})$$

which yields instead $1/\sqrt{L'C'} = 1/\sqrt{\mu_0 \epsilon_1}$. If we would use the inductance calculated from the ground wire $\epsilon_1 L'/\epsilon_2$, another different result would have been found. From this example, this result clearly differs from the results obtained using an electrostatic approach [33] and magnetostatic approach [32] because no additional polarisation or “bound” currents and charge are included dynamically inside the dielectric at non zero frequencies. These unwanted currents not predicted in a static approach affect the magnetic field inside the dielectrics and may well create a current difference between the signal and the ground wires requiring a full dynamic treatment.

4. The coplanar waveguide

In the case of a coplanar waveguide (CPW) [34] represented in Fig.15, we solve the partial differential Eqs.(C18) with three dielectric constants: ϵ_i in two different regions $i = 1, 2$ of thickness h_i and ϵ_0 otherwise. The shielding to the ground in the lower part is assumed at a distance $h_0 + h_1 + h_2$. Generally, this distance is large and can be taken to infinity. Typically the first region is silicon and the region 2 is silicon oxide [34]. The thickness of the superconducting plates are negligible. In these conditions Eq.(C18) reduces to the Laplace equation except at the surface of the dielectric where, for both interfaces 2-1 and 1-0, the boundary conditions over the normal component of the field apply, respectively $\epsilon_2 \partial_{r_y} \chi(\mathbf{r}_\perp) = \epsilon_1 \partial_{r_y} \chi(\mathbf{r}_\perp)$ and $\epsilon_1 \partial_{r_y} \chi(\mathbf{r}_\perp) = \epsilon_0 \partial_{r_y} \chi(\mathbf{r}_\perp)$.

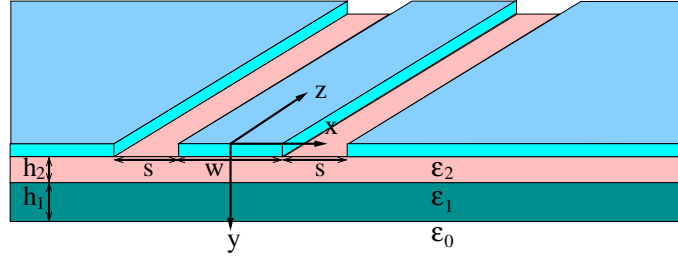


FIG. 15. Schematic representation of the coplanar waveguide with two layers of dielectric materials.

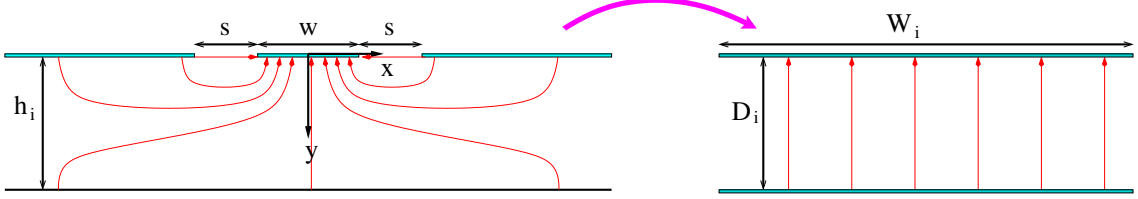


FIG. 16. Schematic representation of the conformal transformation for the line force of the field $\chi_i(\mathbf{r}_\perp)$ for a CPW.

The capacitance is a sum of two capacitances for each half plane $C' = C'_0 + C'_d$. In the upper half plane, we recover the result $C'_0 = \epsilon_0 W_0 / D_0$ of the previous section for the vacuum case. In the lower half plane, the solution is of the form $\chi = \chi_0 + \chi_1 + \chi_2$ where χ_0 is the vacuum solution of the entire half space, χ_1 is the non zero solution only in the regions 1 and 2 and χ_2 is the non zero solution only in the region 2. These are solutions of the Laplace equation and obey the whole set of boundary conditions:

1	$\chi_i(r_x, r_y = 0) = \chi_{s,i}$ for $r_x \in [-w/2, w/2]$
2	$\chi_i(r_x, r_y = 0) = 0$ for $r_x \in [-\infty, -s - w/2] \cup [s + w/2, \infty]$
3	$\partial_{r_x} \chi_i(r_x, r_y = 0) = 0$ for $r_x \in [-s - w/2, -w/2] \cup [w/2, s + w/2]$
4	$\chi_i(r_x = \pm\infty, r_y = 0) = 0$
5	$\chi_0(r_x, r_y = h_0 + h_1 + h_2) = 0$
6	$\epsilon_0 \partial_{r_y} \chi_0(r_\perp) _{r_y=h_1+h_2+0^+} = \epsilon_1 \partial_{r_y} (\chi_0(r_\perp) + \chi_1(r_\perp)) _{r_y=h_1+h_2-0^+}$
7	$\epsilon_1 \partial_{r_y} (\chi_0(r_\perp) + \chi_1(r_\perp)) _{r_y=h_2+0^+} = \epsilon_2 \partial_{r_y} (\chi_0(r_\perp) + \chi_1(r_\perp) + \chi_2(r_\perp)) _{r_y=h_2-0^+}$

The boundary conditions (1-5) are treated using the techniques of conformal transformation developed in [32, 33] and represented in Fig.16. Using the Gauss and the circulation theorems, it is not difficult to show that any region mapped by χ_i has a boundary value $\chi_{i,s}$ on the signal wire, and zero everywhere else at the other boundaries, with the exception on the line of interdistance s where a zero normal derivative is imposed instead. Therefore, each dielectric region $i = 0, 1, 2$ associated to χ_i can be conformally mapped into a rectangle of width $W_i = 2K(k_i)$ and length $D_i = K(k'_i)$ where we define $k_i = \tanh(\pi w/2 \sum_{i'=i}^2 h_{i'}) / \tanh(\pi(w + 2s)/2 \sum_{i'=i}^2 h_{i'})$ and $k'_i = \sqrt{1 - k_i^2}$ [45]. After the transformation, we deduce also the relation $W_i \chi_{s,i} / D_i = - \int_{-w/2}^{w/2} dr_x \partial_{r_y} \chi_i(\mathbf{r}_\perp)$ which allows to define the vacuum capacitance for each area as $C'_i = \epsilon_0 W_i / D_i$.

The two latest boundary conditions (6,7) correspond to the effective surface charges at the interface 01 and 12. integrating over r_x and using the Gauss theorem at the boundary for each region 1 and 2, we find the following relations between the $\chi_{s,i}$:

$$\epsilon_0 C'_0 \chi_{s,0} = \epsilon_1 (C'_0 \chi_{s,0} + C'_1 \chi_{s,1}) = \epsilon_2 (C'_0 \chi_{s,0} + C'_1 \chi_{s,1} + C'_2 \chi_{s,2}). \quad (C23)$$

Integrating by parts the normalization condition $\int d^2 \mathbf{r}_\perp \epsilon(\mathbf{r}) (\nabla_\perp \chi(\mathbf{r}_\perp))^2 = 1$, we find also that $\chi_s^2 C' = 1$ similarly to the vacuum case. With these relations, we eliminate the variables $\chi_{s,i}$ and we find the line capacitance of the lower plane:

$$C'_d = - \frac{\epsilon_2}{\chi_s} \int_{-w/2}^{w/2} dr_x \partial_{r_y} \chi(r_x, 0^+) = \frac{1}{\frac{1}{C'_0} - \frac{1}{C'_1} \left(\frac{\epsilon_0}{\epsilon_1} - 1 \right) - \frac{1}{C'_2} \left(\frac{\epsilon_0}{\epsilon_2} - \frac{\epsilon_0}{\epsilon_1} \right)}. \quad (C24)$$

Similarly working out $\int d^2\mathbf{r}_\perp (\nabla_\perp \chi(\mathbf{r}_\perp))^2$ through partial integration at the interfaces we determine using Eq.(C20) the speed of light $v = c/\sqrt{\epsilon_{rel}}$ with an effective relative permittivity determined from:

$$\frac{1}{\epsilon_{rel}} = \frac{2C'_0}{C'} + \left[\left(1 - \frac{C'_0}{C'_1}\right) \left(\frac{\epsilon_0}{\epsilon_1} - 1\right) \left[\left(\frac{\epsilon_0}{\epsilon_1} - 1\right) \frac{1}{C'_1} + 2 \left(\frac{\epsilon_0}{\epsilon_2} - \frac{\epsilon_0}{\epsilon_1}\right) \frac{1}{C'_2} \right] + \left(1 - \frac{C'_0}{C'_2}\right) \frac{1}{C'_2} \left(\frac{\epsilon_0}{\epsilon_1} - \frac{\epsilon_0}{\epsilon_2}\right)^2 \right] \frac{C'_d{}^2}{C'}. \quad (C25)$$

In order to have unambiguous definitions for the effective line capacitance and inductance, we require that their values are based on the experimental measurements of phase velocity v and the impedance obtained, using a monochromatic wave of frequency ω , from the ratio:

$$Z = \frac{\langle \hat{V}(r_z, t) \rangle}{\langle \hat{I}(r_z, t) \rangle} = \frac{\mu \int_1^2 d\mathbf{r}_\perp \cdot \mathbf{A}_\perp(\mathbf{r}_\perp) \langle \hat{\alpha}(r_z, t) \rangle}{\oint ds \cdot \mathbf{A}_\perp(\mathbf{r}_\perp) \langle \partial_{r_z} \hat{\alpha}(r_z, t) \rangle} = \frac{\mu \int_1^2 d\mathbf{r}_\perp \cdot \mathbf{A}_\perp(\mathbf{r}_\perp) \omega}{\oint ds \cdot \mathbf{A}_\perp(\mathbf{r}_\perp) k} = \frac{\mu v \int_1^2 d\mathbf{r}_\perp \cdot \mathbf{A}_\perp(\mathbf{r}_\perp)}{\oint ds \cdot \mathbf{A}_\perp(\mathbf{r}_\perp)} = vL'. \quad (C26)$$

In the case of a CPW, we obtain $L' = \mu/(C'_u/\epsilon_0 + C'_d/\epsilon_2)$ using the definition in (C22). From any experimental measurements of the speed v and the impedance Z , we extract the static inductance using $L' = Z/v$. Normally, as for the vacuum case, the experimental extraction of the capacitance C'_{eff} should be done using the formula $v = 1/\sqrt{L'C'_{eff}}$ and impedance $Z = \sqrt{L'/C'_{eff}}$. However, in presence of dielectrics, the deduced formula $C_{eff} = 1/(L'v^2)$ differs from the static formula C' defined in (C21). Using (C22), we find the expression:

$$C'_{eff} = \frac{\oint \mathbf{A}_\perp(\mathbf{r}_\perp) \cdot ds}{\mu v^2 \int_1^2 d\mathbf{r}_\perp \cdot \mathbf{A}_\perp(\mathbf{r}_\perp)} \neq C'. \quad (C27)$$

As a consequence, the measured impedance Z differs also from the static one $Z_{st} = \sqrt{L'/C'}$ determined from electrostatic capacitance and magnetostatic inductance calculations.

The table II displays the parameter values obtained for various model descriptions of the CPW, with comparisons between static capacitance and impedance and effective capacitance and impedance. The two half plane model corresponds to the case where the upper half plane is the vacuum while the lower half plane is filled with silicon; the second model corresponds to the case where the silicon oxide at the interface is not present in contrast to the full model. We note that the full model provides the best prediction for the effective permittivity, but with an impedance very low in comparison to the usual chosen value of 50Ω as a standard in a waveguide. In contrast, the absence of the silicon oxide prevents a leaked polarisation current at the interface which results in a higher inductance and thus an impedance close the desired value. Therefore the interface current has to be taken into account and probably could also contribute to the total current at the output of the quantum circuit through ac capacitive coupling.

The conclusion of this section is that in presence of dielectrics, we should distinguish between the real capacitance measured in static conditions and the effective capacitance. It is caused by additional polarisation currents at the dielectric interfaces and results also in line loss caused by their intrinsic resistance but that are not studied in this work.

For simplicity, in the main text and in what follows, we shall keep the notation of c and C' to actually mean v and C'_{eff} instead.

Cases	C'	v/c	ϵ_{eff}	L'	C_{eff}	$Z = vL'$	$Z_{st} = \sqrt{\frac{L'}{C'}}$
	$10^{-10} F$			$10^{-7} H$	$10^{-10} F$	Ω	Ω
2 half planes	1.55	0.398	6.3	8.32	0.84	99.4	73
$\epsilon_2 = \epsilon_1$	1.54	0.409	5.99	4.54	1.47	55.6	54.3
Full model	1.44	0.434	5.30	2.36	2.49	30.8	40.5
Simulation [34]	1.27	0.438	5.22	4.53	NA	NA	59.7
Experiment [34]		0.455	5.05				

TABLE II. Comparison of various model description with experiment and simulation for the CPW waveguide. Parameter values of [34] are $s = 6.6\mu m$, $w = 10\mu m$, $h_1 = 500\mu m$, $h_2 = 550nm$, $\epsilon_1/\epsilon_0 = 11.6$, $\epsilon_2/\epsilon_0 = 3.78$.

Appendix D: Accounting for the resonator capacitances

1. Hamiltonian term derivation

The phenomenological treatment of the resonator [34] is based on the lumped-element representation and is an efficient approach for a classical description of the microwave radiation in the system. In order to address the quantum aspects here, we derive the Hamiltonian term for the resonator cavity in the waveguide. In the following sections we will show how it leads to the consistent quantum derivation of the resonator's spectrum and damping.

The resonator is located between the position $r_z = -L, 0$ respectively where the signal line is disrupted by a cut or an insulator gap (see Fig.1). Both gaps are assumed identical with their charges located at $r_z^\pm = -L^\pm, 0^\pm$ and the width $w_g = |L^+ - L^-| = |0^+ - 0^-|$. Physically, the electric current transporting electrical charge to the gap leads to a net electrical charge at the cut of the wire. As a result, we need to modify the quantum field description of the waveguide as:

$$\sqrt{N_{s,0}}\psi(\mathbf{r}) \rightarrow \hat{\psi}(\mathbf{r}, t) = \sqrt{N_{s,0}}\psi_0(\mathbf{r}) + \delta\hat{\psi}(\mathbf{r}, t), \quad (\text{D1})$$

with a net local charge distribution described by the perturbation $\delta\hat{\psi}(\mathbf{r}, t)$. If the wavefunction abruptly drops to zero beyond the position $r_z = -L^-$ at the left end of the gap, the variation of charge is determined from the conservation law as:

$$(2e)\partial_t|\hat{\psi}(\mathbf{r}, t)|^2 = -\nabla \cdot \hat{\mathbf{j}}(\mathbf{r}, t) \cong \delta(r_z + L_z^-)\hat{j}_z(\mathbf{r}, t). \quad (\text{D2})$$

From integration over the transverse plane, the net total charge accumulated at $-L^-$ is:

$$\hat{Q}_-(-L^-, t) = (2e) \int_{-\infty}^{-L^-} dr_z \int d^2\mathbf{r} (|\hat{\psi}(\mathbf{r}, t)|^2 - N_{s,0}|\psi_0(\mathbf{r})|^2). \quad (\text{D3})$$

Integrating over the transverse coordinates and using Eq.(D2) and the local equation for the surface charge conservation with the current (C7), we obtain:

$$\partial_t \hat{Q}_-(-L^-, t) \cong \int d^2\mathbf{r}_\perp \hat{j}_z(\mathbf{r}_\perp, -L^-, t) = \hat{I}(r_z, t) = - \int_{-\infty}^{-L^-} dr_z \partial_t \partial_{r_z} \hat{Q}(r_z, t) + \hat{I}(-\infty, t) \quad (\text{D4})$$

where we can assume that the effect of far distant current $\hat{I}(-\infty, t)$ is negligible for any signal localized in time and space. The integration over time produces:

$$\hat{Q}_-(-L^-, t) = - \int_{-\infty}^{-L^-} dr_z \partial_{r_z} \hat{Q}(r_z, t). \quad (\text{D5})$$

That is, the charge at the signal wire ends is opposite of the total charge obtained from integration over the line. A similar expression holds for a charge coming from the right: $\hat{Q}_+(0^+, t) = \int_{-\infty}^{0^+} dr_z \partial_{r_z} \hat{Q}(r_z, t)$. However, for the charge accumulated inside the resonator, we find instead the neutrality constraint:

$$\hat{Q}_+(-L^+, t) + \hat{Q}_-(0^-, t) = - \int_{-L^+}^{0^-} dr_z \partial_{r_z} \hat{Q}(r_z, t) = - \int_{-L^+}^{0^-} dr_z \epsilon \oint ds \cdot \hat{\mathbf{E}}(\mathbf{r}, t), \quad (\text{D6})$$

where the last equality results from the Gauss theorem applied to the resonator. For each gap of the resonator, we define the self capacitance C and the interaction capacitance C_I such that the Hamiltonian term associated with these charges located at $r_z^\pm = -L^\pm, 0^\pm$ is:

$$\hat{H}_c = \sum_{r_z=0, -L} \frac{\hat{Q}_+^2(r_z^+, t) + \hat{Q}_-^2(r_z^-, t)}{2C} + \frac{\hat{Q}_+(r_z^+, t)\hat{Q}_-(r_z^-, t)}{C_I}. \quad (\text{D7})$$

Assuming a conductor of cross section S over which the excess charges are uniformly distributed, we identify by comparison with the Coulombian term in Eq.(A3) the self capacitance formula and the interaction capacitance:

$$\frac{1}{C} = \frac{1}{S^2} \int_S d^2\mathbf{r}_\perp \int_S d^2\mathbf{r}'_\perp \frac{1}{4\pi\epsilon\sqrt{(\mathbf{r}_\perp - \mathbf{r}'_\perp)^2}}, \quad \frac{1}{C_I} = \frac{1}{S^2} \int_S d^2\mathbf{r}_\perp \int_S d^2\mathbf{r}'_\perp \frac{1}{4\pi\epsilon\sqrt{(\mathbf{r}_\perp - \mathbf{r}'_\perp)^2 + w_g^2}}. \quad (\text{D8})$$

Usually in a classical circuit, the neutrality conditions is fulfilled so that the left and right charges are opposite $\hat{Q}_+(r_z^+, t) = -\hat{Q}_-(r_z^-, t)$. In our case, however, we deal with a sufficiently large gap so that $C_I \gg C$ and the

interaction capacitance term does not contribute in (D7). The validity of this assumption relies on the experimentally confirmed results Eqs.(7) and (8), but the term C_I should be generally included as well. Also, a too high gap may induce the loss in the line leading to a saturation of the quality factor [34].

Doing an *a posteriori* reasoning over the result of the appendix H, the resonating modes of the cavity cancels the integral over the electric field in Eq.(D6) and imposes neutrality of the edge charges $\hat{Q}_+(-L^+, t) = -\hat{Q}_-(0^-, t)$. In addition, if we note that the only remaining independent operator variable $\hat{Q}_+(-L^+, t) - \hat{Q}_-(0^-, t)$ minimizes the Hamiltonian (D7) for a zero value, we conclude that these charges inside the resonator are zero resulting in a charge asymmetry at each capacitance. Therefore, the Hamiltonian Eq.(D7) becomes:

$$\hat{H}_c = \frac{\hat{Q}_-^2(-L^-, t) + \hat{Q}_+^2(0^+, t)}{2C}, \quad \hat{Q}_\pm(r_z, t) = \pm \int_{-\infty}^{\infty} dr'_z 1^+(\pm(r_z - r'_z))\sqrt{C'}\hat{\alpha}(r'_z, t). \quad (\text{D9})$$

where $1^+(r_z)$ is the Heaviside function. Since the gap is very small compared to the wavelength, we will assume that $-L^- \cong -L$ and $0^+ \cong 0$ in the following.

2. The quantum circuit formulation with a resonator

As a result of the new term (D9), the Hamiltonian (C15) becomes:

$$\begin{aligned} \hat{H} = & \int_{-\infty}^{\infty} dr_z \frac{1}{2} \left[\hat{\alpha}^2(r_z, t) - c^2 \hat{\alpha}(r_z, t) \partial_z^2 \hat{\alpha}(r_z, t) \right] + \frac{C'}{2C} \left[\left(\int_{-\infty}^L dr'_z \hat{\alpha}(r'_z, t) \right)^2 + \left(\int_0^{\infty} dr'_z \hat{\alpha}(r'_z, t) \right)^2 \right] \\ & + \sum_{j=1}^N E_{J,j} \left[1 - \cos \left(\frac{2e}{\hbar} \hat{\Phi}_j(t) \right) \right] + \frac{1}{2} \sum_{j,j'=1}^N C_{j,j'}^{-1} \hat{q}_j(t) \hat{q}_{j'}(t) - \sum_{j=1}^N \frac{\hat{\alpha}(-l_j, t)}{\sqrt{C'}} f_j \hat{q}_j(t). \end{aligned} \quad (\text{D10})$$

This Hamiltonian is nonlocal in the field $\hat{\alpha}(r_z, t)$ which makes the resulting quantum field theory unconventional. In terms of the effective charge and flux of the waveguide field expressed in (C12), the Hamiltonian takes the more recognizable quantum circuit form:

$$\begin{aligned} \hat{H} = & \int \left[\frac{d\hat{Q}^2}{2dC} + \frac{d\hat{\Phi}_B^2}{2dL} \right] + \frac{\hat{Q}_-^2(-L, t) + \hat{Q}_+^2(0, t)}{2C} \\ & + \sum_{j=1}^N E_{J,j} \left[1 - \cos \left(\frac{2e}{\hbar} \hat{\Phi}_j(t) \right) \right] + \frac{1}{2} \sum_{j,j'=1}^N C_{j,j'}^{-1} \hat{q}_j(t) \hat{q}_{j'}(t) + \sum_{j=1}^N f_j \frac{d\hat{Q}(-l_j, t)}{dC} \hat{q}_j(t). \end{aligned} \quad (\text{D11})$$

Appendix E: The qubit Hamiltonian and the energy balance relation

1. Derivation

For renormalisation purposes, the Hamiltonian (D11) is rewritten using a unitary transformation: $\hat{\Phi}_j(t) \rightarrow \hat{\Phi}_j(t) - \frac{f_j}{\sqrt{C}} \hat{\alpha}(-l_j, t)$ and $\hat{\alpha}(r_z, t) \rightarrow \hat{\alpha}(r_z, t) + \sum_{j=1}^N \frac{f_j}{\sqrt{C'}} \hat{q}_j \delta(r_z + l_j)$. This result yields:

$$\begin{aligned} \hat{H} = & \int dr_z \frac{1}{2} \left[\hat{\alpha}^2(r_z, t) - c^2 \hat{\alpha}(r_z, t) \partial_z^2 \hat{\alpha}(r_z, t) \right] + \frac{\hat{Q}_-^2(-L, t) + \hat{Q}_+^2(0, t)}{2C} \\ & + \sum_{j=1}^N E_{J,j} \left[1 - \cos \left(\frac{2e}{\hbar} \left(\hat{\Phi}_j(t) - \frac{f_j}{\sqrt{C'}} \hat{\alpha}(-l_j, t) \right) \right) \right] + \frac{\hat{q}_j^2(t)}{2C_j}, \end{aligned} \quad (\text{E1})$$

where $1/C_j = 1/C_{j,j} + f_j^2 \delta(0)/C'$ in which “ $\delta(0)$ ” $\simeq 1/\Delta r$ with Δr is the size of the transmon.

From inspection of the Hamiltonian (D11) when we omit the coupling term, we recover the well known anharmonic oscillator dynamics of each transmon characterized by the Josephson energy much larger than the capacitance energy and that leads to a non equidistant spectrum [8]. In these conditions and if the transmons are sufficiently far from each other to neglect their mutual capacitance interaction, we can restrict the description to the two first states so that the transmon becomes in good approximation a qubit.

Using the notation:

$$\hat{\Phi}_j = \frac{\hbar}{2e} \left(\frac{8E_{C,j}}{E_{J,j}} \right)^{1/4} \frac{\hat{b}_j + \hat{b}_j^\dagger}{\sqrt{2}}, \quad \hat{q}_j = 2e \left(\frac{E_{J,j}}{8E_{C,j}} \right)^{1/4} \frac{\hat{b}_j - \hat{b}_j^\dagger}{\sqrt{2i}}, \quad E_C = \frac{e^2}{2C_j}, \quad \hbar\omega_j = \sqrt{8E_{C,j}E_{J,j}}, \quad (\text{E2})$$

we reexpress the Hamiltonian using the creation annihilation operators \hat{b}_j^\dagger and \hat{b}_j . In the limit $E_{C,j} \ll E_{J,j}$, we can limit the expansion up to the quadratic terms:

$$\begin{aligned} \hat{H} = & \int dr_z \frac{1}{2} \left[\hat{\alpha}^2(r_z, t) - c^2 \hat{\alpha}(r_z, t) \partial_z^2 \hat{\alpha}(r_z, t) \right] + \frac{\hat{Q}_-^2(-L, t) + \hat{Q}_+^2(0, t)}{2C} + \sum_{j=1}^N \frac{c\kappa_j^2}{\omega_j} \hat{\alpha}^2(-l_j, t) \\ & + \hbar\omega_j \hat{b}_j^\dagger(t) \hat{b}_j(t) - \sqrt{\hbar c \kappa_j} \left(\hat{b}_j(t) + \hat{b}_j^\dagger(t) \right) \hat{\alpha}(-l, t), \end{aligned} \quad (\text{E3})$$

where we define the coupling with electromagnetic field $\kappa_j = \frac{2e f_j E_{J,j}}{\hbar \sqrt{2cC'}} \left(\frac{8E_{C,j}}{E_{J,j}} \right)^{1/4} = \frac{2e f_j \sqrt{E_{J,j} \omega_j}}{\hbar \sqrt{2cC'}}$. We shall omit the third quadratic term proportional to κ_j^2/ω_j in the field as it gives a negligible contribution to the detuning frequency much smaller than the microwave frequency. Since we are interested in the two first levels, we replace the transmon operators by the qubit Pauli operators and obtain finally:

$$\hat{H} = \int dr_z \frac{1}{2} \left[\hat{\alpha}^2(r_z, t) - c^2 \hat{\alpha}(r_z, t) \partial_z^2 \hat{\alpha}(r_z, t) \right] + \frac{\hat{Q}_-^2(-L, t) + \hat{Q}_+^2(0, t)}{2C} + \sum_{j=1}^N \frac{\hbar\omega_j}{2} \hat{\sigma}_j^z(t) - \sqrt{\hbar c \kappa_j} \hat{\sigma}_j^x(t) \hat{\alpha}(-l_j, t). \quad (\text{E4})$$

Corrections due to the anharmonicity renormalize this energy into $\omega_j = \sqrt{8E_{C,j}E_{J,j}} - E_{C,j}$ as established in [8]. We set $\hbar = 1$ in what follows to simplify the formulas.

2. Heisenberg and scattering equations

Using $\partial_t \hat{A} = i[\hat{H}, \hat{A}]$ and the Pauli matrix algebra $[\hat{\sigma}^+, \hat{\sigma}^-] = \hat{\sigma}^z$, $[\hat{\sigma}^z, \hat{\sigma}^\pm] = \pm 2\hat{\sigma}^\pm$, the Heisenberg equations are:

$$\partial_t \hat{\alpha}(r_z, t) = \hat{\alpha}(r_z, t) + \frac{C'}{C} \left[1^+(L - r_z) \int_{-\infty}^L dr'_z \hat{\alpha}(r'_z, t) + 1^+(r_z) \int_0^\infty dr'_z \hat{\alpha}(r'_z, t) \right] \quad (\text{E5})$$

$$\partial_t \hat{\alpha}(r_z, t) = c^2 \partial_z^2 \hat{\alpha}(r_z, t) + \sum_{j=1}^N \sqrt{c\kappa_j} \hat{\sigma}_j^x(t) \delta(r_z + l_j) \quad (\text{E6})$$

$$\partial_t \hat{\sigma}_j^z(t) = -\sqrt{c\kappa_j} [\hat{\sigma}_j^y(t), \hat{\alpha}(-l_j, t)]_+ \quad (\text{E7})$$

$$\partial_t \hat{\sigma}_j^\pm(t) = \pm i\omega_j \hat{\sigma}_j^\pm(t) \pm i\sqrt{c\kappa_j} [\hat{\sigma}_j^z(t), \hat{\alpha}(-l_j, t)]_+ / 2, \quad (\text{E8})$$

where $[\cdot, \cdot]_+$ represents the anticommutator. For any quantum field operator $\hat{O}(r_z, t)$, we define its Fourier transform in space and time with various associated notations as:

$$\hat{O}(r_z, t) = \int_{-\infty}^\infty \frac{d\omega}{2\pi} e^{-i(\omega+i\eta)t} \hat{O}_\omega(r_z) = \int_{-\infty}^\infty \frac{dk}{2\pi} e^{ikr_z} \hat{O}_k(t) = \int_{-\infty}^\infty \frac{d\omega}{2\pi} \int_{-\infty}^\infty \frac{dk}{2\pi} e^{i[kr_z - (\omega+i\eta)t]} \hat{O}_{k,\omega}, \quad (\text{E9})$$

where we have introduced the positive and infinitesimal parameter $\eta \rightarrow 0$ to ensure an adiabatic switching essential to study the retarded response to any input wave [40]. Using the Heaviside function expressed in the integral form:

$$1^+(\pm r_z) = \mp \int_{-\infty}^\infty \frac{dk}{2\pi i} \frac{e^{-ikr_z}}{k^\pm}, \quad k^\pm = k \pm i\varepsilon, \quad (\text{E10})$$

with the infinitesimal positive parameter $\varepsilon \rightarrow 0$. they become:

$$\partial_t \hat{\alpha}_k(t) = \hat{\alpha}_k(t) + \int_{-\infty}^\infty \frac{dk'}{2\pi} \frac{C'}{C} \left[\frac{1}{k^- k'^+} + \frac{e^{i(k-k')L}}{k^+ k'^-} \right] \hat{\alpha}_{k'}(t) \quad (\text{E11})$$

$$\partial_t \hat{\alpha}_k(t) = -c^2 k^2 \hat{\alpha}_k(t) + \sum_{j=1}^N e^{ikl_j} \sqrt{c\kappa_j} \hat{\sigma}_j^x(t). \quad (\text{E12})$$

We solve the electromagnetic wave equation for the field operator by decomposing the field operator into an input and scattered component

$$\hat{\alpha}_k(t) = \hat{\alpha}_k^{in}(t) + \hat{\alpha}_k^{sc}(t), \quad \hat{\alpha}_k(t) = \hat{\alpha}_k^{in}(t) + \hat{\alpha}_k^{sc}(t). \quad (\text{E13})$$

The input field operators have a simple noninteracting dynamics and are decomposed into creation-annihilation operators as

$$\hat{\alpha}_k^{in}(t) = e^{\eta t} \frac{e^{-ic|k|t} \hat{a}_k^{in} + e^{ic|k|t} \hat{a}_{-k}^{in\dagger}}{\sqrt{2c|k|}}, \quad \hat{\alpha}_k^{in}(t) = \sqrt{c|k|} e^{\eta t} \frac{e^{-ic|k|t} \hat{a}_k^{in} - e^{ic|k|t} \hat{a}_{-k}^{in\dagger}}{\sqrt{2}i}, \quad (\text{E14})$$

with the nontrivial commutation relation $[\hat{a}_k^{in}, \hat{a}_{k'}^{in\dagger}] = 2\pi\delta(k-k')$. These obey the noninteracting part of Eq.(E11,E12). By eliminating them and using the time Fourier transform (E9), we obtain the following equations for the scattering field part:

$$-i(\omega + i\eta)\hat{\alpha}_{k,\omega}^{sc} = \hat{\alpha}_{k,\omega}^{sc} + \int_{-\infty}^{\infty} \frac{dk' C'}{2\pi C} \left[\frac{1}{k-k'+} + \frac{e^{i(k-k')L}}{k+k'-} \right] \hat{\alpha}_{k',\omega} \quad (\text{E15})$$

$$-i(\omega + i\eta)\hat{\alpha}_{k,\omega}^{sc} = -c^2 k^2 \hat{\alpha}_{k,\omega}^{sc} + \sum_{j=1}^N e^{ikl_j} \sqrt{c\kappa_j} \hat{\sigma}_{\omega,j}^x. \quad (\text{E16})$$

3. Energy balance equation

In the absence of dissipation, the energy conservation requires that the net power received within the cavity is equal to the input power radiation minus the output power radiation in a steady state regime. The Noether theorem usually ensures that the variation of the energy in a volume is equal to the energy incoming energy flux minus the outgoing flux. More specifically, assuming a waveguide beginning at $r_z = -L$ before the capacitance and finishing at $r_z = 0$ after the capacitance, we define the energy within the waveguide volume as:

$$\hat{H}(t) \Big|_{-L}^0 = \int_{-L}^0 dr_z \frac{1}{2} \left[\hat{\alpha}^2(r_z, t) - c^2 \hat{\alpha}(r_z, t) \partial_z^2 \hat{\alpha}(r_z, t) \right] + \frac{\hat{Q}_+^2(-L, t) + \hat{Q}_-^2(0, t)}{2C} + \sum_{j=1}^N \frac{\omega_j}{2} \hat{\sigma}_j^z(t) - \sqrt{c\kappa_j} \hat{\sigma}_j^x(t) \hat{\alpha}(-l_j, t). \quad (\text{E17})$$

The time variation of this energy is found using the Heisenberg equation (E5-E8). We obtain

$$\frac{d\hat{H}(t)}{dt} \Big|_{-L}^0 = \frac{c^2}{2} [\partial_{r_z} \hat{\alpha}(r_z, t), \hat{\alpha}(r_z, t)] \Big|_{r_z=-L}^{r_z=0} = \hat{A}_+^2(-L, t) - \hat{A}_-^2(-L, t) + \hat{A}_-^2(0, t) - \hat{A}_+^2(0, t). \quad (\text{E18})$$

The last operators are easy to determine using the results of subsection C 2 in terms of the voltage and current operators and impedance by:

$$\hat{A}_{\pm}(r_z, t) = \frac{\hat{V}(r_z, t) \pm Z\hat{I}(r_z, t)}{2\sqrt{Z}} = \frac{\pm c^{3/2} \partial_{r_z} \hat{\alpha}(r_z, t) - c^{1/2} \hat{\alpha}(r_z, t)}{2}, \quad Z = \sqrt{L'/C'}. \quad (\text{E19})$$

These are Hermitian and correspond to the quantum analog of forward + and backward - wave respectively, while their square are the forward and backward energy fluxes. Similarly the operators can be decomposed into an input and scattered fields:

$$\hat{A}_{\pm}(r_z, t) = \hat{A}_{\pm}^{in}(r_z, t) + \hat{A}_{\pm}^{sc}(r_z, t). \quad (\text{E20})$$

Using (E14), the left and right input wave operator in the spatial and Fourier modes is expressed in terms of creation annihilation field operator \hat{a}_k as:

$$\hat{A}_{k,\omega,\pm}^{in} = \frac{\pm ick \hat{\alpha}_{k,\omega}^{in} - \hat{\alpha}_{k,\omega}^{in}}{2} = 2\pi\delta(\omega \mp ck) \sqrt{c|\omega|/2} [1^+(\omega) \hat{a}_{\pm\omega/c} - 1^+(-\omega) \hat{a}_{\mp\omega/c}^\dagger] \quad (\text{E21})$$

$$\hat{A}_{\omega,\pm}^{in}(r_z) = e^{\pm i\omega r_z/c} i \sqrt{c|\omega|/2} [1^+(\omega) \hat{a}_{\pm\omega/c} - 1^+(-\omega) \hat{a}_{\mp\omega/c}^\dagger], \quad (\text{E22})$$

with the property that $\hat{A}_{\omega,\pm}^{in*}(r_z) = \hat{A}_{-\omega,\pm}^{in}(r_z)$. From the absence of scattering coming outside the resonator, we deduce that $\hat{A}_{\omega,+}^{sc}(-L) = 0$ and $\hat{A}_{\omega,-}^{sc}(0) = 0$.

In a steady state regime, the energy balance equation (E17) after averaging is rewritten as a sum of uncorrelated and correlated (fluorescent) part:

$$\langle \hat{A}_+^{in}(-L, t) \rangle^2 - \langle \hat{A}_-(-L, t) \rangle^2 + \langle \hat{A}_-^{in}(0, t) \rangle^2 - \langle \hat{A}_+(0, t) \rangle^2 = -\langle \delta^2 \hat{A}_+^{in}(-L, t) - \delta^2 \hat{A}_-(-L, t) + \delta^2 \hat{A}_-^{in}(0, t) - \delta^2 \hat{A}_+(0, t) \rangle. \quad (\text{E23})$$

The left hand side corresponds to signal reflection and transmission of the resonator while the right hand side appears when some relaxation occurs such as spontaneous emission or fluorescence of the qubits [38]. Thus, the Hamiltonian Eq.(E4) models the relaxation rate T_1 characterizing the decay of a qubit in its ground state.

Without the correlation, the balance equation is simplified and, after integration over infinite interval of time and the use of time Fourier transform, reads:

$$\int_{-\infty}^{\infty} \frac{d\omega}{2\pi} |\langle \hat{A}_{\omega,+}^{in}(-L) \rangle|^2 - |\langle \hat{A}_{\omega,-}(-L) \rangle|^2 + |\langle \hat{A}_{\omega,-}^{in}(0) \rangle|^2 - |\langle \hat{A}_{\omega,+}(0) \rangle|^2 = 0. \quad (\text{E24})$$

Appendix F: The transmission and reflection formalism

1. Reflection and Transmission: definitions

Since the transmission and reflection are usually concepts defined for classical circuit, this section aims at establishing their link with quantum field theory. Within the classical consideration (for instance any standard microwave engineering handbook like [31]), one often introduces input and output for forward and backward waves, $a_1 = \langle \hat{A}_{\omega,+}^{in}(-L) \rangle$ $a_2 = \langle \hat{A}_{\omega,-}^{in}(0) \rangle$ $b_1 = \langle \hat{A}_{\omega,-}(-L) \rangle$ $b_2 = \langle \hat{A}_{\omega,+}(0) \rangle$ where $a_{1,2}$ ($b_{1,2}$) represents the input (output), while the index 1(2) corresponds to forward (backward) wave.

The transmission and reflection are defined from the matrix relation:

$$\begin{pmatrix} b_1 \\ b_2 \end{pmatrix} = \begin{pmatrix} \langle \hat{A}_{\omega,-}(-L) \rangle \\ \langle \hat{A}_{\omega,+}(0) \rangle \end{pmatrix} = \begin{pmatrix} S_{11} & S_{12} \\ S_{21} & S_{22} \end{pmatrix} \begin{pmatrix} a_1 \\ a_2 \end{pmatrix} = \begin{pmatrix} S_{11} & S_{12} \\ S_{21} & S_{22} \end{pmatrix} \begin{pmatrix} \langle \hat{A}_{\omega,+}^{in}(0) \rangle \\ \langle \hat{A}_{\omega,-}^{in}(-L) \rangle \end{pmatrix}. \quad (\text{F1})$$

In what follows we consider only the case where $\langle \hat{A}_{\omega,-}^{in}(0) \rangle = 0$. In absence of scattering or fluorescence, any signal frequency remains unchanged and, thus, satisfies the unitary property $|S_{21}(\omega)|^2 + |S_{11}(\omega)|^2 = 1$. Otherwise, interactions may transfer the input signal into another frequency channel or the fluorescence broadens the signal into a continuum of frequencies which should be analyzed using correlations. Note that the spectral function of the voltage fluctuations is another quantity also used for analyzing the transmission [19].

2. Scattered wave operators

As quantities of interest for the transmission and reflection, we use the Heisenberg equations for the wave operators. Using the definition (E19) and applying the Fourier transform to Eqs.(E11) and (E12), we find

$$[\omega + i\eta \mp ck] \hat{A}_{k,\omega,\pm}^{sc} = \mp \frac{C' \sqrt{c}}{2C} \int_{-\infty}^{\infty} \frac{dk'}{2\pi} \left(\frac{1}{k'^+} + \frac{e^{i(k-k')L}}{k'^-} \right) \hat{\alpha}_{k',\omega} - \frac{ic}{2} \sum_{j=1}^N e^{ikl_j} \kappa_j \hat{\sigma}_{\omega,j}^x. \quad (\text{F2})$$

Multiplying by the propagator both sides, we determine after a contour integration over k' the non trivial scattered waves:

$$\hat{A}_{\omega,+}^{sc}(0^+) = i \frac{C'}{2C} \int_{-\infty}^{\infty} \frac{dk'}{2\pi \sqrt{c}} \left(\frac{1}{k'^+} + \frac{e^{i(\omega/c-k')L}}{k'^-} \right) \hat{\alpha}_{k',\omega} - \sum_{j=1}^N e^{i\omega l_j/c} \frac{\kappa_j}{2} \hat{\sigma}_{\omega,j}^x \quad (\text{F3})$$

$$\hat{A}_{\omega,-}^{sc}(-L^-) = -i \frac{C'}{2C} \int_{-\infty}^{\infty} \frac{dk'}{2\pi \sqrt{c}} \left(\frac{e^{i\omega L/c}}{k'^+} + \frac{e^{-ik'L}}{k'^-} \right) \hat{\alpha}_{k',\omega} - \sum_{j=1}^N e^{i\omega(L-l_j)/c} \frac{\kappa_j}{2} \hat{\sigma}_{\omega,j}^x. \quad (\text{F4})$$

The superscripts in 0^+ and L^- are here to indicate that the scattered wave functions are defined outside the cavity and ensure the convergence of the integration. They will be omitted subsequently. Taking also into account that

$\hat{\alpha}_{k,\omega}^{sc} = -(\hat{A}_{k,\omega,+}^{sc} + \hat{A}_{k,\omega,-}^{sc})/\sqrt{c}$, we deduce from Eq.(F2) an integral equation for $\hat{\alpha}_{k,\omega}^{sc}$ only. We integrate the latter as:

$$\hat{T}_{\pm} = \int_{-\infty}^{\infty} \frac{dk}{2\pi} \left(\frac{1}{k^+} \pm \frac{e^{-ikL}}{k^-} \right) \hat{\alpha}_{k,\omega}^{sc}, \quad (\text{F5})$$

to deduce:

$$\hat{T}_{\pm} = \int_{-\infty}^{\infty} \frac{dk}{2\pi} \frac{1/k^+ \pm e^{-ikL}/k^-}{(\omega + i\eta)^2 - c^2k^2} \left[\int_{-\infty}^{\infty} \frac{dk'}{2\pi} \frac{kC'}{C} \left(\frac{1}{k'^+} + \frac{e^{i(k-k')L}}{k'^-} \right) \hat{\alpha}_{k',\omega}^{sc} + \frac{i\omega}{\sqrt{c}} \sum_{j=1}^N e^{ikl_j} \kappa_j \hat{\sigma}_{\omega,j}^x \right]. \quad (\text{F6})$$

Using the integral results for any real parameter $a \geq 0$:

$$\int_{-\infty}^{\infty} \frac{dk}{2\pi} \frac{\cos(ka)}{(\omega + i\eta)^2 - c^2k^2} = \frac{\exp(ia\omega/c)}{2i(\omega + i\eta)c}, \quad \int_{-\infty}^{\infty} \frac{dk}{2\pi} \frac{\exp(\pm ika)}{(k \pm i\varepsilon)(\omega + i\eta)^2 - c^2k^2} = \pm \frac{\exp(ia\omega/c)}{2i(\omega + i\eta)^2}, \quad (\text{F7})$$

we obtain an algebraic linear equation for \hat{T}_{\pm} . Combining its solution with the input component, we find the result:

$$\int_{-\infty}^{\infty} \frac{dk}{2\pi} \left(\frac{1}{k^+} \pm \frac{e^{-ikL}}{k^-} \right) \hat{\alpha}_{k,\omega}^{sc} = \frac{2i\omega \int_{-\infty}^{\infty} \frac{dk}{2\pi} \left(\frac{1}{k^+} \pm \frac{e^{-ikL}}{k^-} \right) \hat{\alpha}_{k,\omega}^{in} + i\sqrt{c} \sum_{j=1}^N \kappa_j \hat{\sigma}_{\omega,j}^x [e^{i\omega l_j/c} \mp e^{i\omega(L-l_j)/c}]}{2i\omega - C'c(1 \pm e^{i\omega L/c})/C}. \quad (\text{F8})$$

After substitution of a linear combination of Eq.(F8) into the left hand side of (F3) and (F4), we obtain finally for the scattered wave operators:

$$\hat{A}_{\omega,+}^{sc}(0) = \sum_{\pm} \frac{C'(1 \pm e^{i\omega L/c})}{4C} \frac{2(1 \pm e^{-i\omega L/c})(\hat{A}_{\omega,+}^{in}(0) \pm e^{i\omega L/c} \hat{A}_{\omega,-}^{in}(0)) - \sum_{j=1}^N \kappa_j \hat{\sigma}_{\omega,j}^x [e^{i\omega l_j/c} \mp e^{i\omega(L-l_j)/c}]}{2i\omega - C'c(1 \pm e^{i\omega L/c})/C} - \sum_{j=1}^N e^{i\omega l_j/c} \frac{\kappa_j}{2c} \hat{\sigma}_{\omega,j}^x \quad (\text{F9})$$

$$\hat{A}_{\omega,-}^{sc}(-L) = \sum_{\pm} \pm \frac{C'(1 \pm e^{i\omega L/c})}{4C} \frac{2(1 \pm e^{-i\omega L/c})(\hat{A}_{\omega,+}^{in}(0) \pm e^{i\omega L/c} \hat{A}_{\omega,-}^{in}(0)) - \sum_{j=1}^N \kappa_j \hat{\sigma}_{\omega,j}^x [e^{i\omega l_j/c} \mp e^{i\omega(L-l_j)/c}]}{2i\omega - C'c(1 \pm e^{i\omega L/c})/C} - \sum_{j=1}^N e^{i\omega(L-l_j)/c} \frac{\kappa_j}{2c} \hat{\sigma}_{\omega,j}^x. \quad (\text{F10})$$

3. Transmission and reflection spectrum of the resonator

In the absence of any qubits, $\kappa_j = 0$. In this case, the transmission and reflection is found using the formula (F1):

$$S_{21}(\omega) = \frac{(2i\omega C/cC')^2}{(1 - 2i\omega C/cC')^2 - \exp(2iL\omega/c)} \quad (\text{F11})$$

$$S_{11}(\omega) = \frac{2i[2\omega C/cC' \cos(L\omega/c) + \sin(L\omega/c)]}{(1 - 2i\omega C/cC')^2 - \exp(2iL\omega/c)}, \quad (\text{F12})$$

that fulfills $|S_{21}(\omega)|^2 + |S_{11}(\omega)|^2 = 1$. The poles of Eqs.(F11) and (F12) are the same and correspond to the resonance frequencies ω_n and the half widths γ_n or damping. These are given in terms of the Lambert special function $W(k, x)$ as:

$$\omega_n - i\gamma_n/2 = i\frac{C'c}{2C} - i\frac{c}{L}W\left(\frac{1 - (-1)^n}{4} + \frac{n}{2}, \frac{C'L}{2C}(-1)^n \exp(C'L/2C)\right). \quad (\text{F13})$$

Figure 17 depicts these reflection and transmission response functions in the frequency ranges for the first three resonances. Although the broadening has been taken larger than usual, transmission is close to unity around the resonance while the reflection is dominant outside the resonance. Figure 18 represents the spectrum as a function

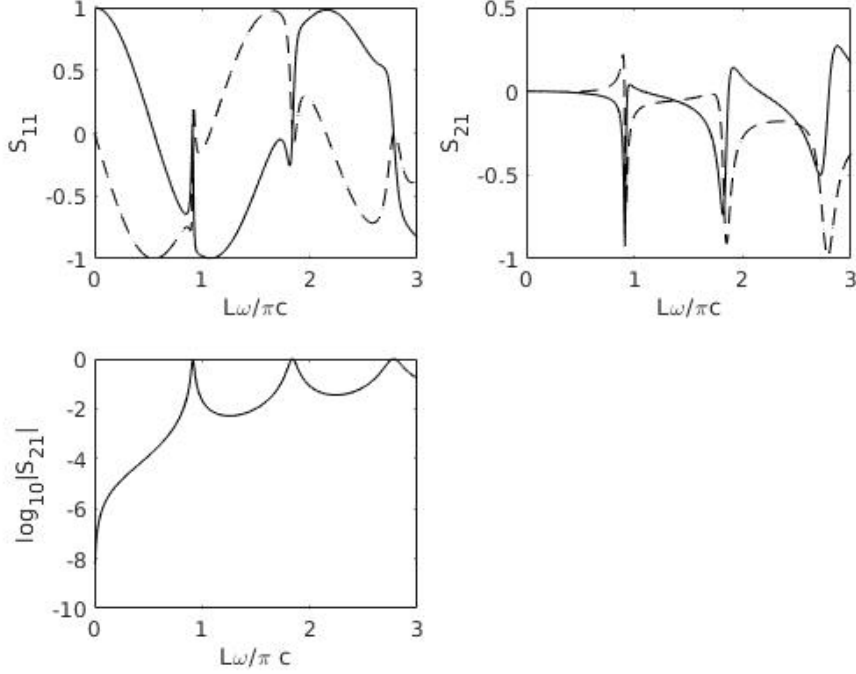


FIG. 17. Reflection and Transmission quadrature components for a cavity with $C/(C'L) = 20$. The solid curve is for the real part and the dashed curve is for the imaginary part (see Eq.(F11)). Lower: absolute value of the transmission in logarithm scale.

of $C/C'L$. For high quality factor ($C \rightarrow 0$), we recover the steady resonance $\omega_{n,0} = n\pi c/L$. For small capacitance $C \leq 0.04C'L$, we deduce the correction and a non-zero half width:

$$\omega_n - \omega_{n,0} \cong -\frac{2C}{C'L}\omega_{n,0}, \quad \gamma_n \cong \frac{4c}{L} \left(\frac{n\pi C}{LC'} \right)^2, \quad (\text{F14})$$

in agreement with the reference [34]. The quality factor and the peak intensity are:

$$Q_n = \frac{\omega_n}{\gamma_n} \cong \frac{C'^2 L^2}{2n\pi C^2} = \frac{C'L}{2\omega_{n,0} Z C^2}. \quad (\text{F15})$$

In comparison, in the equivalent circuit model proposed in [34], ones find $Q_n = \frac{C'L}{2\omega_n R_L C^2}$ where R_L is defined as the charge resistance outside the resonator. Since this resistance is generally adjusted to correspond to the impedance Z , we may conclude that both results are equivalent. However, we should point out that the model developed in [34] addresses one resonance only in the limit of weak capacitance $C \ll C'L$.

On the other hand, our expression does not account for the saturation effect at high quality factor [34]. The latter is likely due to the additional currents at the dielectric interfaces caused by the polarisation or some dissipation effect around the capacitance C due to the finite charge mobility.

Appendix G: The “artificial atom” without a cavity

1. Quantum stochastic and Master equation derivation

In this appendix we utilize our framework to reproduce the results for reflection and transmission of a “artificial atom” previously discussed in [13, 38]. The interest of the approach here is the use of a stochastic operator technique [36] that will be a useful tool to address the cavity case. We focus on the case without cavity ($C \rightarrow \infty$) and derive a master equation using the stochastic formalism.

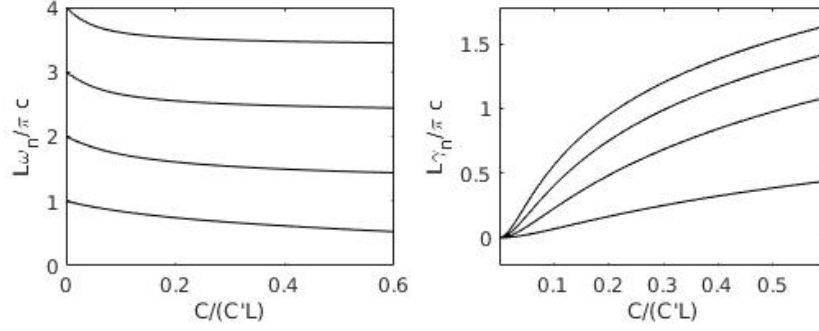


FIG. 18. Representation of the spectrum ω_n and the damping γ_n as a function of the capacitance at the cavity ends and $n = 1, 2, 3, 4$. For both graphics, n labels each curve from its lowest to its highest in ascending order.

Using the decomposition into input and scattering component, the Hamiltonian (E4) in spatial Fourier components form becomes:

$$\begin{aligned} \hat{H} = & \int_{-\infty}^{\infty} \frac{dk}{2\pi} c|k| \hat{a}_k^{\dagger in}(t) \hat{a}_k^{in}(t) + \int dr_z \frac{1}{2} \left[\hat{\alpha}^{sc^2}(r_z, t) - c^2 \hat{\alpha}^{sc}(r_z, t) \partial_z^2 \hat{\alpha}^{sc}(r_z, t) \right] \\ & + \sum_{j=1}^N \frac{\omega_j}{2} \hat{\sigma}_j^z(t) - \sqrt{c} \kappa_j \hat{\sigma}_j^x(t) \left(\int_{-\infty}^{\infty} \frac{dk}{2\pi} e^{ikl_j} \frac{\hat{a}_k^{in}(t) + \hat{a}_{-k}^{\dagger in}(t)}{\sqrt{2c|k|}} + \hat{\alpha}^{sc}(r_z, t) \right). \end{aligned} \quad (G1)$$

Here we define the time dependent free operator $\hat{a}_k(t) = e^{-ic|k|t + \eta t} \hat{a}_k$. Solving Eqs.(E15) and (E16) for $C \rightarrow \infty$, we find the scattered radiation amplitude from the qubits:

$$\hat{\alpha}_{\omega}^{sc}(r_z) = \int_{-\infty}^{\infty} \frac{dk}{2\pi} e^{ikr_z} \hat{\alpha}_{k,\omega}^{sc} = - \int_{-\infty}^{\infty} \frac{dk}{2\pi} \sum_{j=1}^N \frac{e^{ik(r_z + l_j)} \sqrt{c} \kappa_j \hat{\sigma}_{\omega,j}^x}{(\omega + i\eta)^2 - c^2 k^2} = \sum_{j=1}^N \frac{i \exp(i|r_z + l_j|\omega/c) \kappa_j \hat{\sigma}_{\omega,j}^x}{2\omega\sqrt{c}}. \quad (G2)$$

For a nearly monochromatic input field involving frequencies close and centered around $\omega > 0$, this last expression can be made Markovian in the time domain. As a result, we obtain the decomposition in positive and negative frequencies for the raising and lowering operators respectively:

$$\hat{\alpha}^{sc}(r_z, t) \cong \sum_{\pm} \sum_{j=1}^N \frac{\pm i \exp(\pm i|r_z + l_j|\omega/c) \kappa_j \hat{\sigma}_j^{\mp}(t)}{2\omega\sqrt{c}}, \quad \hat{\alpha}^{sc}(r_z, t) \cong \sum_{\pm} \sum_{j=1}^N \frac{\exp(\pm i|r_z + l_j|\omega/c) \kappa_j \hat{\sigma}_j^{\mp}(t)}{2\sqrt{c}}. \quad (G3)$$

This procedure amounts to neglecting the Lamb shift effect which appears to have an infrared divergence [36] that does not concern us here. Eliminating the scattering component (G3), we express the Hamiltonian (G1) only in terms of the input field components in the Schrödinger picture:

$$\hat{H} = \int_{-\infty}^{\infty} \frac{dk}{2\pi} c|k| \hat{a}_k^{\dagger in} \hat{a}_k^{in} + \sum_{j=1}^N \frac{\omega_j}{2} \hat{\sigma}_j^z - \kappa_j \int_{-\infty}^{\infty} \frac{dk}{2\pi} e^{ikl_j} \frac{\hat{\sigma}_j^+ \hat{a}_k^{in} + \hat{a}_{-k}^{\dagger in} \hat{\sigma}_j^-}{\sqrt{2|k|}} + \sum_{j,j'=1}^N \frac{\kappa'_{jj'}}{2} \hat{\sigma}_j^+ \hat{\sigma}_{j'}^-, \quad (G4)$$

where $\kappa'_{jj'} = \kappa_j \kappa_{j'} \sin(|l_j - l_{j'}|\omega/c)/\omega$ are the interaction constant responsible for mutual scattering between the qubits [13, 19]. For field frequencies ω close to the qubit frequencies, we can do the rotating wave approximation (RWA) by making the unitary transformation $\hat{a}_k^{in} \rightarrow e^{-i\omega t} \hat{a}_k^{in}$ and $\hat{\sigma}_i^{\pm} \rightarrow e^{\pm i\omega t} \hat{\sigma}_i^{\pm}$. The input field in the interaction term can be rewritten approximately as:

$$\int_{-\infty}^{\infty} \frac{dk}{2\pi} e^{ikl_j} \frac{e^{-ic|k|t} \hat{a}_k^{in}}{\sqrt{2|k|}} \cong \sum_{\pm} \frac{e^{\pm i\omega l_j/c}}{\sqrt{2\omega}} \hat{a}_{\pm,t}, \quad (G5)$$

where we define the forward (+) and backward (-) wave time dependent operators $\hat{a}_{\pm,t} = \int_{-\infty}^{\infty} \frac{d\omega'}{2\pi} e^{-i\omega't} \hat{a}_{\pm\omega'}^{in}$. The latter can be viewed as stochastic quantum variables expressing the influence of the vacuum noise on the artificial atoms. As long as we operate with frequency field around ω , they are held in a good approximation, the commutation

relation $[\hat{a}_{\pm,t}, \hat{a}_{\pm,t'}^\dagger] = \delta(t-t')$ and $[\hat{a}_{\pm,t}, \hat{a}_{\mp,t'}^\dagger] = 0$ and therefore time-dependent backward and forward quantum waves are independent. In the new base of operators using Eq.(G5), we find the time-dependent stochastic Hamiltonian:

$$\hat{H}'(t) = \sum_{j=1}^N -\frac{\delta\omega_j}{2} \hat{\sigma}_j^z + \sum_{j,j'=1}^N \frac{\kappa'_{jj'}}{2} \hat{\sigma}_j^+ \hat{\sigma}_{j'}^- + \sum_{j=1}^N \frac{\kappa_j}{\sqrt{2\omega}} \left[(e^{i\omega l_j/c} \hat{a}_{+,t} + e^{-i\omega l_j/c} \hat{a}_{-,t}) e^{i\omega t} \hat{\sigma}_j^+ + c.c. \right], \quad (\text{G6})$$

where we define the detuning $\delta\omega_j = \omega - \omega_j$. With a forward coherent input field of frequency ω and no backward input, one has $\langle \hat{A}_+^{in}(r_z, t) \rangle = \sqrt{Z} \langle \hat{I}^{in}(r_z, t) \rangle = \sqrt{Z} I_0 \cos[\omega(r_z/c - t)]$. For a well defined frequency the forward quantum stochastic field is decomposed into a coherent and an quantum radiation field contribution: $\hat{a}_{+,t} = -i\sqrt{2/c\omega} \langle \hat{A}_+^{in}(0, t) \rangle + \delta\hat{a}_{+,t}$. Using the Rabi frequency notation $\Omega_{\pm,j} = \pm \frac{\kappa_j \sqrt{Z} I_0}{i\omega}$, the Hamiltonian becomes:

$$\hat{H}'(t) = \hat{H}_S + \hat{H}_I(t), \quad \hat{H}_S = \sum_{j=1}^N -\frac{\delta\omega_j}{2} \hat{\sigma}_j^z - \sum_{\pm} \frac{\Omega_{\pm,\omega,j}}{2} \hat{\sigma}_j^{\pm} + \sum_{j,j'=1}^N \frac{\kappa'_{jj'}}{2} \hat{\sigma}_j^+ \hat{\sigma}_{j'}^- \quad (\text{G7})$$

$$\hat{H}_I(t) = \sum_{j=1}^N \frac{\kappa_j}{\sqrt{2\omega}} \left[(e^{i\omega l_j/c} \delta\hat{a}_{+,t} + e^{-i\omega l_j/c} \delta\hat{a}_{-,t}) e^{i\omega t} \hat{\sigma}_j^+ + c.c. \right]. \quad (\text{G8})$$

The last term is responsible for the relaxation of the excited qubit state into the ground state by spontaneous photon emission in vacuum. We eliminate the quantum radiation field component using the master equation for the density matrix $\hat{\rho}(t)$ developed up to the second order in the interaction:

$$\partial_t \hat{\rho}(t) + i[\hat{H}_S, \hat{\rho}(t)] = - \int_0^t d\tau \text{Tr}_B \left\{ [\hat{H}_I(t), [\hat{H}_I(t-\tau), \hat{\rho}_B(0) \hat{\rho}(t-\tau)]] \right\}. \quad (\text{G9})$$

In the absence of thermal field noise, we use the vacuum state $\hat{\rho}_B(0) = |0\rangle_B \langle 0|$ for the radiation. We make the Markovian approximation so that the effective equation is:

$$\partial_t \hat{\rho}(t) + i[\hat{H}_S, \hat{\rho}(t)] = - \int_0^\infty d\tau \text{Tr}_B \left\{ [\hat{H}_I(t), [\hat{H}_I(t-\tau), |0\rangle_B \langle 0| \hat{\rho}(t)]] \right\}. \quad (\text{G10})$$

Determining the matrix element over the vacuum state in the right hand side of Eq.(G10) and carry out the integration over τ (as done in detail for instance in [36]), we obtain the master equation [19]:

$$\partial_t \hat{\rho}(t) - i \left[\sum_{j=1}^N \frac{\delta\omega_j}{2} \hat{\sigma}_j^z + \sum_{\pm} \frac{\Omega_{\pm,\omega,j}}{2} \hat{\sigma}_j^{\pm} + \sum_{j,j'=1}^N \frac{\kappa'_{jj'}}{2} \hat{\sigma}_j^+ \hat{\sigma}_{j'}^-, \hat{\rho}(t) \right] = - \sum_{j,j'=1}^N \frac{\kappa_{jj'}}{2} \left[[\hat{\sigma}_j^+ \hat{\sigma}_{j'}^-, \hat{\rho}(t)]_+ - \hat{\sigma}_j^- 2\hat{\rho}(t) \hat{\sigma}_{j'}^+ \right], \quad (\text{G11})$$

where $\kappa_{jj'} = \kappa_j \kappa_{j'} \cos[(l_j - l_{j'})\omega/c]/\omega$ are the parameters responsible for the relaxation. This equation predicts the possibility of superradiance that has been experimentally analyzed in [13]. It however does not predict the dephasing due to the Josephson junctions themselves which needs to be considered phenomenologically.

2. One qubit without a cavity

Let us solve the master equation Eq.(G11) for the case of one qubit with detuning $\delta\omega_1$, $l_1 = 0$ and decay rate $\Gamma_1 \cong \kappa_1^2/\omega$ and show the equivalence of the approach with [38]. Using (F3) and (F4) for $C \rightarrow \infty$, and defining the average for any operator as $\langle \hat{O} \rangle = \text{Tr}(\hat{\rho}(t) \hat{O})$, we assume the steady state solution:

$$\langle \hat{\sigma}_1^\pm(t) \rangle = \sigma_\omega^\pm, \quad \langle \hat{\sigma}_1^z(t) \rangle = \sigma_\omega^z, \quad \langle \hat{A}_+^{in}(0, t) \rangle = \frac{i\omega\Omega_-}{2\kappa_1} e^{-i\omega t} + c.c., \quad \langle \hat{A}_\pm^{sc}(0, t) \rangle = -\frac{\kappa_1}{2} \sum_{\pm} \sigma_\omega^\pm e^{\pm i\omega t}. \quad (\text{G12})$$

Taking these various averages in Eq.(G11), we obtain for the steady state equations:

$$i(\Omega_+ \sigma_\omega^- - \Omega_- \sigma_\omega^+) + \Gamma_1(1 + \sigma_\omega^z) = 0, \quad (\delta\omega_1 \mp i\Gamma_1) \sigma_\omega^\pm = \frac{\sigma_\omega^z}{2} \Omega_{\pm}, \quad (\text{G13})$$

where for completeness we have added phenomenologically the dephasing rate $\Gamma_{1,\phi}$ in $\Gamma'_1 = \Gamma_1/2 + \Gamma_{1,\phi}$. We find the solution:

$$\sigma_{\omega}^z = -\frac{(\delta\omega_1^2 + \Gamma_1'^2)\Gamma_1}{(\delta\omega_1^2 + \Gamma_1'^2)\Gamma_1 + |\Omega_{\pm}|^2\Gamma_1'}, \quad \sigma_{\omega}^{\pm} = -\frac{1}{2} \frac{(\delta\omega_1 \pm i\Gamma_1')\Gamma_1\Omega_{\pm}}{(\delta\omega_1^2 + \Gamma_1'^2)\Gamma_1 + |\Omega_{\pm}|^2\Gamma_1'}. \quad (\text{G14})$$

For transmission and reflection, we obtain :

$$S_{11} = \frac{\langle \hat{A}_{\omega,-}^{\text{sc}}(0) \rangle}{\langle \hat{A}_{\omega,+}^{\text{in}}(0) \rangle} = -\frac{\Gamma_1}{2\Gamma_1'} \frac{1 + i\delta\omega_1/\Gamma_1'}{1 + (\delta\omega_1^2/\Gamma_1')^2 + |\Omega_{\pm}|^2/(\Gamma_1\Gamma_1')}, \quad S_{21} = \frac{\langle \hat{A}_{\omega,+}(0) \rangle}{\langle \hat{A}_{\omega,+}^{\text{in}}(0) \rangle} = 1 + S_{11}. \quad (\text{G15})$$

The unitary relation $|S_{11}|^2 = 1 - |S_{21}|^2$ is satisfied when $\Omega_{\pm} = 0$ and $\Gamma_{1,\phi} = 0$, otherwise it is violated by quantum wave fluctuations generated from fluorescence. In comparison with [38], the flux parameter ϕ_p defined from the relation $\hbar|\Omega_{\pm}| = \phi_p I_0$ satisfied the identical relation $\Gamma_1 = \omega\phi_p^2/(\hbar Z)$.

The hereafter master equation approach developed here does not take into account the relaxation to radiation modes other than the TEM mode in the waveguide. Using the experiment parameter value in [38], we can predict the relaxation rate for this mode and compare with the measured one Γ . From the input power is given by $\mathcal{P} = ZI_0^2/2$, we can indeed find the relation $\Gamma_1 = |\Omega_{\pm}|^2\hbar\omega_1/(2\mathcal{P})$. We estimate $\Gamma_1/\Gamma \sim 0.15$ within the order of magnitude of unity but with a discrepancy suggesting that other relaxation mechanisms should be taken into account for the specific qubit device used.

Appendix H: The quantum master equation in a cavity

1. Derivation

The qubit model derived in Appendix E is still too complex to be solved exactly as it involves a set of continuous modes interacting both with a cavity and with the qubits. Moreover, for the purpose of single photon detection, we must focus on a frequency range close to a cavity mode frequency which is itself close to the qubit frequency.

In this section, we use the method of the previous section to derive a master equation, with the difference that we need to isolate the cavity mode from the other external fields mode starting from the expression Eq.(E4). The advantage of using a cavity is the enhancement of the coupling of the qubits with the cavity mode field known as the Purcell effect.

We start by separating the electromagnetic field between the photon cavity mode and the other modes according to a discrete and a continuous field :

$$\hat{\alpha}(r_z, t) = \hat{\alpha}_d(r_z, t) + \hat{\alpha}_c(r_z, t), \quad \hat{\alpha}(r_z, t) = \hat{\alpha}_d(r_z, t) + \hat{\alpha}_c(r_z, t). \quad (\text{H1})$$

The discrete field operates on the interval $r_z \in [-L, 0]$ can be decomposed into discrete cavity modes of frequency $\omega_{n,0} = \pi nc/L$ as:

$$\hat{\alpha}_d(r_z, t) = \sum_{n=0}^{\infty} \sqrt{\frac{2 - \delta_{n,0}}{L}} \cos\left(\frac{\pi nr_z}{L}\right) \frac{\hat{a}_n(t) + \hat{a}_n^\dagger(t)}{\sqrt{2\omega_{n,0}}}, \quad \dot{\hat{\alpha}}_d(r_z, t) = \sum_{n=0}^{\infty} \sqrt{\frac{2 - \delta_{n,0}}{L}} \cos\left(\frac{\pi nr_z}{L}\right) \sqrt{\omega_{n,0}} \frac{\hat{a}_n(t) - \hat{a}_n^\dagger(t)}{\sqrt{2i}}. \quad (\text{H2})$$

Using the projector formalism to the full quantum operator, we obtain an explicit expression for each field element of the decomposition:

$$\mathcal{P}\hat{\alpha}(r_z, t) = \hat{\alpha}_d(r_z, t) = \sum_{n=0}^{\infty} \frac{2 - \delta_{n,0}}{L} \cos\left(\frac{\pi nr_z}{L}\right) \int_{-L}^0 dr'_z \cos\left(\frac{\pi nr'_z}{L}\right) \hat{\alpha}(r_z, t), \quad \mathcal{Q} = 1 - \mathcal{P} \quad (\text{H3})$$

$$\mathcal{Q}\hat{\alpha}(r_z, t) = \hat{\alpha}_c(r_z, t), \quad \mathcal{P}\hat{\alpha}(r_z, t) = \hat{\alpha}_d(r_z, t), \quad \mathcal{Q}\hat{\alpha}(r_z, t) = \hat{\alpha}_c(r_z, t). \quad (\text{H4})$$

Inverting the relations Eqs.(H2) and combining with Eq.(H3), the annihilation operator of the cavity mode is expressed to the full quantum field operator through:

$$\hat{a}_n(t) = \sqrt{\frac{2 - \delta_{n,0}}{L}} \int_{-L}^0 dr'_z \cos\left(\frac{\pi nr'_z}{L}\right) \frac{i\hat{\alpha}(r_z, t) + \omega_{n,0}\hat{\alpha}(r_z, t)}{\sqrt{2\omega_{n,0}}}. \quad (\text{H5})$$

Using the notation $\hat{a}_{n,\omega}$ in the time Fourier transform, this relation combined together with the Heisenberg equations (E15, E16) allows to deduce an equation for this discrete set of cavity operators. We find for $n \neq 0$:

$$(\omega + i\eta - \omega_{n,0})\hat{a}_{n,\omega} = \frac{1}{\sqrt{L\omega_{n,0}}} \left(c^2 \int_{-\infty}^{\infty} \frac{dk}{2\pi i} k(1 - (-1)^n e^{-ikL}) \hat{\alpha}_{k,\omega} - \sqrt{c} \sum_{j=1}^N \kappa_j \cos(\omega_{n,0} l_j / c) \hat{\sigma}_{\omega,j}^x \right). \quad (\text{H6})$$

To work out the right hand side of this last equation, we use again the Heisenberg equations to derive the equality:

$$\int_{-\infty}^{\infty} \frac{dk}{2\pi i} k(1 - (-1)^n e^{-ikL}) \hat{\alpha}_{k,\omega} = \frac{i\omega}{c^2} \int_{-\infty}^{\infty} \frac{dk}{2\pi i} \left(\frac{1}{k^+} - \frac{(-1)^n e^{-ikL}}{k^-} \right) \hat{\alpha}_{k,\omega}. \quad (\text{H7})$$

By combining this last relation with Eq.(F8), we find the exact result:

$$\begin{aligned} \hat{a}_{n,\omega} = & \sqrt{c} \sum_j \kappa_j \frac{\cos(\frac{\omega l_j}{c}) - \cos(\frac{\omega_{n,0} l_j}{c})}{\omega - \omega_{n,0}} \hat{\sigma}_{\omega,j}^x + \frac{1}{\omega - \omega_{n,0}} \frac{1}{\sqrt{L\omega_{n,0}}} \frac{1 - (-1)^n e^{-i\omega L/c}}{2i(\omega + i0) - C'c(1 - (-1)^n e^{ikL})/C} \\ & \times \left[-2i\omega (\hat{A}_{\omega,-}^{in}(0) + (-1)^n \hat{A}_{\omega,+}^{in}(-L)) - \sum_{j=1}^N \left(\cos(\omega l_j / c) (i\omega - \frac{C'c}{C}) + \omega \sin(\omega l_j / c) \right) \sqrt{c\kappa_j} \hat{\sigma}_{\omega,j}^x \right]. \end{aligned} \quad (\text{H8})$$

An inspection of this formula shows that the poles is located at $\omega_n - i\frac{\gamma_n}{2}$ with $\omega_n = \omega_{n,0} + \Delta\omega_n$ and that the pole at $\omega_{n,0}$ is apparent. Close to a resonance for $n \neq 0$, the formula for the operator is approximated as:

$$\hat{a}_{n,\omega} \cong \frac{i\sqrt{\frac{\gamma_n}{4c\omega_n}} (\hat{A}_{\omega,-}^{in}(0) + (-1)^n \hat{A}_{\omega,+}^{in}(-L)) - \sum_{j=1}^N \sqrt{1/\pi n} \cos(\omega_{n,0} l_j / c) \sqrt{c\kappa_j} \hat{\sigma}_{\omega,j}^-}{\omega - (\omega_n - i\gamma_n/2)} \quad (\text{H9})$$

$$\cong \frac{-\sqrt{\gamma_n/2} (\hat{a}_{\omega/c} + \hat{a}_{-\omega/c}) - \sum_{j=1}^N \sqrt{1/\pi n} \cos(n\pi l_j / Lc) \sqrt{c\kappa_j} \hat{\sigma}_{\omega,j}^-}{\omega - (\omega_n - i\gamma_n/2)}, \quad (\text{H10})$$

where we used the relation (E22) approximated for frequencies close to ω_n . Similarly to the appendix (G), we define the time dependent stochastic operators $\hat{a}_{\pm,t} = \int_{-\infty}^{\infty} \exp(-i\omega t) \hat{a}_{\pm\omega/c} d\omega / 2\pi$ valid for frequencies around the resonance frequency ω_n and identified as the vacuum noise operators of ingoing wave from the left + and right - of the waveguide. Using this definition and reversing the denominator into the left hand side, the Eq.(H10) can be rewritten back in the time domain to become a quantum stochastic Langevin-like equation:

$$[i\partial_t - (\omega_n - i\frac{\gamma_n}{2})] \hat{a}_n(t) = -\sqrt{\gamma_n/2} \sum_{\pm} \hat{a}_{\pm,t} - \sum_{j=1}^N \frac{\kappa_j}{\sqrt{\pi n}} \cos(n\pi l_j / Lc) \hat{\sigma}_j^-. \quad (\text{H11})$$

Similarly to Appendix G, the stochastic field is decomposed into its coherent and incoherent part $\hat{a}_{\pm,t} = -i\sqrt{2/\omega} \langle \hat{A}_{\pm}^{in}(0,t) \rangle + \delta \hat{a}_{\pm,t}$ where we use the notation $A_{\pm}^{in}(0,t) = \langle \hat{A}_{\pm}^{in}(0,t) \rangle$. We neglect other noise channels (TM or TE or spherical wave) as topologically less favorable for effective interaction. Using the analogy based on stochastic formalism, we obtain eventually the equivalent Hamiltonian:

$$\hat{H}(t) = \hat{H}_S(t) + \hat{H}_I(t) = \hat{H}_c + \hat{H}_{ext}(t) + \hat{H}_I(t) \quad (\text{H12})$$

$$\hat{H}_c = \sum_{j=1}^N -\frac{\delta\omega_j}{2} \hat{\sigma}_j^z - \sum_{n=0}^{\infty} \frac{\kappa_j}{\sqrt{\pi n}} \cos(\pi l_j / L) (\hat{a}_n^\dagger \hat{\sigma}_j^- + \hat{a}_n \hat{\sigma}_j^+) + (\omega_n - \omega) \hat{a}_n^\dagger \hat{a}_n \quad (\text{H13})$$

$$\hat{H}_{ext}(t) = i \sum_{\pm} \sqrt{\frac{\gamma_n}{\omega}} (A_{\pm}^{in*}(0,t) \hat{a}_n e^{-i\omega t} - A_{\pm}^{in}(0,t) \hat{a}_n^\dagger e^{i\omega t}) \quad (\text{H14})$$

$$\hat{H}_I(t) = -\sqrt{\frac{\gamma_n}{2}} \sum_{\pm} (\delta \hat{a}_{\pm,t}^\dagger \hat{a}_n e^{-i\omega t} + \hat{a}_n^\dagger e^{i\omega t} \delta \hat{a}_{\pm,t}). \quad (\text{H15})$$

It contains the Jaynes-Cumming contribution \hat{H}_c with the addition of the external field term $\hat{H}_{ext}(t)$ and the interaction with the vacuum field $\hat{H}_I(t)$. Note that these Eqs.(H12-H15) are formulated in the RWA picture with the substitution $\hat{a}_n \rightarrow e^{-i\omega t} \hat{a}_n$ and $\hat{\sigma}_j^\pm \rightarrow e^{\pm i\omega t} \hat{\sigma}_j^\pm$. To prove the equivalence of this last Hamiltonian with the Langevin

equation (H11), we derive the Heisenberg equations using an Ito-like procedure to obtain the damping term [36]. For a finite time interval, the Heisenberg equation for $\hat{a}_n(t)$ is up to the second order:

$$\frac{\hat{a}_n(t + \Delta t) - \hat{a}_n(t)}{\Delta t} = \frac{1}{i\Delta t} \int_0^{\Delta t} dt' [\hat{H}(t'), \hat{a}_n(t)] - \frac{1}{2\Delta t} \int_0^{\Delta t} dt' \int_0^{t'} dt'' [\hat{H}(t'), [\hat{H}(t''), \hat{a}_n(t)]] + \mathcal{O}(\Delta t^2). \quad (\text{H16})$$

It appears that the second term expansion has a finite contribution in the limit $\Delta t \rightarrow 0$. We notice the nontrivial contribution:

$$\frac{1}{2\Delta t} \int_0^{\Delta t} dt' \int_0^{t'} dt'' [\hat{H}_I(t'), [\hat{H}_I(t''), \hat{a}_n(t)]] \rightarrow \frac{\gamma_n}{\Delta t} \int_0^{\Delta t} dt' \int_0^{t'} dt'' \delta(t'' - t') \hat{a}_n(t') = \frac{\gamma_n}{2\Delta t} \int_0^{\Delta t} dt' \hat{a}_n(t) = \frac{\gamma_n}{2} \hat{a}_n(t), \quad (\text{H17})$$

which corresponds to the damping term of Eq.(H11). The Heisenberg equations for $\hat{\sigma}_j^\pm(t)$ and $\hat{\sigma}_j^z(t)$ are also recovered using (H12) when the quantum radiation field is approximated by its cavity mode component.

For the particular case $n = 1$, the cavity mode is at frequency $\omega_c = \omega_1 \cong \pi c/L$ and damping $\gamma_c = \gamma_1$. The associated system Hamiltonian is:

$$\hat{H}_S(t) = \sum_{j=1}^N -\frac{\delta\omega_j}{2} \hat{\sigma}_j^z - g_j (\hat{a}_1^\dagger \hat{\sigma}_j^- + \hat{a}_1 \hat{\sigma}_j^+) + (\omega_c - \omega) \hat{a}_1^\dagger \hat{a}_1 + i \sum_{\pm} \sqrt{\frac{\gamma_c}{\omega}} (A_{\pm}^{in*}(0, t) \hat{a}_1 e^{-i\omega t} - A_{\pm}^{in}(0, t) \hat{a}_1^\dagger e^{i\omega t}), \quad (\text{H18})$$

where we renormalized the coupling constant into $g_j = \kappa_j \cos(\pi l_j/L)/\sqrt{\pi}$. From this expression, we note that the transmon should be placed ideally close to a cavity end for a maximum coupling to the field. Again we repeat the procedure of the previous section to derive a master equation with the elimination of the radiation field but using instead the interaction term (H15) for $n = 1$. Adding the dephasing $\Gamma_{\phi,j}$ due to Josephson junction and the decay rate Γ_j to a transverse channel (due to other cavity modes), we obtain:

$$\begin{aligned} & \partial_t \hat{\rho}(t) + i[\hat{H}_S, \hat{\rho}(t)] \\ &= -\frac{\gamma_c}{2} \left[\{\hat{a}_1^\dagger \hat{a}_1, \hat{\rho}(t)\} - 2\hat{a}_1 \hat{\rho}(t) \hat{a}_1^\dagger \right] - \sum_{j=1}^N \left(\frac{\Gamma_j}{2} + \Gamma_{\phi,j} \right) \{ \hat{\sigma}_j^+ \hat{\sigma}_j^-, \hat{\rho}(t) \} - \Gamma_j \hat{\sigma}_j^- \hat{\rho}(t) \hat{\sigma}_j^+. \end{aligned} \quad (\text{H19})$$

This simulation is different from the one used for the artificial atom. Now in addition to the relaxation times for decay $T_{1,j} = 1/\Gamma_j$ and for pure dephasing $T_{2,j} = 1/\Gamma_{\phi,j}$, there is a lifetime for the photon within the cavity $T_{ph} = 1/\gamma_c$.

Unlike the model in the absence of cavity Eq.(H19), the qubits interact more strongly only with one field mode. This Purcell effect generates the more complex dressed Jaynes-Cumming Hamiltonian spectrum with anticrossing curves when the qubit frequency is changed by an external magnetic field [35]. The presence of a cavity increases the decoherence time of the whole system as a result of the relaxation mainly due to the cavity field mode [13].

2. Reflection and Transmission for one cavity mode

The master equation (H19) describes only the dynamics of qubit due to an external field. However, we need to specify another relation with the scattered field generated from the qubit evolution. Restricting the frequency domain close to the first cavity mode, the operator relation (F9) and (F10) is approximated for a forward wavevector incident field only as:

$$\hat{A}_{\omega,+}(0) = -\sum_{\pm} \frac{(\gamma_c/2) \hat{A}_{\omega,+}^{in}(0) \pm i\sqrt{\gamma_c\omega_c}/2 \sum_{j=1}^N g_j \hat{\sigma}_{\omega,j}^\mp}{i(\omega - (\pm\omega_c - i\gamma_c/2))} = \hat{A}_{\omega,-}^{sc}(-L) - \hat{A}_{\omega,+}^{in}(0). \quad (\text{H20})$$

Carry out the quantum average of the scattered operators, the transmission is:

$$S_{21} = \frac{\langle \hat{A}_{\omega,+}(0) \rangle}{\langle \hat{A}_{\omega,+}^{in}(0) \rangle} = \sum_{\pm} \frac{-1}{\omega - (\pm\omega_c - i\gamma_c/2)} \left[i\gamma_c/2 \pm \frac{\sqrt{\gamma_c\omega_c}}{2} \sum_{j=1}^N \frac{g_j \langle \hat{\sigma}_{\omega,j}^\mp \rangle}{\langle \hat{A}_{\omega,+}^{in}(0) \rangle} \right], \quad (\text{H21})$$

and the reflection is:

$$S_{11} = \frac{\langle \hat{A}_{\omega,-}^{sc}(-L) \rangle}{\langle \hat{A}_{\omega,+}^{in}(0) \rangle} = 1 - \sum_{\pm} \frac{1}{\omega - (\pm\omega_c - i\gamma_c/2)} \left[i\gamma_c/2 \pm \frac{\sqrt{\gamma_c\omega_c}}{2} \sum_{j=1}^N \frac{g_j \langle \hat{\sigma}_{\omega,j}^\mp \rangle}{\langle \hat{A}_{\omega,+}^{in}(0) \rangle} \right]. \quad (\text{H22})$$

3. The Schrieffer-Wolff transformation for many qubits

For the purpose of a quantum non-demolition measurement, the qubits frequencies must depart strongly from the cavity frequency $|\omega_i - \omega_c| \gg g_i$ but still remains small in comparison to the cavity frequency $|\omega_i - \omega_c| \ll \omega_c$. In that situation, by means of the Schrieffer-Wolff, we can rewrite the Hamiltonian in a diagonal form for interaction between the dressed qubit and cavity states. We start from the Hamiltonian (H18) in absence of external field:

$$\hat{H}_c = \hat{H}_0 + \hat{V} = (\omega_c - \omega)\hat{a}_1^\dagger\hat{a}_1 + \sum_{j=1}^N -\frac{\delta\omega_j}{2}\hat{\sigma}_j^z - g_j(\hat{a}_1^\dagger\hat{\sigma}_j^- + \hat{a}_1\hat{\sigma}_j^+). \quad (\text{H23})$$

The Schrieffer-Wolff transformation consists in finding a unitary transformation $e^{\hat{S}}$ such that: $[\hat{H}_0, \hat{S}] = \hat{V}$ so that the new Hamiltonian $\hat{H}'_c = e^{\hat{S}}\hat{H}_c e^{-\hat{S}} = \hat{H}_0 + [\hat{S}, \hat{V}]/2$ is in the second order in \hat{V} or g_j . We find the operator:

$$\hat{S} = -\sum_{j=1}^N \frac{-g_j}{\omega_j - \omega_c} (\hat{\sigma}_j^+ \hat{a}_1 - \hat{a}_1^\dagger \hat{\sigma}_j^-). \quad (\text{H24})$$

Up to the second order, the qubit and field operators become under this transformation:

$$\hat{\sigma}'_j \cong e^{\hat{S}} \hat{\sigma}_j e^{-\hat{S}} = \hat{\sigma}_j - \frac{g_j}{\omega_j - \omega_c} (\hat{a}_1^\dagger + \hat{a}_1) \hat{\sigma}_j^z, \quad \hat{a}'_1 \cong e^{\hat{S}} \hat{a}_1 e^{-\hat{S}} = \hat{a}_1 - \sum_{j=1}^N \frac{g_j}{\omega_j - \omega_c} \hat{\sigma}_j^-. \quad (\text{H25})$$

Inserting this result into the transformed Hamiltonian, we obtain finally:

$$\hat{H}'_c \cong \sum_{j=1}^N -\frac{\delta\omega_j}{2} \hat{\sigma}_j^z + \left(\sum_{j,j'=1}^N \frac{g_j g_{j'} (\hat{\sigma}_j^+ \hat{\sigma}_{j'}^- + \hat{\sigma}_{j'}^+ \hat{\sigma}_j^-)}{2(\omega_j - \omega_c)} + \sum_{j=1}^N \chi_j \hat{a}_1^\dagger \hat{a}_1 \hat{\sigma}_j^z \right) + (\omega_c - \omega) \hat{a}_1^\dagger \hat{a}_1, \quad (\text{H26})$$

where $\chi_j = g_j^2/(\omega_j - \omega_c)$ is the non-demolition interaction coupling responsible for the Stark shift of the qubit. We note also an additional term of interaction between the qubits that we shall neglect as its amplitude contribution is small in comparison to the detuning energy for a frequency close to cavity frequency $\omega = \omega_c$. The reverse transformation are:

$$\hat{\sigma}_j^- = \hat{\sigma}'_j^- + \frac{g_j}{\omega_j - \omega_c} \hat{a}'_1 \hat{\sigma}'_j^z, \quad \hat{a}_1 = \hat{a}'_1 + \sum_{j=1}^N \frac{g_j}{\omega_j - \omega_c} \hat{\sigma}'_j^-. \quad (\text{H27})$$

Appendix I: Transmission for various profiles of the signal photon

1. Signal field and probe field

In this appendix, we perform the explicit calculation of the linear transmission of an off-resonance probe field of frequency ω_p for various profile of the signal photon field of frequency ω , namely the coherent state, the incoherent state and the thermal state. For each of these cases, we provide analytical formulas that can be directly compared to experiments.

2. Model 1: Coherent state detection

When the signal to be detected has the profile of a coherent state, the external field is expressed in terms of the coherent unknown mode and a probe mode:

$$\langle \hat{A}_+^{in}(0, t) \rangle = i\sqrt{\frac{\omega}{\gamma_c}} \left(\frac{\Omega}{2} e^{-i\omega t} + \frac{\Omega_p}{2} e^{-i\omega_p t} \right) + c.c.. \quad (\text{I1})$$

The external field term (H14) containing the unknown field and the probe field becomes under the Schrieffer-Wolff transformation:

$$\begin{aligned} \hat{H}'_{ext}(t) &= e^{\hat{S}} \hat{H}_{ext}(t) e^{-\hat{S}} \\ &= \frac{\Omega}{2} \left(\hat{a}_1 + \hat{a}_1^\dagger + \sum_{j=1}^N \frac{g_j}{\omega_j - \omega_c} \hat{\sigma}_j^x \right) + \frac{\Omega_p^*}{2} e^{i(\omega_p - \omega)t} \left(\hat{a}_1 - \sum_{j=1}^N \frac{g_j}{\omega_j - \omega_c} \hat{\sigma}_j^- \right) + \frac{\Omega_p}{2} e^{-i(\omega_p - \omega)t} \left(\hat{a}_1^\dagger + \sum_{j=1}^N \frac{g_j}{\omega_j - \omega_c} \hat{\sigma}_j^+ \right). \end{aligned} \quad (I2)$$

Similarly, defining $\hat{\rho}'(t) = e^{\hat{S}} \hat{\rho}(t) e^{-\hat{S}}$, the master equation (H19) becomes:

$$\begin{aligned} \partial_t \hat{\rho}'(t) + i[\hat{H}'_c + \hat{H}'_{ext}(t), \hat{\rho}'(t)] &= \\ -\frac{\gamma_c}{2} \left[\left\{ \hat{a}_1^\dagger \hat{a}_1 + \sum_{j,j'=1}^N \frac{g_j g_{j'}}{(\omega_j - \omega_c)(\omega_{j'} - \omega_c)} \hat{\sigma}_j^+ \hat{\sigma}_{j'}^-, \hat{\rho}'(t) \right\} - 2\hat{a}_1 \hat{\rho}'(t) \hat{a}_1^\dagger - 2 \sum_{j=1}^N \frac{g_j}{\omega_j - \omega_c} \hat{\sigma}_j^- \hat{\rho}'(t) \sum_{j'=1}^N \frac{g_{j'}}{\omega_{j'} - \omega_c} \hat{\sigma}_{j'}^+ \right] \\ - \sum_{j=1}^N \left(\frac{\Gamma_j}{2} + \Gamma_{\phi,j} \right) \left\{ \hat{\sigma}_j^+ \hat{\sigma}_j^- + \frac{g_j^2}{(\omega_j - \omega_c)^2} \hat{a}_1^\dagger \hat{a}_1, \hat{\rho}'(t) \right\} - \Gamma_j \left(\hat{\sigma}_j^- \hat{\rho}'(t) \hat{\sigma}_j^+ + \frac{g_j^2}{(\omega_j - \omega_c)^2} \hat{a}_1 \hat{\sigma}_j^z \hat{\rho}'(t) \hat{a}_1^\dagger \hat{\sigma}_j^z \right). \end{aligned} \quad (I3)$$

In this equation, we shall neglect the smaller higher order terms in g_j^2 . We define β as the amplitude of the coherent field to be detected inside the cavity. It distinguishes from the quantum part of the field operator. Using the Glauber-Sudershan transformation \hat{D} , we rewrite this field as:

$$\hat{a}_1 \rightarrow \hat{D}^\dagger \hat{a}_1 \hat{D} = \hat{a}_1 + \beta = \hat{a}_1 + \frac{\Omega/2}{\omega - \omega_c^* + i\gamma_c/2}, \quad (I4)$$

where $\omega_c^* = \omega_c - \sum_{j=1}^N \chi_j$ is the renormalized cavity frequency due to the presence of the qubits when they are in the ground state. Using $\hat{\rho}''(t) = \hat{D}^\dagger \hat{\rho}'(t) \hat{D}$, we reduce the master equation (I3) into:

$$\begin{aligned} \partial_t \hat{\rho}''(t) + i[\hat{H}^{(2)}(t), \hat{\rho}''(t)] &= -\frac{\gamma_c}{2} \left[\left\{ \hat{a}_1^\dagger \hat{a}_1, \hat{\rho}''(t) \right\} - 2\hat{a}_1 \hat{\rho}''(t) \hat{a}_1^\dagger \right] - \sum_{j=1}^N \left(\frac{\Gamma_j}{2} + \Gamma_{\phi,j} \right) \left\{ \hat{\sigma}_j^+ \hat{\sigma}_j^-, \hat{\rho}''(t) \right\} - \Gamma_j \hat{\sigma}_j^- \hat{\rho}''(t) \hat{\sigma}_j^+ \\ \hat{H}^{(2)}(t) &= \sum_{j=1}^N -\frac{\delta\omega_j}{2} \hat{\sigma}_j^z + \sum_{j=1}^N \chi_j (\hat{a}_1^\dagger + \beta^*) (\hat{a}_1 + \beta) (\hat{\sigma}_j^z + 1) + (\omega_c^* - \omega) \hat{a}_1^\dagger \hat{a}_1 + \frac{\Omega}{2} \sum_{j=1}^N \frac{g_j}{\omega_j - \omega_c} \hat{\sigma}_j^x \\ &+ \frac{\Omega_p^*}{2} e^{i(\omega_p - \omega)t} \left(\hat{a}_1 + \sum_{j=1}^N \frac{g_j}{\omega_j - \omega_c} \hat{\sigma}_j^- \right) + \frac{\Omega_p}{2} e^{-i(\omega_p - \omega)t} \left(\hat{a}_1^\dagger + \sum_{j=1}^N \frac{g_j}{\omega_j - \omega_c} \hat{\sigma}_j^+ \right). \end{aligned} \quad (I5)$$

The term proportional to $\hat{\sigma}_j^x$ can be neglected for sufficiently strong detuning $\delta\omega_j$. Without the probe field, in this dressed picture, the vacuum field together with qubit in their ground state correspond to the solution of this master equation:

$$\hat{\rho}_0 = |0\rangle\langle 0| \prod_{j=1}^N \frac{1 - \hat{\sigma}_j^z}{2}. \quad (I6)$$

A non-zero probe field Ω_p introduces a perturbation of the form:

$$\hat{\rho}_1(t) = \hat{\rho}''(t) - \hat{\rho}_0 = e^{-i(\omega_p - \omega)t} \sum_{j=1}^N \left(\frac{1 - \hat{\sigma}_j^z}{2} |\Psi_{j0}\rangle\langle 0| + \hat{\sigma}_j^+ |\Psi_j\rangle\langle 0| \right) \prod_{j' \neq j=1}^N \frac{1 - \hat{\sigma}_{j'}^z}{2} + c.c.. \quad (I7)$$

The insertion of the latter in Eq.(I5) imposes that the unknown wave function states solve the non-Hermitian state equations:

$$\left[(\omega_p - \omega) - (\omega_c^* - \omega - i\gamma_1/2) \hat{a}_1^\dagger \hat{a}_1 \right] |\Psi_{j0}\rangle = \frac{\Omega_p}{2} \hat{a}_1^\dagger |0\rangle, \quad (I8)$$

$$\left[(\omega_p - \omega_j) - 2\chi_j (\hat{a}_1^\dagger + \beta^*) (\hat{a}_1 + \beta) - (\omega_c^* - \omega - i\gamma_1/2) \hat{a}_1^\dagger \hat{a}_1 + i(\Gamma_j/2 + \Gamma_{\phi,j}) \right] |\Psi_j\rangle = \frac{\Omega_p}{2} \frac{g_j}{\omega_j - \omega_c} |0\rangle. \quad (I9)$$

The former wave function $|\Psi_{j0}\rangle$ has a simple solution:

$$|\Psi_{j0}\rangle = \frac{\Omega_p/2}{(\omega_p - \omega_c^* + i\gamma_1/2)} \hat{a}_1^\dagger |0\rangle. \quad (\text{I10})$$

It corresponds to the free part propagation of probe field transmission and therefore insensitive to the presence of the signal photon field. The latter wave function however is sensitive to the qubit dynamics whose the resonance frequency has a Stark shift depending on the coherent signal field. Inverting formally the operator in the left hand side of (I9), we obtain a formal solution for $|\Psi_j\rangle$ which, after substitution into (I7), gives explicit expressions for the expectation of the lowering and raising qubit operators. Defining the prime representation, we obtain

$$\begin{aligned} g_j \langle \hat{\sigma}_{\omega_p, j}^- \rangle' &= g_j \text{Tr}(\hat{\rho}_1(t) \hat{\sigma}_j^-) e^{i(\omega_p - \omega)t} \\ &= \frac{\Omega_p}{2} \chi_j \langle 0 | \left[(\omega_p - \omega_j) - 2\chi_j (\hat{a}_1^\dagger + \beta^*) (\hat{a}_1 + \beta) - (\omega_c^* - \omega - i\gamma_c/2) \hat{a}_1^\dagger \hat{a}_1 + i(\Gamma_j/2 + \Gamma_{\phi, j}) \right]^{-1} |0\rangle, \end{aligned} \quad (\text{I11})$$

and similarly $\langle \hat{\sigma}_{\omega, j}^- \rangle' = \langle \hat{\sigma}_{j, -\omega}^+ \rangle'$. The vacuum matrix element of the non-Hermitian propagator is determined explicitly. Defining the parameters:

$$w_0 = (\omega_p - \omega_j) - 2\chi_j |\beta|^2 + i(\Gamma_j/2 + \Gamma_{\phi, j}), \quad w = \omega_c^* + 2\chi_j - \omega - i\gamma_c/2, \quad b = 2\chi_j \beta, \quad (\text{I12})$$

and using the creation-annihilation operator algebra, we calculate successively:

$$\begin{aligned} \langle 0 | \frac{1}{w_0 - w \hat{a}_1^\dagger \hat{a}_1 - b \hat{a}_1^\dagger - b^* \hat{a}_1} |0\rangle &= -i \int_0^\infty dt \langle 0 | \exp[i(w_0 - w \hat{a}_1^\dagger \hat{a}_1 - b \hat{a}_1^\dagger - b^* \hat{a}_1)t] |0\rangle \\ &= -i \int_0^\infty dt \langle 0 | e^{i[w_0 - w(\hat{a}_1^\dagger + b^*/w)(\hat{a}_1 + b/w) + |b|^2/w]t} |0\rangle = -i \int_0^\infty dt \langle b/w | e^{i[w_0 - w \hat{a}_1^\dagger \hat{a}_1 + |b|^2/w]t} |b/w\rangle \\ &= -i \int_0^\infty dt \langle b/w | e^{i[w_0 + |b|^2/w]t} |e^{-iwt} b/w\rangle = -i \int_0^\infty dt e^{i[w_0 + |b|^2/w]t} e^{-(1 - \exp(-iwt))|b|^2/w^2} \\ &= e^{-|b|^2/w^2} \sum_{n=0}^\infty \frac{(|b|^2/w^2)^n}{n!} \frac{(-1)^n}{nw - w_0 - |b|^2/w} = \frac{e^{-|b|^2/w^2}}{w_0 + |b|^2/w} {}_1F_1(-w_0/w - |b|^2/w^2; 1 - w_0/w - |b|^2/w^2; |b|^2/w^2), \end{aligned} \quad (\text{I13})$$

where ${}_1F_1(a; b; z)$ is the hypergeometric function. Using this result with the appropriate parameter substitution into Eq.(I11), we obtain a formula with a sideband spectrum:

$$\begin{aligned} g_j \langle \hat{\sigma}_{\omega_p, j}^- \rangle' &= \frac{\Omega_p}{2} \chi_j e^{-W} \sum_{n=0}^\infty \frac{W^n}{n!} \\ &\times \frac{1}{(\omega_p - \omega_j) - 2\chi_j (|\beta|^2 + n) - n(\omega_c^* - \omega - i\gamma_c/2) + i(\Gamma_j/2 + \Gamma_{\phi, j}) + \frac{4\chi_j^2 |\beta|^2}{(\omega_c^* + 2\chi_j - \omega - i\gamma_c/2)}} \end{aligned} \quad (\text{I14})$$

$$\stackrel{\beta=0}{=} \frac{\Omega_p}{2} \chi_j \frac{1}{\omega_p - \omega_j + i(\Gamma_j/2 + \Gamma_{\phi, j})},$$

$$W = \frac{4\chi_j^2 |\beta|^2}{(\omega_c^* + 2\chi_j - \omega - i\gamma_c/2)^2}. \quad (\text{I15})$$

The pole of each term in the infinite sum allows to identify the resonance frequencies and their width revealing a comb structure (as for example in Fig.2). Alternatively we can use also the hypergeometric function in (I13) for a more direct computation. For the case when $\chi_j \gg \gamma_c$ and matching frequency $\omega = \omega_c$, we find the more explicit formula:

$$g_j \langle \hat{\sigma}_{\omega_p, j}^- \rangle' = \frac{\Omega_p}{2} \chi_j e^{-|\beta|^2} \sum_{n=0}^\infty \frac{|\beta|^{2n}}{n!} \frac{1}{(\omega_p - \omega_j) - 2\chi_j n + i(n + |\beta|^2)\gamma_c/2 + i(\Gamma_j/2 + \Gamma_{\phi, j})}. \quad (\text{I16})$$

For high quality factor, the width is mostly controlled by the the radiative and dephasing times T_1 and T_2 . For the opposite case $\chi_j \ll \gamma_c$, we find more simply:

$$g_j \langle \hat{\sigma}_{\omega_p, j}^- \rangle' = \frac{\Omega_p}{2} \frac{\chi_j}{(\omega_p - \omega_j) - 2\chi_j |\beta|^2 + i(\Gamma_j/2 + \Gamma_{\phi, j})}. \quad (\text{I17})$$

For a lower quality factor, we obtain a frequency shift revealing the presence of the photon field of intensity $|\beta|^2$ to be detected.

Determining from Eq.(I10) $\langle \hat{a}_{\omega_p,1} \rangle = \Omega_p/[2(\omega_p - \omega_c^* + i\gamma_c/2)]$ and returning to the original representation Eq.(H27), we determine after averaging finally the qubit dynamics:

$$g_j \langle \hat{\sigma}_j^- \rangle(t) = e^{-i\omega_p t} \left(\langle \hat{\sigma}_{\omega_p,j}^- \rangle' + \frac{\chi_j \Omega_p/2}{(\omega_p - \omega_c^* + i\gamma_c/2)} \right) + e^{-i\omega t} \chi_j \beta. \quad (\text{I18})$$

Using the properties $\langle \hat{\sigma}_{j,\omega}^- \rangle = \langle \hat{\sigma}_{-\omega,j}^+ \rangle$, we determine two transmissions as a result of the input signal frequency ω and the input probe frequency ω_p ,

$$S_{21}|\omega = \sum_{\pm} \frac{-1}{\omega - (\pm\omega_c - i\gamma_c/2)} \left[i\gamma_c/2 \pm \frac{\sqrt{\gamma_c \omega_c}}{2} \sum_{j=1}^N \frac{g_j \langle \hat{\sigma}_{\omega,j}^{\mp} \rangle}{\langle \hat{A}_{\omega,+}^{in}(0) \rangle} \right] \quad (\text{I19})$$

$$\begin{aligned} &= \sum_{\pm} \frac{-i\gamma_c/2}{\omega - (\pm\omega_c - i\gamma_c/2)} \left[1 \pm \sum_{j=1}^N \frac{\mp \chi_j}{(\pm\omega - \omega_c^* \pm i\gamma_c/2)} \right] \\ &= \sum_{\pm} \frac{-i\gamma_c/2}{\omega - (\pm\omega_c^* - i\gamma_c/2)}, \end{aligned} \quad (\text{I20})$$

$$S_{21}^{coh} = S_{21}|\omega_p = \sum_{\pm} \frac{-i\gamma_c/2}{\omega_p - (\pm\omega_c - i\gamma_c/2)} \left[1 \mp \sum_{j=1}^N \frac{g_j \langle \hat{\sigma}_{\omega_p,j}^{\mp} \rangle'}{\Omega_p} - \frac{\chi_j}{\pm\omega_p - \omega_c^* \pm i\gamma_c/2} \right] \quad (\text{I21})$$

$$= \sum_{\pm} \frac{-i\gamma_c/2}{\omega_p - (\pm\omega_c^* - i\gamma_c/2)} \mp \sum_{j=1}^N \frac{i\gamma_c}{\omega_p - (\pm\omega_c - i\gamma_c/2)} \frac{g_j \langle \hat{\sigma}_{\omega_p,j}^{\mp} \rangle'}{\Omega_p}. \quad (\text{I22})$$

The latter is the probe transmission used for the cavity photon detection off cavity resonance while the former corresponds to the signal transmission much larger on resonance. Therefore, we need to use a higher intensity probe in order to detect the small off-resonance response.

Finally, we connect the coherent cavity field β to the forward photon flux given by $\mathcal{J} = c\langle \hat{n}^{in} \rangle/\mathcal{L}$ for a waveguide of large length \mathcal{L} . The input field in the forward $\langle \hat{n}^{in} \rangle$ is related to the input coherent field α^{in} associated to the operator $\hat{a}_{\omega/c}/\sqrt{\mathcal{L}}$. Using the relation in (I1) and (I4), the field amplitude inside the cavity and its average photon number $\bar{n} = |\beta|^2$ are therefore expressed respectively in terms of the input field and the photon flux as:

$$\beta = \frac{\sqrt{\gamma_c/2\mathcal{L}}\alpha^{in}}{\omega - \omega_c^* + i\gamma_c/2}, \quad \bar{n} = \frac{\gamma_c \mathcal{J}/2}{(\omega - \omega_c^*)^2 + \gamma_c^2/4}. \quad (\text{I23})$$

For matching frequency, the cavity photon number becomes $\bar{n} = 2\mathcal{J}/\gamma_c$ which is for high quality factor much higher than the photon density outside the cavity.

3. Model 2: Incoherent input radiation

The incoherent light is a radiation field characterized by an absence of absolute phase [36]. It has the same distribution of black body radiation with the difference that it is assumed here to be monochromatic of frequency ω with an infinite coherence time. Given an input field mode $\hat{a}_{\omega/c}$ in the forward direction and the associated average photon number $\langle \hat{n}^{in} \rangle = \langle \hat{a}_{\omega/c}^\dagger \hat{a}_{\omega/c} \rangle$, its density matrix has the form:

$$\hat{\rho}_B = \sum_{n=0}^{\infty} \frac{\langle \hat{n}^{in} \rangle^n}{(\langle \hat{n}^{in} \rangle + 1)^{n+1}} |n\rangle \langle n|. \quad (\text{I24})$$

To treat this non-classical field, we use the insights so far gained for the coherent case by means of the P representation for the variable α^{in} associated to the operator $\hat{a}_{\omega/c}/\sqrt{\mathcal{L}}$. As in [36], we construct a weight function $P(\alpha^{in})$ with the property that the density matrix is diagonal in the basis of input coherent field states $\{|\alpha^{in}\rangle\}$. More explicitly,

$$\hat{\rho}_B = \int P(\alpha^{in}) |\alpha^{in}\rangle \langle \alpha^{in}| d^2\alpha^{in}, \quad d^2\alpha^{in} \equiv d\text{Re}(\alpha^{in}) d\text{Im}(\alpha^{in}). \quad (\text{I25})$$

The P representation of the fully incoherent light corresponding to (I24) has the form:

$$P(\alpha^{in}) = \frac{1}{\pi \langle \hat{n}^{in} \rangle} e^{-|\alpha^{in}|^2 / \langle \hat{n}^{in} \rangle}. \quad (\text{I26})$$

As a consequence, the transmission becomes phase independent and using the correspondence (I25) is written as:

$$S_{21}^{inc} = \int P(\alpha^{in}) S_{21}^{coh}(\alpha^{in}) d^2 \alpha^{in}. \quad (\text{I27})$$

Using the relations (I23), this integral is expressed in terms of the photon number inside the cavity:

$$S_{21}^{inc} = \int \frac{1}{\pi \bar{n}} e^{-|\beta|^2 / \bar{n}} S_{21}^{coh}(\beta) d^2 \beta \quad \langle \hat{\sigma}_{\omega_p, j}^- \rangle^{inc} = \int \frac{1}{\pi \bar{n}} e^{-|\beta|^2 / \bar{n}} \langle \hat{\sigma}_{\omega_p, j}^- \rangle' d^2 \beta. \quad (\text{I28})$$

In the simplest case of high quality factor obeying $\gamma_c \ll (1 + \bar{n})(\Gamma_j/2 + \Gamma_{\phi, j})/\bar{n}$ and matching frequency, we can use the expression (I16). We find after integration over β a change in the width:

$$g_j \langle \hat{\sigma}_{\omega_p, j}^- \rangle^{inc} = \frac{\Omega_p}{2} \chi_j \sum_{n=0}^{\infty} \frac{\bar{n}^n / (\bar{n} + 1)^{n+1}}{\omega_p - (\omega_j + 2\chi_j n - i(n\gamma_c/2 + \Gamma_j/2 + \Gamma_{\phi, j}))}, \quad (\text{I29})$$

with the spectrum given by

$$\omega_p^{(n)} = \omega_j + 2\chi_j n - i n \gamma_c / 2 - i(\Gamma_j/2 + \Gamma_{\phi, j}). \quad (\text{I30})$$

For the general case, the spectral line is rewritten in terms of the exponential integral functions $E_n(x) = \int_1^{\infty} dt e^{-xt}/t^n$. Using the relations:

$$\int \frac{1}{\pi} e^{-c|\beta|^2} \frac{|\beta|^{2n}}{n!} \frac{1}{a + b|\beta|^2} d^2 \beta = \frac{e^{ac/b}}{bc^n} E_{n+1} \left(\frac{ac}{b} \right), \quad (\text{I31})$$

and applying it to Eq.(I14) with the variable w defined in (I12), we obtain:

$$g_j \langle \hat{\sigma}_{\omega, j}^- \rangle^{inc} = \frac{\Omega_p}{2} \chi_j \sum_{n=0}^{\infty} \frac{1}{\bar{n}} \frac{e^{x_n} E_{n+1}(x_n)}{(2\chi_j - \frac{4\chi_j^2}{w}) \left(1/\bar{n} + \frac{4\chi_j^2}{w^2}\right)^n}, \quad (\text{I32})$$

$$x_n = \frac{i(1/\bar{n} + \frac{4\chi_j^2}{w^2})}{(2\chi_j - \frac{4\chi_j^2}{w})} \left[\frac{\Gamma_j}{2} + \Gamma_{\phi, j} + n\gamma_c/2 - i(\omega_p - \omega_j - 2(\chi_j + \omega_c^* - \omega)n) \right]. \quad (\text{I33})$$

For the purpose of practical computation, we can use alternatively the Kummer function $e^y E_n(y) = y^{n-1} U(n, n, y)$. At the singularity for $x_n \sim 0$, we have $E_1(x_1) \sim -\gamma - \ln(x_n)$ and $E_{n+1}(x_n) \sim 1/n$ for $n > 0$. Asymptotically, $E_{n+1}(x_n) \sim \exp(-x_n)/x_n$. In the limit of strong $\gamma_c \gg \chi_j$, the first term in the sum is dominant and Eq.(I32) becomes:

$$g_j \langle \hat{\sigma}_{\omega, j}^- \rangle^{inc} = \frac{\Omega_p}{4\bar{n}} \exp\left[[(\omega_p - \omega_j) + i(\frac{\Gamma_j}{2} + \Gamma_{\phi, j})]/(2\bar{n}\chi_j)\right] E_1 \left([(\omega_p - \omega_j) + i(\frac{\Gamma_j}{2} + \Gamma_{\phi, j})]/(2\bar{n}\chi_j) \right). \quad (\text{I34})$$

4. Model 3: Incoherent state detection with coherence time (thermal bath states)

In the previous subsection, we assume a pure input monochromatic beam which means that the frequency broadening is much smaller than the cavity broadening. In this subsection, we assume the opposite case where the broadening is much larger so that the coherence time τ_c fulfills the condition $\gamma_c \tau_c \ll 1$. In that situation, the amplitude average is still zero and the averaged photon number is distributed continuously in the momentum space so that the radiation signal can be viewed as a thermal bath for the cavity system. As a consequence, the treatment of such photon signal requires to change the density matrix $\hat{\rho}_B(0)$ from the vacuum state into a thermal-like state. It is in fact sufficient to define this incoherent state by the stationary average:

$$\langle \hat{a}_{k, in}^\dagger \hat{a}_{k', in} \rangle = 2\pi 1^+(k) \delta(k - k') \frac{2\mathcal{J}/\tau_c}{(\omega - \omega_k)^2 + 1/\tau_c^2}, \quad \langle \hat{a}_{k, in} \hat{a}_{k', in}^\dagger \rangle = 2\pi \delta(k - k') \left((1 + 1^+(k)) \frac{2\mathcal{J}/\tau_c}{(\omega - \omega_k)^2 + 1/\tau_c^2} \right), \quad (\text{I35})$$

where \mathcal{J} is the photon flux coming from the left side of the cavity. The distribution has a Lorentzian form centered around the input frequency ω but with a frequency broadening large enough as to be indistinguishable from a thermal state.

With these different assumptions, the master equation (I5) has to be modified by replacing the vacuum from the Lorentzian state and setting $\Omega = 0$ and choosing the reference frequency for detuning in the RWA as $\omega = \omega_c^*$. This procedure leads to the following non-Markovian master equation:

$$\begin{aligned} \partial_t \hat{\rho}'(t) + i[\hat{H}^{(3)}(t), \hat{\rho}'(t)] &= -\frac{\gamma_c}{2} \int_0^\infty dt' \mathcal{J} \cos[(\omega - \omega_c^*)t'] e^{-t'/\tau_c} \left[\{\hat{a}_1 \hat{a}_1^\dagger, \hat{\rho}'(t-t')\} - 2\hat{a}_1^\dagger \hat{\rho}'(t-t') \hat{a}_1 \right] + \\ (2\delta(t') + \mathcal{J} \cos[(\omega - \omega_c^*)t'] e^{-t'/\tau_c}) &\left[\{\hat{a}_1^\dagger \hat{a}_1, \hat{\rho}(t-t')\} - 2\hat{a}_1 \hat{\rho}'(t-t') \hat{a}_1^\dagger \right] - \sum_{j=1}^N \left(\frac{\Gamma_j}{2} + \Gamma_{\phi,j} \right) \{\hat{\sigma}_j^+ \hat{\sigma}_j^-, \hat{\rho}'(t)\} - \Gamma_j \hat{\sigma}_j^- \hat{\rho}'(t) \hat{\sigma}_j^+ \\ \hat{H}^{(3)}(t) &= \sum_{j=1}^N \frac{(\omega_j - \omega_c^*)}{2} \hat{\sigma}_j^z + \sum_{j=1}^N \chi_j \hat{a}_1^\dagger \hat{a}_1 (\hat{\sigma}_j^z + 1) + \sum_{j=1}^N \left[\frac{\Omega_p^*}{2} \left(\hat{a}_1 - \frac{g_j}{\omega_c - \omega_j} \hat{\sigma}_j^- \right) e^{i(\omega_p - \omega_c^*)t} + c.c. \right]. \end{aligned} \quad (\text{I36})$$

In absence of the probe field ($\Omega_p = 0$), the stationary solution has a form where the qubits are in their ground state and the radiation has a thermal distribution:

$$\hat{\rho}_0 = \hat{\rho}_T \prod_{j=1}^n \frac{1 - \hat{\sigma}_j^z}{2}, \quad \hat{\rho}_T = \frac{\exp(-\hbar\omega_c^* \hat{a}_1^\dagger \hat{a}_1 / k_B T_e)}{\bar{n} + 1}. \quad (\text{I37})$$

The effective temperature T_e is defined from the effective Bose Einstein factor for average population inside the cavity \bar{n} which is itself related to the Lorentzian distribution parameter:

$$\bar{n} = \frac{1}{\exp(\hbar\omega_c^* / k_B T_e) - 1} = \frac{\mathcal{J} / \tau_c}{(\omega - \omega_c^*)^2 + 1 / \tau_c^2} \stackrel{\omega = \omega_c^*}{=} \tau_c \mathcal{J}. \quad (\text{I38})$$

Therefore, because of the larger broadband, the rate of signal photon passing through the cavity is considerably reduced by a factor $\tau_c \gamma_c / 2$ in comparison to the monochromatic beams defined in subsection 1 and 2. The probe field introduces a perturbation:

$$\hat{\rho}'(t) = \hat{\rho}_0 + \delta\hat{\rho}(t) = \hat{\rho}_0 + \left[e^{-i(\omega_p - \omega_c^*)t} \left(\sum_{j=1}^N \frac{1 - \hat{\sigma}_j^z}{2} \hat{\rho}_{j0} + \hat{\sigma}_j^+ \hat{\rho}_j \right) \prod_{j' \neq j=1}^N \frac{1 - \hat{\sigma}_{j'}^z}{2} + c.c. \right], \quad (\text{I39})$$

whose matrix elements $\hat{\rho}_{j0}$ and $\hat{\rho}_j$ solve respectively:

$$\begin{aligned} -i(\omega_p - \omega) \hat{\rho}_{j0} + \frac{i\Omega_p}{2} [\hat{a}_1^\dagger, \hat{\rho}_T] \\ = -\frac{\gamma_c}{2} \bar{n}_p \left[\{\hat{a}_1 \hat{a}_1^\dagger, \hat{\rho}_{j0}\} - 2\hat{a}_1^\dagger \hat{\rho}_{j0} \hat{a}_1 \right] - \frac{\gamma_c}{2} (1 + \bar{n}_p) \left[\{\hat{a}_1^\dagger \hat{a}_1, \hat{\rho}_{j0}\} - 2\hat{a}_1 \hat{\rho}_{j0} \hat{a}_1^\dagger \right], \end{aligned} \quad (\text{I40})$$

$$\begin{aligned} -i[\omega_p - \omega_j + i(\frac{\Gamma_j}{2} + \Gamma_{\phi,j})] \hat{\rho}_j + \hat{a}_1^\dagger \hat{a}_1 \hat{\rho}_j + \frac{i\Omega_p}{2} \frac{g_j \hat{\rho}_T}{\omega_j - \omega_c} \\ = -\frac{\gamma_c}{2} \bar{n}_p \left[\{\hat{a}_1 \hat{a}_1^\dagger, \hat{\rho}_j\} - 2\hat{a}_1^\dagger \hat{\rho}_j \hat{a}_1 \right] - \frac{\gamma_c}{2} (1 + \bar{n}_p) \left[\{\hat{a}_1^\dagger \hat{a}_1, \hat{\rho}_j\} - 2\hat{a}_1 \hat{\rho}_j \hat{a}_1^\dagger \right]. \end{aligned} \quad (\text{I41})$$

In both equations, the effective Bose enhancement factor is defined as $\bar{n}_p = \bar{n}|_{\tau_c = \tau_p}$ where $\tau_p = \tau_c / (1 + i\tau_c(\omega_p - \omega))$ and is much less sensitive to the signal for large detuning between the signal and probe frequency. On the contrary, for relatively long coherence time satisfying $\tau_c(\omega_p - \omega) \ll 1$, the master equation corresponding to a markovian process, this enhancement is maximal $\bar{n}_p \simeq \bar{n}$.

The first equation (I41) is similar to the case (I10) developed in subsection 1 and provides an identical shift in the photon transmission spectrum. We need to take only the first order average in the field to obtain the same response $\langle \hat{a}_{\omega_p,1} \rangle$. The second equation (I41) is solved using the following steps. First, we use the Fock representation $f_j(n) = \langle n | \hat{\rho}_j | n \rangle$, this second equation is rewritten as:

$$\begin{aligned} [i(\omega_p - \omega_j) - (\frac{\Gamma_j}{2} + \Gamma_{\phi,j}) - i2n\chi_j] f_j(n) = \gamma_c (1 + \bar{n}_p) (n f_j(n) - (n+1) f_j(n+1)) + \gamma_c \bar{n}_p ((n+1) f_j(n) - n f_j(n-1)) \\ + \frac{i\Omega_p}{2} \frac{g_j e^{-\hbar\omega_c^* n / k_B T_e}}{(\omega_j - \omega_c)(1 + \bar{n})}. \end{aligned} \quad (\text{I42})$$

Second, we define from this representation the generating function: $h_j(x) = e^{v_j x} \sum_{n=0}^{\infty} x^n f_j(n)/n!$. This function obeys the differential equation:

$$\begin{aligned} & \left[\gamma_c(1 + \bar{n}_p)(x\partial_x^2 + \partial_x) + [2\gamma_c(v_j - 1)(\bar{n}_p + 1) + \gamma_c - 2i\chi_j]x\partial_x + i[\omega_p - \omega_j + i(\frac{\Gamma_j}{2} + \Gamma_{\phi,j})] + \gamma_c(v_j(\bar{n}_p + 1) - \bar{n}_p) \right] h_j(x) \\ &= \frac{i\Omega_p}{2} \frac{g_j e^{[\bar{n}/(1+\bar{n})-v_j]x}}{(1 + \bar{n})(\omega_j - \omega_c)} \end{aligned} \quad (\text{I43})$$

where we choose $v_j = 1 + (i\chi_j - \gamma_c/2 - S_j)/[\gamma_c(1 + \bar{n}_p)]$ with $S_j = \sqrt{\gamma_c^2/4 + \gamma_c(2\bar{n}_p + 1)i\chi_j - \chi_j^2}$. Third, we solve the differential equation using the Laguerre polynomials expansion: $h_j(x) = \sum_{k=0}^{\infty} c_n L_n(2S_j x/\gamma_c(\bar{n}_p + 1))$. These polynomials are eigenfunctions of the differential operator and leads to a quantification condition of the spectrum for ω_p according to

$$\omega_p^{(n)} = \omega_j - i(\frac{\Gamma_j}{2} + \Gamma_{\phi,j}) - i(2n + 1)S_j - \chi_j + i\gamma_c/2. \quad (\text{I44})$$

Fourth, we determine the coefficient c_n using the variation of constants and then determine $\langle \hat{\sigma}_{\omega,j}^- \rangle' = \text{Tr}(\hat{\rho}_j)$. After a straightforward calculation, we find the general expression:

$$g_j \langle \hat{\sigma}_{\omega,j}^- \rangle' = \frac{\Omega_p \chi_j}{2} \sum_{n=0}^{\infty} \frac{2S_j \gamma_c}{\omega_p - \omega_p^{(n)}} \frac{[\gamma_c/2 - S_j - i\chi_j]^n}{[\gamma_c/2 + S_j - i\chi_j]^{n+1}} \frac{[\gamma_c(v_j - \bar{n}/(1 + \bar{n})) (1 + \bar{n}_p)]^n}{[\gamma_c(v_j - \bar{n}/(1 + \bar{n})) (1 + \bar{n}_p) + 2S_j]^{n+1}}. \quad (\text{I45})$$

Similarly to previous models, the summation is done over propagators with poles that represent the resonance of the spectrum. For practical computation of the infinite sum, we may use the related hypergeometric function defined as $\Phi(x, 1, a) = {}_2F_1(1, a; 1 + a; x)/a = \sum_{n=0}^{\infty} x^n/(n + a)$. For the case of vanishing coherence time, we recover the thermal case with $\bar{N} = \bar{N}_p$. We find successively in the limit of high quality factor and no signal photon:

$$g_j \langle \hat{\sigma}_{\omega,j}^- \rangle' = \frac{\Omega_p}{2} \chi_j \sum_{n=0}^{\infty} \frac{2S_j \gamma_c}{\omega_p - \omega_p^{(n)}} \frac{[(S_j - \gamma_c/2)^2 + \chi_j^2]^n}{[(S_j + \gamma_c/2)^2 + \chi_j^2]^{n+1}} \quad (\text{I46})$$

$$\stackrel{\gamma_c \ll \chi_j}{=} \sum_{n=0}^{\infty} \frac{(\Omega_p/2) \chi_j \bar{n}^n / (\bar{n} + 1)^{n+1}}{\omega_p - (\omega_j + 2\chi_j n - i(\gamma_c[(2\bar{n} + 1)n +] + \frac{\Gamma_j}{2} + \Gamma_{\phi,j}))} \quad (\text{I47})$$

$$\stackrel{\bar{n}=0}{=} \frac{\Omega_p}{2} \chi_j \frac{1}{\omega_p - \omega_j + i(\frac{\Gamma_j}{2} + \Gamma_{\phi,j})}. \quad (\text{I48})$$